ACCURATE AND EFFICIENT CALCULATION OF SINGULAR ELECTROSTATIC POTENTIALS IN CHARGE-DIELECTRIC SPHERICAL AND JANUS PARTICLE SYSTEMS

by

Caylah Natielle Retz

A dissertation submitted to the faculty of
The University of North Carolina at Charlotte
in partial fulfillment of the requirements
for the degree of Doctor of Philosophy in
Applied Mathematics

Charlotte

2018

Approved by:

_____

Xingjie Li

_____

Wei Cai

_____

Duan Chen

_____

Gregory Gbur

ABSTRACT

CAYLAH NATIELLE RETZ. Accurate and efficient calculation of singular electrostatic potentials in charge-dielectric spherical and Janus particle systems. (Under the direction of DR. WEI CAI)

We introduce an efficient and accurate boundary element method for computing the electrostatic potential in closely-packed dielectric spheres and Janus particles. Close physical proximity occurs in modeling molecular ion interactions or colloidal materials. The electrostatic potential, which is described by the Poisson-Boltzmann equation, becomes highly singular under close interactions, resulting in difficulties in computational results. We select a boundary element approach due to the natural reduction of the dimension of the problem from volume to surface elements. The singular behavior caused by the close proximity of the system due to the source charge and part of the reaction field is removed from the potential via a subtraction de-singularization technique within a hyper-singular, high order second kind integral equation formulation.

The resulting system of equations has a number of right-hand-side integrals that do not contain basis elements and contain the bulk of the singular behavior. These auxiliary integrals require treatment in order to best capture the singular behavior while keeping cost at a minimum. So long as these integrals are calculated accurately, the system can be readily, easily solved. Regularization techniques for the Hadamard finite part integral that appears in this method are then presented, where mathematical identities and adaptive meshes offer a means to compute the singular integral with the required level of accuracy at a much reduced computational cost. Adaptive quadrature is presented and used for other less challenging, but still singular integrals. We demonstrate that numerical results of the singular potential for one and two closely-packed spheres have validated the effectiveness and accuracy of the proposed method.

ACKNOWLEDGMENTS

My journey through graduate school has been an extended stay amongst magnificent professors and brilliant peers who have contributed to shaping my experience and, by extension, this work. I have had the pleasure to learn from and interact with friends, colleagues and professors alike, all of whom I hold dear to my heart and will never, ever forget. I would not have been able to accomplish even a fraction of the work required for obtaining a Doctorate of Philosophy without their assistance and unconditional support. Here follows a partial list of people who have my infinite gratitude for their part in my long journey to this point.

Firstly, I would like to acknowledge my advisor, Dr. Wei Cai. I began my tutelage under his guidance at the most elementary of levels, and somehow he took that and made me into a researcher. He provides the perfect blend of cheer and honesty in his instruction, leaving one with both direction and optimism. His patience, kindness, understanding and generosity have all been pivotal to my learning and, ultimately, to finishing at all. Dr. Cai is an excellent advisor, and one of the best decisions I have made was asking if he would be mine.

I would next like to express my gratitude to Dr. Xingjie Li for her part on my committee and for her invaluable assistance with this dissertation in Dr. Cai's absence. Her willingness to meet with me over the summer and give feedback and suggestions helped drag me across the finish line. This generosity with her time and her amazing abilities to be nurturing and supportive are virtues that I benefited from just at the perfect time. I would like to thank my other committee member, Dr. Duan Chen for his feedback, suggestions and personal qualities that make him a pleasure to be around. Together, these three professors made a perfect, well-rounded mathematical committee, and I am forever grateful for their participation in this endeavor of mine. Thanks goes out to my graduate faculty representative, Dr. Greg

TABLE OF CONTENTS

LIST OF TABLES

LIST OF FIGURES

CHAPTER 1: Introduction

1.1 Motivation

The topic of electrostatic interactions encompasses many scientific disciplines. Electrostatic interactions exert important influences in applications such as protein folding [41], biomolecular processes [24], colloidal materials sciences [46] and optics [13]. As a result of such broad applications, integral equations for finding electrostatic fields have been extensively studied and used. The electrostatic potential itself is described by the Poisson or Poisson-Boltzmann differential equation [19] and is a scalar quantity equaling the amount of work necessary to move a test unit positive charge from a reference point to a designated endpoint. When given a system of interacting objects that have specific dielectric and/or ionization properties, one can find the electric potential at any point in space through solving the Poisson or Poisson-Boltzmann equation by one of the many existing numerical techniques. In this dissertation, we choose the numerical, boundary element method approach [9, 28, 12]. Our primary goal is the accurate computation of the electric potential for a chosen system when the objects in question are in close proximity. The singular nature of the Green's function to the Poisson-Boltzmann equation indicates that there are limitations to how close two objects can get (< 0.2 units usually) before the singularity unfavorably impacts the results of a solver algorithm. In this work we develop and utilize techniques that seek to mitigate a substantial portion of the singular behavior that arises in particular close-proximity systems when using boundary element methods. These techniques result in more accurate electric potential results than otherwise. We then

demonstrate the effectiveness of our methods through several examples of physical systems of choice.

1.2 Background and Previous Work

Differential equations present themselves as mathematical descriptions of many physical problems. Wave phenomena and heat conduction are among the more elementary of these. Along with a plethora of significant partial differential equations comes numerous methods by which they may be solved. Choosing the best mathematical framework for solving a differential equation depends on what restrictions or characteristics must be considered. In general, there are two types of solutions to differential equations: analytical (exact) solutions and numerical solutions. Analytical solutions have the advantage of being fast, accurate and computationally inexpensive. However, it is not always possible or preferable to solve a problem analytically, as an analytic solution may not exist, and in the event that it does, it may not be easy to directly compute. Numerical methods is a natural alternative to analytic solutions, with the disadvantage sometimes being that they are computationally expensive.

In this dissertation, we are interested in modeling electrostatic interactions in and around systems of source charges with dielectric spheres and Janus particles. The electric potential at any point in space is described by the Poisson or Poisson-Boltzmann partial differential equation, depending on if ionic material is involved [19]. An analytic approach to solving for the electrostatic potential might include image charge methods [14, 48, 18] or generalized Born approximations [42]. On the other hand, numerically we have the choice of finite differences [32, 17], finite elements [16, 23], and boundary element techniques [11, 32, 33]. In this work we are interested in the electrostatic potential within a physical geometry similar to that of colloidal materials [47], where charges, ions and molecules interact in very close physical proximity. This means that the value of the potential must be reliable and accurate since

small changes in proximity may have significant impact. This naturally lends to the use of numerical methods to solve the Poisson-Boltzmann (PB) equation. We will use boundary element methods for boundary integral equations to solve, due to the reduction of the problem to lower dimensional manifolds [7, 8].

Boundary element methods blossomed and gained popularity in the last half century due to advances in computing capabilities made possible by modern technology. The method's development has a long history [15, 5], with foundations laid by a number of well-known mathematicians, leading up to the use of integral equations and boundary element methods to describe and numerically solve electrostatic potential problems in independent works by Jaswon, Ponter, Symm, and Rizzo [26, 25, 44, 38]. From there, the modern boundary element method condensed and found its name in a research group consisting of Brebbia, Dominguez, and others [9, 12]. Boundary element methods afford the luxury of only having to discretize the boundary of a volume using surface elements, instead of having to use volume elements as in finite element methods. Thus boundary element methods spare some computational cost compared to finite element techniques. Since ultimately we desire to model several objects in a system, any reduction in computation time is much valued. However, a notable disadvantage to using boundary element techniques is the need to have a fundamental solution to the differential equation already known [33]. For our purposes, fundamental solutions used in [29], [50], and [13] will be appropriate for our systems.

A classical approach for electric potential integral equations calls for the use of single and double layer potentials for the respective solutions of the Neumann and Dirichlet problems of the Poisson-Boltzmann equation [39]. This results in a so-called second kind integral equation, which satisfies the conditions of Fredholm theorems and results in asymptotically stable solution algorithms when in a discretized system [34, 4].

We follow an approach used in Juffer [27] and Lu [31], and recently implemented

in the immediate predecessors to this work [50, 30], that results in a hypersingular integral equation and whose second kind integral formulation is well-conditioned. The hypersingularity of order $\mathcal{O}(|\mathbf{r}-\mathbf{r}'|^{-3})$ is the result of taking the second derivative of the Green's function kernel. In those works the hypersingularity is treated using a singularity subtraction technique outlined in Müller [35] and Rokhlin [39], which ultimately ensures very good accuracy in the electric potential. However, the Green's function fundamental solution $G(\mathbf{r}, \mathbf{r}')$ corresponding to the Poisson-Boltzmann equation can only be treated to result in such nicely behaved hypersingular integral equations when $\mathbf{r}$ and $\mathbf{r}'$ are sufficiently far apart. For geometries and physical problems in which we are interested, that require close proximity of the two points, such treatments are largely unsuccessful at ensuring that the kernel's singular behavior does not severely degenerate the results of the algorithm.

The specific Green's function solution to be used depends on the geometries and setup of the problem. In particular, in many topics the physical problem can involve layered media, where special "layered" Green's functions must be used when discussing boundary integral techniques [37, 50, 29]. For example, inhomogeneous (ionized) media may be considered, as in ion transport through a cell membrane, where the membrane is a layered structure whose dielectric properties vary and whose electrostatic forces influence the dynamics of the ions. In another example, and the one most relevant to this work, the polarization of particles in inhomogeneous media can influence the building of materials, as in colloidal material sciences involving Janus particles, which are themselves layered. Janus particles are micro-objects that contain asymmetrical physical and chemical traits that influence self-assembled materials and their overall properties, such as mechanical strength, magnetism and conductivity [47]. When scientists are interested in building some new, structured material, the building blocks are colloidal particles, which themselves can be built by a combination of homogeneous (dielectric) or inhomogeneous (Janus) particles. Therefore, we will

be working with homogeneous, inhomogeneous and layered media situations, each of which requires different fundamental solutions.

In adapting the physical problem of electrostatically interacting particles to a mathematical one, we must be able to model more than one particle at a time, with those particles interacting in close range. In this dissertation we will derive a set of hypersingular integral equations and further treat the hypersingularity and resulting computational difficulty through the use of change of variables, in addition to the techniques outlined in [50, 30]. As a result, the singular behavior of the potential is moved to a number of right-hand side integrals of the resulting matrix equation, which can then be treated using adaptive quadratures and a mathematical identity similar to that used in [49].

1.3   Layout of Dissertation

This dissertation is laid out as follows: Chapter 2 starts with introducing the Poisson-Boltzmann equation and the functions which will be used in a change of variables to a new smooth de-singularized variable. A system of two hypersingular boundary integral equations will then be derived for a physical system consisting of a single dielectric sphere and a source charge. The system of equations will result in a matrix equation that contains a few right-hand-side auxiliary integrals that contain the bulk of the singular behavior of the electrostatic potential. Then we will derive a mathematical identity which exists over a purely mathematical boundary and apply it to the integral equations so that the right-hand-side integrals contain integrands with more manageable singular behavior. In Chapter 3, the integral equations from Chapter 2 are discretized and we demonstrate the improved results we obtain compared to previous results where the subtraction de-singularization method has not been used. In Chapter 4, we refine the Gauss quadrature used when calculating the right-hand-side integrals so that calculation time is reduced while maintaining the integrity of the

results. The resulting adaptive quadrature places dense "patches" of Gauss points around areas of the integrals where singular behavior is most pronounced, with fewer points spread elsewhere.

Chapter 5 re-derives the boundary integral equations, using the same substitution and integral techniques, to systems of more than one dielectric sphere and a source charge. We then present a few examples where a system of dielectric spheres exist, but one of them is "fake," where its dielectric properties are identical to the background medium. This lets us reduce a system of two spheres to the results as if there were only one. This is in an effort to show that the results are identical to those for only one sphere and that our computer code correctly works for systems. Other examples featuring perturbed dielectric constants and a second non-fake sphere are also shown and elaborated upon. In Chapter 6 we re-derive the boundary integral equations to those where Janus particles are involved instead of dielectric spheres. The mathematical identity we used in the integral equations for dielectric spheres is altered and adapted for Janus particles, which slightly changes the system of boundary integral equations from what they were for dielectric spheres. A few interesting examples about Janus particle interactions are then presented.

CHAPTER 2: Single-sphere system setup and its boundary integral equations

2.1   Differential equation and charge-sphere system

Consider a sphere in an infinite medium. Denote regions of this system as Ω_j, where $j = i, o$, the interior and exterior regions of the spheroid, respectively. We further denote dielectric constants by ε_j and the inverse Debye Hückel lengths [22] by λ_j, where $j = i, o$. Assume that there is a charge with magnitude q_s at $\mathbf{r}_s$ located outside the sphere. For convenience, we let $q_s = 1$.
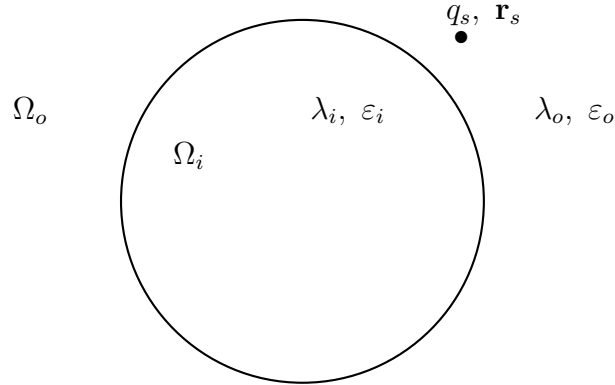
Figure 2.1: Dielectric sphere and source charge system

In this model, the sphere represents a homogeneous particle interacting with a source charge in a medium that may or may not be ionic in nature. Assuming ionicity of the exterior domain, the potential field ϕ at arbitrary position $\mathbf{r}$ satisfies the Poisson-Boltzmann equation in free space

$$\nabla^2 \phi(\mathbf{r}) - \lambda^2(\mathbf{r})\phi(\mathbf{r}) = -\frac{4\pi}{\varepsilon(\mathbf{r})} q_s \delta(\mathbf{r} - \mathbf{r}_s) \tag{2.1}$$

with boundary conditions

$$[\phi(\mathbf{r})] = 0 \text{ and } \left[\varepsilon(\mathbf{r})\frac{\partial\phi(\mathbf{r})}{\partial\mathbf{n}}\right] = 0, \tag{2.2}$$

where δ is the dirac delta function and $[\cdot]$ is the jump across a boundary. Here, we have that

$$\varepsilon(\mathbf{r}) = \begin{cases} \varepsilon_i & \mathbf{r} \in \Omega_i \\ \varepsilon_o & \mathbf{r} \in \Omega_o \end{cases} \tag{2.3}$$

and

$$\lambda(\mathbf{r}) = \begin{cases} \lambda_i & \mathbf{r} \in \Omega_i \\ \lambda_o & \mathbf{r} \in \Omega_o \end{cases}. \tag{2.4}$$

Let the fundamental solution for (2.1) be given by G, where

$$G(\mathbf{r}, \mathbf{r}') = \frac{e^{-\lambda(\mathbf{r})|\mathbf{r}-\mathbf{r}'|}}{4\pi\varepsilon(\mathbf{r})|\mathbf{r}-\mathbf{r}'|}. \tag{2.5}$$

Then G satisfies the PDE

$$\varepsilon(\mathbf{r})[\nabla^2 G(\mathbf{r}, \mathbf{r}') - \lambda^2(\mathbf{r})G(\mathbf{r}, \mathbf{r}')] = -\delta(\mathbf{r} - \mathbf{r}') \tag{2.6}$$

with boundary conditions on the surface of the sphere:

$$[G(\mathbf{r}, \mathbf{r}')] = 0, \left[\varepsilon(\mathbf{r})\frac{\partial G}{\partial\mathbf{n}}(\mathbf{r}, \mathbf{r}')\right] = 0. \tag{2.7}$$

In work by B. Zinser [50] and H. Lin [29], a system of hypersingular integral equations was derived for the domain of a round-topped cylinder, which allows for the reduction of the domain to a sphere if the height of the cylinder is set to zero. That paper showed an example of such a reduction by finding the potential for a Janus particle and source charge system. The limitations of those hypersingular integral equations, written in terms of the potential ϕ, arise when we let the source

charge $\mathbf{r}_s$ approach the surface of the sphere, inducing singular behavior. The closer the source charge gets to the particle, the less accurate the potential is and the harder the iterative solver, GMRES [40], has to work to converge. This dissertation uses BIE derivations similar to those used in [50], taking advantage of the methods developed in that work that tackle the hypersingularity that appears in the matrix part of the eventual matrix equation. Our contribution then focuses on developing means to gain accuracy when considering close-body interactions, a scenery by which previous works fall short. We set about our task by introducing a new function $w(\mathbf{r})$ that is much smoother than the potential $\phi(\mathbf{r})$ when the source charge $\mathbf{r}_s$ is close to the particle. We re-derive the integral equations in terms of $w(\mathbf{r})$. The resulting discretized matrix equation is then easy to solve, since most of the singular behavior of the Green's function kernel is captured by right-hand-side auxiliary integrals. We then tackle the issue of accurately capturing the hypersingularity in these auxiliary integrals through specific treatments.

2.2 De-singularized variables

In general, the potential $\phi(\mathbf{r})$ can be decomposed into the sum of the potential due to the source charge and the reaction field potential $\phi_{\mathrm{rf}}(\mathbf{r})$, the latter of which reflects the polarization of the material outside the sphere Ω_o. That is,

$$\phi(\mathbf{r}) = \frac{q_s}{\varepsilon(\mathbf{r})|\mathbf{r} - \mathbf{r}_s|} + \phi_{\mathrm{rf}}(\mathbf{r}). \tag{2.8}$$

Using Kelvin image location $\mathbf{x}_1$ [45] and Jacobi-Gauss-Radau locations $\mathbf{x}_{m=2}^{M-1}$ [43][20], we estimate the reaction field potential using image charges [14] as

$$\phi_{\mathrm{rf}}(\mathbf{r}) \approx \frac{q_1}{\varepsilon(\mathbf{r})|\mathbf{r} - \mathbf{x}_1|} + \sum_{m=2}^{M-1} \frac{q_m}{\varepsilon(\mathbf{r})|\mathbf{r} - \mathbf{x}_m|}, \tag{2.9}$$

where M is a pre-determined number of image charge locations. We choose M according to the guidelines indicated in [14]. We note here that to use the estimation of the reaction field as outlined in [14], we must stipulate that $\lambda = 0$ in the Poisson-Boltzmann equation. However, we will continue to derive the integral equations in terms of the Poisson-Poltzmann equation (instead of the Poisson equation) for later use. The reaction field can be re-defined as necessary for the cases where $\lambda \neq 0$.

We define a "de-singularized" solution variable such that the potential due to the source charge in (2.8) as well as the dominant part of the reaction field from the image charges (2.9) are explicitly removed from the potential. For this purpose, let

$$G_o(\mathbf{r}, \mathbf{r}') = \frac{e^{-\lambda_o(\mathbf{r})|\mathbf{r}-\mathbf{r}'|}}{4\pi\varepsilon_o(\mathbf{r})|\mathbf{r} - \mathbf{r}'|} \tag{2.10}$$

and define a function H by

$$H(\mathbf{r}, \mathbf{r}_s) = 4\pi q_s G_o(\mathbf{r}, \mathbf{r}_s), \tag{2.11}$$

where H satisfies the P-B equation

$$\varepsilon_o(\nabla^2 H(\mathbf{r}, \mathbf{r}_s) - \lambda_o^2 H(\mathbf{r}, \mathbf{r}_s)) = -\rho(\mathbf{r}), \tag{2.12}$$

and, for sphere Ω,

$$\rho(\mathbf{r}) = \begin{cases} 4\pi q_s \delta(\mathbf{r} - \mathbf{r}_s) & \text{if } \mathbf{r} \in \Omega_o \\ 0 & \text{if } \mathbf{r} \in \Omega_i \end{cases} \tag{2.13}$$

Secondly, define $T(\mathbf{r}, \mathbf{r}_s)$ equal to the sum of n terms of the M screened Coulomb potential terms used to approximate the reaction field [14], where $n < M$,

$$T(\mathbf{r}, \mathbf{r}_s) = \frac{q_1}{\varepsilon_o|\mathbf{r} - \mathbf{x}_1|} + \sum_{j=2}^{n-1} \frac{q_j}{\varepsilon_o|\mathbf{r} - \mathbf{x}_j|}, \tag{2.14}$$

where, for each image location $\mathbf{x}_j$, $T(\mathbf{r}, \mathbf{r}_s)$ satisfies the P-B equation

$$\varepsilon_o(\nabla^2 T(\mathbf{r}, \mathbf{r}_s) - \lambda_o^2 T(\mathbf{r}, \mathbf{r}_s)) = -\nu(\mathbf{r}), \tag{2.15}$$

and, for a sphere Ω,

$$\nu(\mathbf{r}) = \begin{cases} 0 & \text{if } \mathbf{r} \in \Omega_o \\ 4\pi \sum_{j=1}^{n} q_i \delta(\mathbf{r} - \mathbf{x}_j) & \text{if } \mathbf{r} \in \Omega_i \end{cases}. \tag{2.16}$$

Finally, we introduce a de-singularized solution variable w, with which we will derive the boundary integral equations,

$$w(\mathbf{r}) = \begin{cases} \phi_o(\mathbf{r}) - H(\mathbf{r}, \mathbf{r}_s) - T(\mathbf{r}, \mathbf{r}_s) & \text{if } \mathbf{r} \in \Omega_o \\ \phi_i(\mathbf{r}) & \text{if } \mathbf{r} \in \Omega_i \end{cases}, \tag{2.17}$$

which can be shown to satisfy a homogeneous P-B equation in Ω_o and Ω_i, respectively. This definition will result in different interface conditions on the surface of the sphere than in (2.7), to be given a little later. First we will re-write the partial differential equation in terms of this new variable $w(\mathbf{r})$.

For $\mathbf{r}$ outside the sphere, first we subtract equations (2.1) and (2.12) as follows:

$$\varepsilon_o(\nabla^2 \phi_o(\mathbf{r}) - \lambda_o^2 \phi_o(\mathbf{r})) = -4\pi q_s \delta(\mathbf{r} - \mathbf{r}_s)$$

$$-\left(\varepsilon_o(\nabla^2 H(\mathbf{r}, \mathbf{r}_s) - \lambda_o^2 H(\mathbf{r}, \mathbf{r}_s)) = -4\pi q_k \delta(\mathbf{r} - \mathbf{r}_s) \right) \tag{2.18}$$

$$\Rightarrow \quad \varepsilon_o(\nabla^2 \big(\phi_o(\mathbf{r}) - H(\mathbf{r}, \mathbf{r}_s) \big) - \lambda_o^2 \big(\phi_o(\mathbf{r}) - H(\mathbf{r}, \mathbf{r}_s) \big)) = 0.$$

Next we subtract (2.15) from (2.18)

$$\varepsilon_o(\nabla^2\big(\phi_o(\mathbf{r}) - H(\mathbf{r}, \mathbf{r}_s)\big) - \lambda_o^2\big(\phi_o(\mathbf{r}) - H(\mathbf{r}, \mathbf{r}_s)\big)) = 0$$

$$-\left(\varepsilon_o(\nabla^2 T(\mathbf{r}, \mathbf{r}_s) - \lambda_o^2 T(\mathbf{r}, \mathbf{r}_s)) = 0\right) \tag{2.19}$$

$$\Rightarrow \varepsilon_o\nabla^2(\phi_o(\mathbf{r}) - H(\mathbf{r}, \mathbf{r}_s) - T(\mathbf{r}, \mathbf{r}_s)) - \lambda_o^2(\phi_o(\mathbf{r}) - H(\mathbf{r}, \mathbf{r}_s) - T(\mathbf{r}, \mathbf{r}_s)) = 0.$$

Substituting in for the variable w, we have

$$\varepsilon_o\nabla^2 w_o(\mathbf{r}) - \lambda_o^2 w_o(\mathbf{r}) = 0. \tag{2.20}$$

For the case that $\mathbf{r}$ is inside the sphere, we have

$$\varepsilon_i(\nabla^2 w_i(\mathbf{r}) - \lambda_i^2 w_i(\mathbf{r})) = \varepsilon_i[\nabla^2\phi_i(\mathbf{r}) - \lambda_i^2\phi_i(\mathbf{r})] = 0.$$

In addition, we have new jump condition on the interface for w as

$$w_i - w_o = \phi_i - (\phi_o - H - T) = H + T$$

and

$$\varepsilon_i\frac{\partial w_i}{\partial\mathbf{n}} - \varepsilon_o\frac{\partial w_o}{\partial\mathbf{n}} = \varepsilon_i\frac{\partial\phi_i}{\partial\mathbf{n}} - \varepsilon_o\left(\frac{\partial\phi_o}{\partial\mathbf{n}} - \frac{\partial H}{\partial\mathbf{n}} - \frac{\partial T}{\partial\mathbf{n}}\right) = \varepsilon_o\frac{\partial H(\mathbf{r}, \mathbf{r}_s)}{\partial\mathbf{n}} + \varepsilon_o\frac{\partial T(\mathbf{r}, \mathbf{r}_s)}{\partial\mathbf{n}}.$$

That is, after changing variables, the boundary conditions are

$$[w(\mathbf{r})] = H(\mathbf{r}, \mathbf{r}_s) + T(\mathbf{r}, \mathbf{r}_s), \quad \left[\varepsilon(\mathbf{r})\frac{\partial w(\mathbf{r})}{\partial\mathbf{n}}\right] = \varepsilon_o\frac{\partial H(\mathbf{r}, \mathbf{r}_s)}{\partial\mathbf{n}} + \varepsilon_o\frac{\partial T(\mathbf{r}, \mathbf{r}_s)}{\partial\mathbf{n}}. \tag{2.21}$$

2.3   Boundary integral equations

In this section we will derive hypersingular boundary integral equations of the second kind in terms of the variable $w(\mathbf{r})$. The process starts by finding the integral equations of the first kind and then taking appropriate derivatives of the integral equations. We then use them to derive the integral equations of the second kind. Afterward, we will derive an identity on a purely mathematical, non-physical boundary and apply it to the integral equations so that the auxiliary integrals that result from the change of variables from ϕ to w will be more manageable.

2.3.1   Integral equations of first kind on the outside of the boundary

The two PDE's for $\mathbf{r}'$ outside the sphere Ω are:

$$\varepsilon_o \nabla^2 w_o(\mathbf{r}) - \lambda_o^2 w_o(\mathbf{r}) = 0 \tag{2.22}$$

$$\varepsilon_o (\nabla^2 G_o(\mathbf{r},\mathbf{r}') - \lambda_o^2 G_o(\mathbf{r},\mathbf{r}')) = -\delta(\mathbf{r} - \mathbf{r}'), \tag{2.23}$$

where $G_o(\mathbf{r},\mathbf{r}') = \dfrac{e^{-\lambda_o(\mathbf{r})|\mathbf{r}-\mathbf{r}'|}}{4\pi\varepsilon_o(\mathbf{r})|\mathbf{r} - \mathbf{r}'|}$ Multiply (2.22) by $G_o(\mathbf{r},\mathbf{r}')$ and (2.23) by $w_o(\mathbf{r})$ and take their difference

$$\varepsilon_o (G_o(\mathbf{r},\mathbf{r}')\nabla^2 w_o(\mathbf{r}) - \lambda_o^2 w_o(\mathbf{r})G_o(\mathbf{r},\mathbf{r}')) = 0$$

$$-\left(\varepsilon_o(w_o(\mathbf{r})\nabla^2 G_o(\mathbf{r},\mathbf{r}') - \lambda_o^2 w_o(\mathbf{r})G_o(\mathbf{r},\mathbf{r}')) = -w_o(\mathbf{r})\delta(\mathbf{r} - \mathbf{r}') \right) \tag{2.24}$$

$$\varepsilon_o (G_o(\mathbf{r},\mathbf{r}')\nabla^2 w_o(\mathbf{r}) - w_o(\mathbf{r})\nabla^2 G_o(\mathbf{r},\mathbf{r}')) = w_o(\mathbf{r})\delta(\mathbf{r} - \mathbf{r}')$$

and then integrate over the exterior of Ω and a ball $B(\mathbf{r}', \rho)$ of radius ρ centered at $\mathbf{r}'$

$$\int_{\mathbb{R}^3 \setminus (\Omega \cup B(\mathbf{r}', \rho))} \varepsilon_o (G_o(\mathbf{r}, \mathbf{r}') \nabla^2 w_o(\mathbf{r}) - w_o(\mathbf{r}) \nabla^2 G_o(\mathbf{r}, \mathbf{r}')) \, d\mathbf{r} = \int_{\mathbb{R}^3 \setminus (\Omega \cup B(\mathbf{r}', \rho))} w_o(\mathbf{r}) \delta(\mathbf{r} - \mathbf{r}') \, d\mathbf{r}$$

$$\Rightarrow \int_{\mathbb{R}^3 \setminus (\Omega \cup B(\mathbf{r}', \rho))} \varepsilon_o (G_o(\mathbf{r}, \mathbf{r}') \nabla^2 w_o(\mathbf{r}) - w_o(\mathbf{r}) \nabla^2 G_o(\mathbf{r}, \mathbf{r}')) \, d\mathbf{r} = 0.$$

$$(2.25)$$

Using Green's second identity, we move the domain of integration to the boundary.

$$\oint_{\partial(\mathbb{R}^3 \setminus (\Omega \cup B(\mathbf{r}', \rho)))} \varepsilon_o \left(G_o(\mathbf{r}, \mathbf{r}') \frac{\partial w_o(\mathbf{r})}{\partial \mathbf{n}} - w_o(\mathbf{r}) \frac{\partial G_o(\mathbf{r}, \mathbf{r}')}{\partial \mathbf{n}} \right) dS(\mathbf{r}) = 0. \qquad (2.26)$$

Considering separate parts of the boundary that the integral is calculated over, we have that the integral on the infinite interface is zero, as both G_o and w_o vanish at infinity. So that leaves 1) the integral on the surface dielectric sphere S, and 2) the integral on the boundary of $B(\mathbf{r}', \rho)$.

$$\oint_{\partial(\mathbb{R}^3 \setminus (\Omega \cup B(\mathbf{r}', \rho)))} \varepsilon_o \left(G_o(\mathbf{r}, \mathbf{r}') \frac{\partial w_o(\mathbf{r})}{\partial \mathbf{n}} - w_o(\mathbf{r}) \frac{\partial G_o(\mathbf{r}, \mathbf{r}')}{\partial \mathbf{n}} \right) dS(\mathbf{r})$$

$$= - \oint_S \varepsilon_o \left(G_o(\mathbf{r}, \mathbf{r}') \frac{\partial w_o(\mathbf{r})}{\partial \mathbf{n}} - w_o(\mathbf{r}) \frac{\partial G_o(\mathbf{r}, \mathbf{r}')}{\partial \mathbf{n}} \right) dS(\mathbf{r})$$

$$- \oint_{\partial B(\mathbf{r}', \rho)} \varepsilon_o \left(G_o(\mathbf{r}, \mathbf{r}') \frac{\partial w_o(\mathbf{r})}{\partial \mathbf{n}} - w_o(\mathbf{r}) \frac{\partial G_o(\mathbf{r}, \mathbf{r}')}{\partial \mathbf{n}} \right) dS(\mathbf{r})$$

$$= \oint_S \varepsilon_o \left(w_o(\mathbf{r}) \frac{\partial G_o(\mathbf{r}, \mathbf{r}')}{\partial \mathbf{n}} - G_o(\mathbf{r}, \mathbf{r}') \frac{\partial w_o(\mathbf{r})}{\partial \mathbf{n}} \right) dS(\mathbf{r}) + (-w_o(\mathbf{r}')),$$

$$(2.27)$$

where the negative is due to the normal vector pointing into the domain. So then we have for boundary S

$$\oint_S \varepsilon_o (w_o(\mathbf{r}) \frac{\partial G_o(\mathbf{r}, \mathbf{r}')}{\partial \mathbf{n}} - G_o(\mathbf{r}, \mathbf{r}') \frac{\partial w_o(\mathbf{r})}{\partial \mathbf{n}}) \, dS(\mathbf{r}) + (-w_o(\mathbf{r}')) = 0$$

$$\implies w_o(\mathbf{r}') = \oint_S \varepsilon_o (w_o(\mathbf{r}) \frac{\partial G_o(\mathbf{r}, \mathbf{r}')}{\partial \mathbf{n}} - G_o(\mathbf{r}, \mathbf{r}') \frac{\partial w_o(\mathbf{r})}{\partial \mathbf{n}}) \, dS(\mathbf{r})$$

$$(2.28)$$

Taking the limit as $\mathbf{r}'$ approaches some $\mathbf{p}$ in S, we have

$$\implies \quad \frac{1}{2}w_o(\mathbf{p}) = \oint_S \varepsilon_o\left(w_o(\mathbf{r})\frac{\partial G_o(\mathbf{r},\mathbf{p})}{\partial \mathbf{n}} - G_o(\mathbf{r},\mathbf{p})\frac{\partial w_o(\mathbf{r})}{\partial \mathbf{n}}\right)\mathrm{d}S(\mathbf{r}), \qquad (2.29)$$

resulting in the one-half out front [36, 13].

2.3.2 Integral equations of first kind on the inside of the boundary

Let $\mathbf{r}'$ be inside Ω. Then the two PDEs are:

$$\varepsilon_i(\nabla^2 w_i(\mathbf{r}) - \lambda_i^2 w_i(\mathbf{r})) = 0 \qquad (2.30)$$

$$\varepsilon_i(\nabla^2 G_i(\mathbf{r},\mathbf{r}') - \lambda_i^2 G_i(\mathbf{r},\mathbf{r}')) = -\delta(\mathbf{r} - \mathbf{r}'). \qquad (2.31)$$

We then multiply (2.30) by $G_i(\mathbf{r},\mathbf{r}')$ and (2.31) by $w_i(\mathbf{r})$ and integrate their difference

$$\int_{\Omega\smallsetminus B(\mathbf{r}',\rho)} \varepsilon_i(G_i(\mathbf{r},\mathbf{r}')\nabla^2 w_i(\mathbf{r}) - w_i(\mathbf{r})\nabla^2 G_i(\mathbf{r},\mathbf{r}'))\,\mathrm{d}\mathbf{r} = \int_{\Omega\smallsetminus B(\mathbf{r}',\rho)} w_i(\mathbf{r})\delta(\mathbf{r} - \mathbf{r}')\,\mathrm{d}\mathbf{r} = 0$$

$$(2.32)$$

where $B(\mathbf{r}',\rho)$ is a ball of radius ρ at $\mathbf{r}'$. Applying Green's second identity, we move the integral to the boundary S and take the limit as ρ goes to zero:

$$w_i(\mathbf{r}') = \oint_S \varepsilon_i\left(G_i(\mathbf{r},\mathbf{r}')\frac{\partial w_i(\mathbf{r})}{\partial \mathbf{n}} - w_i(\mathbf{r})\frac{\partial G_i(\mathbf{r},\mathbf{r}')}{\partial \mathbf{n}}\right)\mathrm{d}S(\mathbf{r}). \qquad (2.33)$$

Taking the limit as $\mathbf{r}'$ approaches a point $\mathbf{p}$ in S from the inside and using the boundary conditions (2.21), we have

$$\frac{1}{2}w_i(\mathbf{p}) = \oint_S \varepsilon_i \left(G_i(\mathbf{r}, \mathbf{p}) \frac{\partial w_i(\mathbf{r})}{\partial \mathbf{n}} - w_i(\mathbf{r}) \frac{\partial G_i(\mathbf{r}, \mathbf{p})}{\partial \mathbf{n}} \right) dS(\mathbf{r})$$

$$\Rightarrow \frac{1}{2}(w_o(\mathbf{p}) + H(\mathbf{p}, \mathbf{r}_s) + T(\mathbf{p}, \mathbf{r}_s)) = \oint_S \varepsilon_i \left(G_i(\mathbf{r}, \mathbf{p}) \left(\frac{\varepsilon_o}{\varepsilon_i} \frac{\partial H(\mathbf{r}, \mathbf{r}_s)}{\partial \mathbf{n}} + \frac{\varepsilon_o}{\varepsilon_i} \frac{\partial w_o(\mathbf{r})}{\partial \mathbf{n}} + \frac{\varepsilon_o}{\varepsilon_i} \frac{\partial T(\mathbf{r}, \mathbf{r}_s)}{\partial \mathbf{n}} \right) \right.$$

$$\left. - (w_o(\mathbf{r}) + H(\mathbf{r}, \mathbf{r}_s) + T(\mathbf{r}, \mathbf{r}_s)) \frac{\partial G_i(\mathbf{r}, \mathbf{p})}{\partial \mathbf{n}} \right) dS(\mathbf{r})$$

$$\Rightarrow \frac{1}{2}w_o(\mathbf{p}) = \oint_S \left(\varepsilon_o G_i(\mathbf{r}, \mathbf{p}) \frac{\partial w_o(\mathbf{r})}{\partial \mathbf{n}} - \varepsilon_i w_o(\mathbf{r}) \frac{\partial G_i(\mathbf{r}, \mathbf{p})}{\partial \mathbf{n}} \right) dS(\mathbf{r}) \tag{2.34}$$

$$+ \oint_S \left(\varepsilon_o G_i(\mathbf{r}, \mathbf{p}) \frac{\partial H(\mathbf{r}, \mathbf{r}_s)}{\partial \mathbf{n}} - \varepsilon_i H(\mathbf{r}, \mathbf{r}_s) \frac{\partial G_i(\mathbf{r}, \mathbf{p})}{\partial \mathbf{n}} \right) dS(\mathbf{r})$$

$$+ \oint_S \left(\varepsilon_o G_i(\mathbf{r}, \mathbf{p}) \frac{\partial T(\mathbf{r}, \mathbf{r}_s)}{\partial \mathbf{n}} - \varepsilon_i T(\mathbf{r}, \mathbf{r}_s) \frac{\partial G_i(\mathbf{r}, \mathbf{p})}{\partial \mathbf{n}} \right) dS(\mathbf{r})$$

$$- \frac{1}{2}H(\mathbf{p}, \mathbf{r}_s) - \frac{1}{2}T(\mathbf{p}, \mathbf{r}_s).$$

Together equations (2.29) and (2.34) make up the integral equations of the first kind. However, they form an ill-conditioned system of equations [13][50]. So we must consider integral equations of the second kind.

2.3.3   Integral equations of the second kind

The integral equations of the second kind are made by taking the sum of equations (2.29) and (2.34) and by taking the sum of normal derivatives of (2.29) and (2.34) with respect to $\mathbf{r}'$. So we need to find the normal derivatives and then sum the equations.

Taking the derivative of (2.28) with respect to $\mathbf{r}'$, we get the following equation for when $\mathbf{r}'$ is outside of Ω

$$\frac{\partial w_o(\mathbf{r}')}{\partial \mathbf{n}'} = \oint_S \varepsilon_o \left(w_o(\mathbf{r}) \frac{\partial^2 G_o(\mathbf{r}, \mathbf{r}')}{\partial \mathbf{n}' \partial \mathbf{n}} - \frac{\partial G_o(\mathbf{r}, \mathbf{r}')}{\partial \mathbf{n}'} \frac{\partial w_o(\mathbf{r})}{\partial \mathbf{n}} \right) dS(\mathbf{r}). \tag{2.35}$$

Taking the limit from the outside as $\mathbf{r}'$ approaches a point $\mathbf{p}$ in S, we have

$$\frac{1}{2}\frac{\partial w_o(\mathbf{p})}{\partial \mathbf{n}} = \oint_S \varepsilon_o \left(w_o(\mathbf{r})\frac{\partial^2 G_o(\mathbf{r},\mathbf{p})}{\partial \mathbf{n}'\partial \mathbf{n}} - \frac{\partial G_o(\mathbf{r},\mathbf{p})}{\partial \mathbf{n}'}\frac{\partial w_o(\mathbf{r})}{\partial \mathbf{n}} \right) \mathrm{d}S(\mathbf{r}). \qquad (2.36)$$

Taking the normal derivative of (2.33) with respect to $\mathbf{r}'$, we get the following equation for when $\mathbf{r}'$ is inside Ω.

$$\frac{w_i(\mathbf{r}')}{\partial \mathbf{n}'} = \oint_S \varepsilon_i \left(\frac{\partial G_i(\mathbf{r},\mathbf{r}')}{\partial \mathbf{n}'}\frac{\partial w_i(\mathbf{r})}{\partial \mathbf{n}} - w_i(\mathbf{r})\frac{\partial^2 G_i(\mathbf{r},\mathbf{r}')}{\partial \mathbf{n}'\partial \mathbf{n}} \right) \mathrm{d}S(\mathbf{r}) \qquad (2.37)$$

Taking the limit as $\mathbf{r}'$ approaches a point $\mathbf{p}$ in S from the inside and using the boundary conditions (2.21)

$$\frac{1}{2}\frac{w_i(\mathbf{p})}{\partial \mathbf{n}} = \oint_S \varepsilon_i \left(\frac{\partial G_i(\mathbf{r},\mathbf{p})}{\partial \mathbf{n}'}\frac{\partial w_i(\mathbf{r})}{\partial \mathbf{n}} - w_i(\mathbf{r})\frac{\partial^2 G_i(\mathbf{r},\mathbf{p})}{\partial \mathbf{n}'\partial \mathbf{n}} \right) \mathrm{d}S(\mathbf{r})$$

$$\Rightarrow \quad \frac{1}{2}\frac{\varepsilon_o}{\varepsilon_i}\left(\frac{\partial H(\mathbf{p},\mathbf{r}_s)}{\partial \mathbf{n}} + \frac{\partial w_o(\mathbf{p})}{\partial \mathbf{n}} + \frac{\partial T(\mathbf{p},\mathbf{r}_s)}{\partial \mathbf{n}} \right) = \oint_S \varepsilon_i \frac{\partial G_i(\mathbf{r},\mathbf{p})}{\partial \mathbf{n}'}\left(\frac{\varepsilon_o}{\varepsilon_i}\frac{\partial H(\mathbf{r},\mathbf{r}_s)}{\partial \mathbf{n}} + \frac{\varepsilon_o}{\varepsilon_i}\frac{\partial w_o(\mathbf{r})}{\partial \mathbf{n}} + \frac{\varepsilon_o}{\varepsilon_i}\frac{\partial T(\mathbf{r},\mathbf{r}_s)}{\partial \mathbf{n}} \right) \mathrm{d}S(\mathbf{r})$$

$$- \oint_S \varepsilon_i(w_o(\mathbf{r}) + H(\mathbf{r},\mathbf{r}_s) + T(\mathbf{r},\mathbf{r}_s))\frac{\partial^2 G_i(\mathbf{r},\mathbf{p})}{\partial \mathbf{n}'\partial \mathbf{n}}\, \mathrm{d}S(\mathbf{r})$$

$$\Rightarrow \quad \frac{1}{2}\frac{\varepsilon_o}{\varepsilon_i}\frac{\partial w_o(\mathbf{p})}{\partial \mathbf{n}} = \oint_S \left(\varepsilon_o \frac{\partial G_i(\mathbf{r},\mathbf{p})}{\partial \mathbf{n}'}\frac{\partial w_o(\mathbf{r})}{\partial \mathbf{n}} - \varepsilon_i w_o(\mathbf{r})\frac{\partial^2 G_i(\mathbf{r},\mathbf{p})}{\partial \mathbf{n}'\partial \mathbf{n}} \right) \mathrm{d}S(\mathbf{r})$$

$$+ \oint_S \left(\varepsilon_o \frac{\partial G_i(\mathbf{r},\mathbf{p})}{\partial \mathbf{n}'}\frac{\partial H(\mathbf{r},\mathbf{r}_s)}{\partial \mathbf{n}} - \varepsilon_i H(\mathbf{r},\mathbf{r}_s)\frac{\partial^2 G_i(\mathbf{r},\mathbf{p})}{\partial \mathbf{n}'\partial \mathbf{n}} \right) \mathrm{d}S(\mathbf{r})$$

$$+ \oint_S \left(\varepsilon_o \frac{\partial G_i(\mathbf{r},\mathbf{p})}{\partial \mathbf{n}'}\frac{\partial T(\mathbf{r},\mathbf{r}_s)}{\partial \mathbf{n}} - \varepsilon_i T(\mathbf{r},\mathbf{r}_s)\frac{\partial^2 G_i(\mathbf{r},\mathbf{p})}{\partial \mathbf{n}'\partial \mathbf{n}} \right) \mathrm{d}S(\mathbf{r})$$

$$- \frac{1}{2}\frac{\varepsilon_o}{\varepsilon_i}\frac{\partial H(\mathbf{p},\mathbf{r}_s)}{\partial \mathbf{n}} - \frac{1}{2}\frac{\varepsilon_o}{\varepsilon_i}\frac{\partial T(\mathbf{p},\mathbf{r}_s)}{\partial \mathbf{n}}.$$

$$(2.38)$$

2.3.4 Second kind integral equations

The first integral equation of the second kind is the sum of (2.29) and (2.34):

$$
\begin{aligned}
w_o(\mathbf{p}) = & \oint_S \varepsilon_o \left(G_i(\mathbf{r},\mathbf{p}) - G_o(\mathbf{r},\mathbf{p}) \right) \frac{\partial w_o(\mathbf{r})}{\partial \mathbf{n}} \, dS(\mathbf{r}) + \oint_S \left(\varepsilon_o \frac{\partial G_o(\mathbf{r},\mathbf{p})}{\partial \mathbf{n}} - \varepsilon_i \frac{\partial G_i(\mathbf{r},\mathbf{p})}{\partial \mathbf{n}} \right) w_o(\mathbf{r}) \, dS(\mathbf{r}) \\
& + \oint_S \left(\varepsilon_o G_i(\mathbf{r},\mathbf{p}) \frac{\partial H(\mathbf{r},\mathbf{r}_s)}{\partial \mathbf{n}} - \varepsilon_i H(\mathbf{r},\mathbf{r}_s) \frac{G_i(\mathbf{r},\mathbf{p})}{\partial \mathbf{n}} \right) dS(\mathbf{r}) \\
& + \oint_S \left(\varepsilon_o G_i(\mathbf{r},\mathbf{p}) \frac{\partial T(\mathbf{r},\mathbf{r}_s)}{\partial \mathbf{n}} - \varepsilon_i T(\mathbf{r},\mathbf{r}_s) \frac{\partial G_i(\mathbf{r},\mathbf{p})}{\partial \mathbf{n}} \right) dS(\mathbf{r}) \\
& - \frac{1}{2} H(\mathbf{p},\mathbf{r}_s) - \frac{1}{2} T(\mathbf{p},\mathbf{r}_s).
\end{aligned}
\tag{2.39}
$$

The second equation of the second kind is the sum of (2.36) and (2.38)

$$
\begin{aligned}
\left(\frac{1}{2} + \frac{1}{2} \frac{\varepsilon_o}{\varepsilon_i} \right) \frac{\partial w_o(\mathbf{p})}{\partial \mathbf{n}} = & \oint_S \left(\varepsilon_o \frac{\partial^2 G_o(\mathbf{r},\mathbf{p})}{\partial \mathbf{n}' \partial \mathbf{n}} - \varepsilon_i \frac{\partial^2 G_i(\mathbf{r},\mathbf{p})}{\partial \mathbf{n}' \partial \mathbf{n}} \right) w_o(\mathbf{r}) \, dS(\mathbf{r}) \\
& + \oint_S \left(\varepsilon_o \frac{\partial G_i(\mathbf{r},\mathbf{p})}{\partial \mathbf{n}'} - \varepsilon_o \frac{\partial G_o(\mathbf{r},\mathbf{p})}{\partial \mathbf{n}'} \right) \frac{\partial w_o(\mathbf{r})}{\partial \mathbf{n}} \, dS(\mathbf{r}) \\
& - \text{p.f.} \oint_S \varepsilon_i H(\mathbf{r},\mathbf{r}_s) \frac{\partial^2 G_i(\mathbf{r},\mathbf{p})}{\partial \mathbf{n}' \partial \mathbf{n}} \, dS(\mathbf{r}) - \text{p.f.} \oint_S \varepsilon_i T(\mathbf{r},\mathbf{r}_s) \frac{\partial^2 G_i(\mathbf{r},\mathbf{p})}{\partial \mathbf{n}' \partial \mathbf{n}} \, dS(\mathbf{r}) \\
& + \oint_S \varepsilon_o \frac{\partial H(\mathbf{r},\mathbf{r}_s)}{\partial \mathbf{n}} \frac{\partial G_i(\mathbf{r},\mathbf{p})}{\partial \mathbf{n}'} \, dS(\mathbf{r}) + \oint_S \varepsilon_o \frac{\partial T(\mathbf{r},\mathbf{r}_s)}{\partial \mathbf{n}} \frac{\partial G_i(\mathbf{r},\mathbf{p})}{\partial \mathbf{n}'} \, dS(\mathbf{r}) \\
& - \frac{1}{2} \frac{\varepsilon_o}{\varepsilon_i} \frac{\partial H(\mathbf{p},\mathbf{r}_s)}{\partial \mathbf{n}} - \frac{1}{2} \frac{\varepsilon_o}{\varepsilon_i} \frac{\partial T(\mathbf{p},\mathbf{r}_s)}{\partial \mathbf{n}}.
\end{aligned}
\tag{2.40}
$$

Together equations (2.39) and (2.40) make a system of hypersingular second kind boundary integral equations. The hypersingularity is seen in the Hadamard finite part integrals, where the second derivatives of the Green's function give the integrands singular behavior of order $\mathcal{O}(|\mathbf{r} - \mathbf{r}'|^{-3})$. These finite part integrals need regularization so that they can be accurately calculated for source charges very close to the boundary of the sphere. In the next section, we introduce a new mathematical boundary on the surface of the spherical particle in the system and derive a mathematical identity [49] that we can apply to the Hadamard finite part integrals. The result is the extension of the single Hadamard finite part integral into several other integrals, each of which divvies up the load of handling the hypersingular behavior.

2.4 Regularization of the hyper-singular integral

We would like to regularize the finite part integrals in (2.40). Let Σ denote the integral(s) of interest, namely

$$\Sigma = -\text{p.f.} \oint_S \varepsilon_o (H(\mathbf{r}, \mathbf{r}_s) + T(\mathbf{r}, \mathbf{r}_s)) \frac{\partial^2 G_i(\mathbf{r}, \mathbf{p})}{\partial \mathbf{n}' \partial \mathbf{n}} \, dS(\mathbf{r}). \tag{2.41}$$

This integral is being calculated at a point $\mathbf{p} \in \partial\Omega$. When $\mathbf{r} \to \mathbf{p}$, the integrand of Σ has order $\frac{1}{|\mathbf{r}-\mathbf{p}|^3}$. The method to be discussed here, which we call the "bubble" technique, will remove one order of the singularity, making the integrand to be of order $\frac{1}{|\mathbf{r}-\mathbf{p}|^2}$. While this reduction still leaves strongly singular integrands, significant improvement in the ability to accurately calculate the integrals is observed nonetheless.

2.4.1 Hemisphere and special solution $v(\mathbf{r})$

Let us construct a hemisphere of radius a and center it at the point $\mathbf{p}$ along the inside of the surface of our sphere. The hemispherical surface is denoted by Γ and the intersection of the hemisphere and the boundary of Ω is denoted by $S_a \equiv S_a(\mathbf{p})$. We call the region enclosed by this hemisphere Ω_p. For some $\mathbf{z} \in \Omega_i$, $\mathbf{z} \notin \Omega_p$ and for some constant C, let us construct a special solution for the potential of a charge at $\mathbf{z}$:
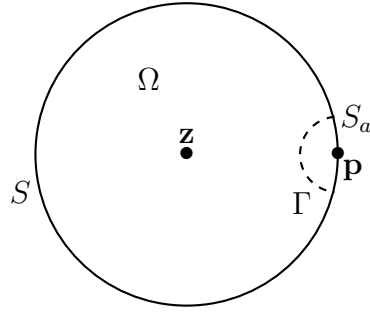
Figure 2.2: Sphere and hemisphere setup

$$v(\mathbf{r}) = \frac{e^{-\lambda(\mathbf{r})|\mathbf{r}-\mathbf{z}|}}{\varepsilon(\mathbf{r})|\mathbf{r} - \mathbf{z}|} C. \tag{2.42}$$

Details about the value of constant C will be discussed a little later in this section. In addition, for ease of calculating the constant C, we generally take $\mathbf{z}$ to be located in the center of the sphere. We then have that v satisfies the PDE

$$\varepsilon(\mathbf{r})(\nabla^2 v(\mathbf{r}) - \lambda^2(\mathbf{r})v(\mathbf{r})) = -C \cdot 4\pi\delta(\mathbf{r} - \mathbf{z}). \tag{2.43}$$

Given the radius r of the sphere Ω, if we impose the restriction for the hemisphere that $a < \frac{1}{2}r$, then the pde for $v(\mathbf{r})$ in Ω_p is given by

$$\varepsilon_o\big[\nabla^2 v(\mathbf{r}) - \lambda_i^2 v(\mathbf{r})\big] = 0. \tag{2.44}$$

We wish to derive the boundary integral equations for v on the domain Ω_p. The two PDE's for $\mathbf{r}$ inside the sphere Ω are:

$$\varepsilon_i(\nabla^2 v(\mathbf{r}) - \lambda_i^2 v(\mathbf{r})) = 0 \tag{2.45}$$

$$\varepsilon_i(\nabla^2 G_i(\mathbf{r}, \mathbf{r}') - \lambda_i^2 G_i(\mathbf{r}, \mathbf{r}')) = -\delta(\mathbf{r} - \mathbf{r}'), \tag{2.46}$$

so multiplying (2.45) by $G_i(\mathbf{r}, \mathbf{r}')$ and (2.46) by $v(\mathbf{r})$, and taking their difference, we get

$$\varepsilon_i(G_i(\mathbf{r}, \mathbf{r}')\nabla^2 v(\mathbf{r}) - v(\mathbf{r})\nabla^2 G_i(\mathbf{r}, \mathbf{r}')) = v(\mathbf{r})\delta(\mathbf{r} - \mathbf{r}'). \tag{2.47}$$

Integrating over $\Omega_p \setminus B(\mathbf{r}', \rho)$ and using Green's identity yields

$$\oint_{\partial(\Omega_p \setminus B(\mathbf{r}', \rho))} \varepsilon_i \left(G_i(\mathbf{r}, \mathbf{r}')\frac{\partial v(\mathbf{r})}{\partial \mathbf{n}} - v(\mathbf{r})\frac{\partial G_i(\mathbf{r}, \mathbf{r}')}{\partial \mathbf{n}} \right) dS(\mathbf{r}) = 0,$$

which, using a previous argument, becomes

$$v(\mathbf{r}') = \oint_{S_a \cup \Gamma} \varepsilon_i \left(G_i(\mathbf{r}, \mathbf{r}')\frac{\partial v(\mathbf{r})}{\partial \mathbf{n}} - v(\mathbf{r})\frac{\partial G_i(\mathbf{r}, \mathbf{r}')}{\partial \mathbf{n}} \right) dS(\mathbf{r}). \tag{2.48}$$

Care must be taken when considering normal derivatives on the boundary of Ω_p. For clarity, we introduce the notation $\mathbf{n}_o = -\mathbf{n}_i$, where $\mathbf{n}_i$ is the unit normal on the surface of the sphere, at point $\mathbf{p}$, pointing into domain Ω_p. Furthermore, we denote $\mathbf{n}_\Gamma$ as the outward unit normal on Γ. Instituting this new notation, (2.48) becomes

$$
\begin{aligned}
v(\mathbf{r}') = \oint_{S_a} \varepsilon_i \left(G_i(\mathbf{r}, \mathbf{r}') \frac{\partial v(\mathbf{r})}{\partial \mathbf{n}_o} - v(\mathbf{r}) \frac{\partial G_i(\mathbf{r}, \mathbf{r}')}{\partial \mathbf{n}_o} \right) \mathrm{d}S(\mathbf{r}) \\
+ \oint_{\Gamma} \varepsilon_i \left(G_i(\mathbf{r}, \mathbf{r}') \frac{\partial v(\mathbf{r})}{\partial \mathbf{n}_\Gamma} - v(\mathbf{r}) \frac{\partial G_i(\mathbf{r}, \mathbf{r}')}{\partial \mathbf{n}_\Gamma} \right) \mathrm{d}S(\mathbf{r})
\end{aligned}
\tag{2.49}
$$

Taking the normal derivative of (2.49) with respect to $\mathbf{r}'$

$$
\begin{aligned}
\frac{\partial v(\mathbf{r}')}{\partial \mathbf{n}_o'} = \oint_{S_a} \varepsilon_i \left(\frac{\partial G_i(\mathbf{r}, \mathbf{r}')}{\partial \mathbf{n}_o'} \frac{\partial v(\mathbf{r})}{\partial \mathbf{n}_o} - v(\mathbf{r}) \frac{\partial^2 G_i(\mathbf{r}, \mathbf{r}')}{\partial \mathbf{n}_o' \partial \mathbf{n}_o} \right) \mathrm{d}S(\mathbf{r}) \\
+ \oint_{\Gamma} \varepsilon_i \left(\frac{\partial G_i(\mathbf{r}, \mathbf{r}')}{\partial \mathbf{n}_o'} \frac{\partial v(\mathbf{r})}{\partial \mathbf{n}_\Gamma} - v(\mathbf{r}) \frac{\partial^2 G_i(\mathbf{r}, \mathbf{r}')}{\partial \mathbf{n}_o' \partial \mathbf{n}_\Gamma} \right) \mathrm{d}S(\mathbf{r})
\end{aligned}
\tag{2.50}
$$

and taking the limit as $\mathbf{r}'$ approaches $\mathbf{p}$ in S from the inside yields the following identity:

$$
\begin{aligned}
\frac{1}{2} \frac{\partial v(\mathbf{p})}{\partial \mathbf{n}_o} - \oint_{S_a} \varepsilon_i \left(\frac{\partial G_i(\mathbf{r}, \mathbf{p})}{\partial \mathbf{n}_o'} \frac{\partial v(\mathbf{r})}{\partial \mathbf{n}_o} - v(\mathbf{r}) \frac{\partial^2 G_i(\mathbf{r}, \mathbf{p})}{\partial \mathbf{n}_o' \partial \mathbf{n}_o} \right) \mathrm{d}S(\mathbf{r}) \\
- \oint_{\Gamma} \varepsilon_i \left(\frac{\partial G_i(\mathbf{r}, \mathbf{p})}{\partial \mathbf{n}_o'} \frac{\partial v(\mathbf{r})}{\partial \mathbf{n}_\Gamma} - v(\mathbf{r}) \frac{\partial^2 G_i(\mathbf{r}, \mathbf{p})}{\partial \mathbf{n}_o' \partial \mathbf{n}_\Gamma} \right) \mathrm{d}S(\mathbf{r}) = 0.
\end{aligned}
\tag{2.51}
$$

2.4.2 De-singularized Hadamard finite part integral

We now treat (2.51) as the value zero and add it to our hyper-singular integral Σ. But first let us split Σ up over the union $(S \setminus S_a) \cup S_a$ and use the above identity

$$\Sigma = - \oint_{(S \smallsetminus S_a)} \varepsilon_i (H(\mathbf{r}, \mathbf{r}_s) + T(\mathbf{r}, \mathbf{r}_s)) \frac{\partial^2 G_i(\mathbf{r}, \mathbf{p})}{\partial \mathbf{n}'_o \partial \mathbf{n}_o} \, \mathrm{d}S(\mathbf{r}) - \oint_{S_a} \varepsilon_i (H(\mathbf{r}, \mathbf{r}_s) + T(\mathbf{r}, \mathbf{r}_s)) \frac{\partial^2 G_i(\mathbf{r}, \mathbf{p})}{\partial \mathbf{n}'_o \partial \mathbf{n}_o} \, \mathrm{d}S(\mathbf{r}). \tag{2.52}$$

Add 0 to Σ:

$$
\begin{aligned}
\Sigma + 0 = & - \oint_{(S \smallsetminus S_a)} \varepsilon_i (H(\mathbf{r}, \mathbf{r}_s) + T(\mathbf{r}, \mathbf{r}_s)) \frac{\partial^2 G_i(\mathbf{r}, \mathbf{p})}{\partial \mathbf{n}'_o \partial \mathbf{n}_o} \, \mathrm{d}S(\mathbf{r}) + \oint_{S_a} \varepsilon_i \left(v(\mathbf{r}) - H(\mathbf{r}, \mathbf{r}_s) - T(\mathbf{r}, \mathbf{r}_s) \right) \frac{\partial^2 G_i(\mathbf{r}, \mathbf{p})}{\partial \mathbf{n}'_o \partial \mathbf{n}_o} \, \mathrm{d}S(\mathbf{r}) \\
& - \oint_{S_a} \varepsilon_i \left(\frac{\partial G_i(\mathbf{r}, \mathbf{p})}{\partial \mathbf{n}'_o} \frac{\partial v(\mathbf{r})}{\partial \mathbf{n}_o} \right) \mathrm{d}S(\mathbf{r}) - \oint_{\Gamma} \varepsilon_i \left(\frac{\partial G_i(\mathbf{r}, \mathbf{p})}{\partial \mathbf{n}'_o} \frac{\partial v(\mathbf{r})}{\partial \mathbf{n}_\Gamma} \right) \mathrm{d}S(\mathbf{r}) \\
& + \oint_{\Gamma} \varepsilon_i \left(v(\mathbf{r}) \frac{\partial^2 G_i(\mathbf{r}, \mathbf{p})}{\partial \mathbf{n}'_o \partial \mathbf{n}_\Gamma} \right) \mathrm{d}S(\mathbf{r}) + \frac{1}{2} \frac{\partial v(\mathbf{p})}{\partial \mathbf{n}_o}.
\end{aligned}
\tag{2.53}
$$

It can be shown using Taylor series that $v(\mathbf{r}) - H(\mathbf{r}, \mathbf{r}_s) - T(\mathbf{r}, \mathbf{r}_s) = \mathcal{O}(|\mathbf{r} - \mathbf{p}|)$ as $\mathbf{r}$ goes to $\mathbf{p}$. The details can be found in Appendix C. As a result, the second integral in (2.53), which contains the majority of the singular behavior of Σ, is of order $\mathcal{O}\left(\dfrac{1}{|\mathbf{r} - \mathbf{p}|^2}\right)$. We then replace Σ in (2.40) with the additional integrals shown in (2.53). With the introduction of the function $v(\mathbf{r})$ and subsequent identity on the mathematical hemisphere, we traded one computationally difficult integral for several simpler, less challenging integrals. Further, we now declare that the constant C is chosen so that $v(\mathbf{r}) - H(\mathbf{r}, \mathbf{r}_s) - T(\mathbf{r}, \mathbf{r}_s)$ vanishes at a point $\mathbf{p}$ on the surface of the sphere. Given that we know $v(\mathbf{r})$, $H(\mathbf{r}, \mathbf{r}_s)$, and $T(\mathbf{r}, \mathbf{r}_s)$, then C is easily found.

After all these changes, equation (2.38) is re-written as

$$
\begin{aligned}
\frac{1}{2}\frac{\varepsilon_o}{\varepsilon_i}\frac{\partial w_o(\mathbf{p})}{\partial \mathbf{n}_o'} &= \oint_S \left(\varepsilon_o \frac{\partial G_i(\mathbf{r},\mathbf{p})}{\partial \mathbf{n}_o'}\frac{\partial w_o(\mathbf{r})}{\partial \mathbf{n}_o} - \varepsilon_i w_o(\mathbf{r})\frac{\partial^2 G_i(\mathbf{r},\mathbf{p})}{\partial \mathbf{n}_o'\partial \mathbf{n}_o} \right) \mathrm{d}S(\mathbf{r}) \\
&\quad + \oint_S \varepsilon_o \frac{\partial G_i(\mathbf{r},\mathbf{p})}{\partial \mathbf{n}_o'}\left(\frac{\partial H(\mathbf{r},\mathbf{r}_s)}{\partial \mathbf{n}_o} + \frac{\partial T(\mathbf{r},\mathbf{r}_s)}{\partial \mathbf{n}_o} \right)\mathrm{d}S(\mathbf{r}) \\
&\quad - \oint_{S\smallsetminus S_a} \varepsilon_i (H(\mathbf{r},\mathbf{r}_s)+T(\mathbf{r},\mathbf{r}_s))\frac{\partial^2 G_i(\mathbf{r},\mathbf{p})}{\partial \mathbf{n}_o'\partial \mathbf{n}_o}\,\mathrm{d}S(\mathbf{r}) \\
&\quad + \oint_\Gamma \varepsilon_i v(\mathbf{r})\frac{\partial^2 G_i(\mathbf{r},\mathbf{p})}{\partial \mathbf{n}_o'\partial \mathbf{n}_\Gamma}\,\mathrm{d}S(\mathbf{r}) - \oint_{S_a} \varepsilon_i \frac{\partial G_i(\mathbf{r},\mathbf{p})}{\partial \mathbf{n}_o'}\frac{\partial v(\mathbf{r})}{\partial \mathbf{n}_o}\,\mathrm{d}S(\mathbf{r}) \\
&\quad - \oint_\Gamma \varepsilon_i \frac{\partial G_i(\mathbf{r},\mathbf{p})}{\partial \mathbf{n}_o}\frac{\partial v(\mathbf{r})}{\partial \mathbf{n}_\Gamma}\,\mathrm{d}S(\mathbf{r}) + \frac{1}{2}\frac{\partial v(\mathbf{p})}{\partial \mathbf{n}_o} \\
&\quad - \frac{1}{2}\frac{\varepsilon_o}{\varepsilon_i}\frac{\partial H(\mathbf{p},\mathbf{r}_s)}{\partial \mathbf{n}_o} - \frac{1}{2}\frac{\varepsilon_o}{\varepsilon_i}\frac{\partial T(\mathbf{p},\mathbf{r}_s)}{\partial \mathbf{n}_o}.
\end{aligned}
\tag{2.54}
$$

2.4.3 Modified second kind integral equations

Now that we have altered significant portions of one of the integral equations, we write the complete set of second kind integral equations here for ease of reference. The first integral equation of the second kind is the sum of (2.29) and (2.34):

$$
\begin{aligned}
w_o(\mathbf{p}) &= \oint_S \varepsilon_o (G_i(\mathbf{r},\mathbf{p}) - G_o(\mathbf{r},\mathbf{p}))\frac{\partial w_i(\mathbf{r})}{\partial \mathbf{n}_o}\,\mathrm{d}S(\mathbf{r}) \\
&\quad + \oint_S \left(\varepsilon_o \frac{\partial G_o(\mathbf{r},\mathbf{p})}{\partial \mathbf{n}_o} - \varepsilon_i \frac{\partial G_i(\mathbf{r},\mathbf{p})}{\partial \mathbf{n}_o} \right) w_o(\mathbf{r})\,\mathrm{d}S(\mathbf{r}) \\
&\quad + \oint_S \left(\varepsilon_o G_i(\mathbf{r},\mathbf{p})\frac{\partial H(\mathbf{r},\mathbf{r}_s)}{\partial \mathbf{n}_o} - \varepsilon_i H(\mathbf{r},\mathbf{r}_s)\frac{G_i(\mathbf{r},\mathbf{p})}{\partial \mathbf{n}_o} \right)\mathrm{d}S(\mathbf{r}) \\
&\quad + \oint_S \left(\varepsilon_o G_i(\mathbf{r},\mathbf{p})\frac{\partial T(\mathbf{r},\mathbf{r}_s)}{\partial \mathbf{n}_o} - \varepsilon_i T(\mathbf{r},\mathbf{r}_s)\frac{G_i(\mathbf{r},\mathbf{p})}{\partial \mathbf{n}_o} \right)\mathrm{d}S(\mathbf{r}) \\
&\quad - \frac{1}{2}H(\mathbf{p},\mathbf{r}_s) - \frac{1}{2}T(\mathbf{p},\mathbf{r}_s).
\end{aligned}
\tag{2.55}
$$

The second equation of the second kind is the sum of (2.36) and (2.54), which yields

$$
\left(\frac{1}{2} + \frac{1}{2}\frac{\varepsilon_o}{\varepsilon_i}\right)\frac{\partial w_o(\mathbf{p})}{\partial \mathbf{n}_o} = \oint_S \left(\varepsilon_o \frac{\partial^2 G_o(\mathbf{r},\mathbf{p})}{\partial \mathbf{n}_o'\partial \mathbf{n}_o} - \varepsilon_i \frac{\partial^2 G_i(\mathbf{r},\mathbf{p})}{\partial \mathbf{n}_o'\partial \mathbf{n}_o}\right) w_o(\mathbf{r})\,\mathrm{d}S(\mathbf{r})
$$

$$
+ \oint_S \varepsilon_o \left(\frac{\partial G_i(\mathbf{r},\mathbf{p})}{\partial \mathbf{n}_o'} - \frac{\partial G_o(\mathbf{r},\mathbf{p})}{\partial \mathbf{n}_o'}\right)\frac{\partial w_o(\mathbf{r})}{\partial \mathbf{n}_o}\,\mathrm{d}S(\mathbf{r})
$$

$$
+ \oint_S \varepsilon_o \frac{\partial G_i(\mathbf{r},\mathbf{p})}{\partial \mathbf{n}_o'}\left(\frac{\partial H(\mathbf{r},\mathbf{r}_s)}{\partial \mathbf{n}_o} + \frac{\partial T(\mathbf{r},\mathbf{r}_s)}{\partial \mathbf{n}_o}\right)\,\mathrm{d}S(\mathbf{r})
$$

$$
- \oint_{S\setminus S_a} \varepsilon_i(H(\mathbf{r},\mathbf{r}_s) + T(\mathbf{r},\mathbf{r}_s))\frac{\partial^2 G_i(\mathbf{r},\mathbf{p})}{\partial \mathbf{n}_o'\partial \mathbf{n}_o}\,\mathrm{d}S(\mathbf{r})
$$

$$
+ \oint_{S_a} \varepsilon_i(v(\mathbf{r}) - H(\mathbf{r},\mathbf{r}_s) - T(\mathbf{r},\mathbf{r}_s))\frac{\partial^2 G_i(\mathbf{r},\mathbf{p})}{\partial \mathbf{n}_o'\partial \mathbf{n}_o}\,\mathrm{d}S(\mathbf{r}) \qquad (2.56)
$$

$$
+ \oint_\Gamma \varepsilon_i v(\mathbf{r})\frac{\partial^2 G_i(\mathbf{r},\mathbf{p})}{\partial \mathbf{n}_o'\partial \mathbf{n}_\Gamma}\,\mathrm{d}S(\mathbf{r})
$$

$$
- \oint_{S_a} \varepsilon_i \frac{\partial G_i(\mathbf{r},\mathbf{p})}{\partial \mathbf{n}_o'}\frac{\partial v(\mathbf{r})}{\partial \mathbf{n}_o}\,\mathrm{d}S(\mathbf{r})
$$

$$
- \oint_\Gamma \varepsilon_i \frac{\partial G_i(\mathbf{r},\mathbf{p})}{\partial \mathbf{n}_o}\frac{\partial v(\mathbf{r})}{\partial \mathbf{n}_\Gamma}\,\mathrm{d}S(\mathbf{r}) + \frac{1}{2}\frac{\partial v(\mathbf{p})}{\partial \mathbf{n}_o}
$$

$$
- \frac{1}{2}\frac{\varepsilon_o}{\varepsilon_i}\frac{\partial H(\mathbf{p},\mathbf{r}_s)}{\partial \mathbf{n}_o} - \frac{1}{2}\frac{\varepsilon_o}{\varepsilon_i}\frac{\partial T(\mathbf{p},\mathbf{r}_s)}{\partial \mathbf{n}_o}.
$$

In the next chapter we discretize these boundary integral equations and state the corresponding matrix equation. We then show how we calculate the right-hand-side integrals of the matrix equation and give a few examples showcasing the improved electric potential results that these integral equations give when compared to integral equations where the change of variables to $w(\mathbf{r})$ was not used [50].

CHAPTER 3: Discretized boundary integral equations and numerical calculations

3.1 Discreted equations and numerical calculations
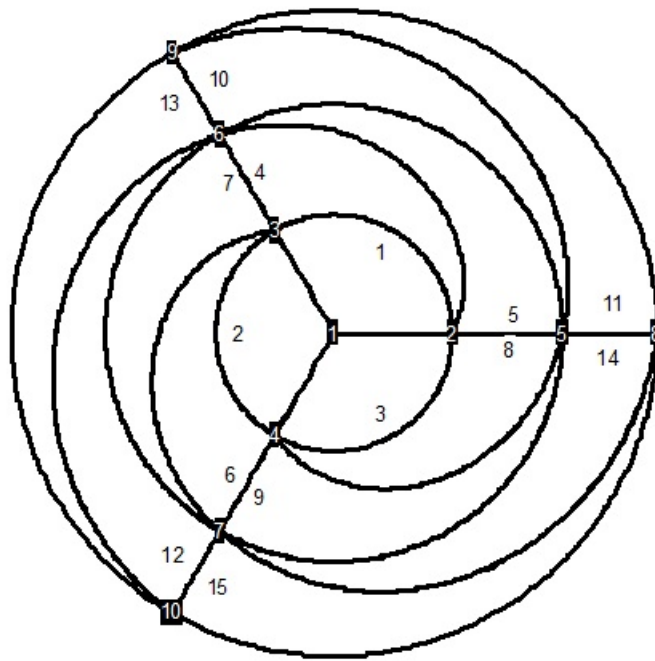
Figure 3.3: Projection of the fitted mesh for one hemisphere of the particle

We now discretize the boundary integral equations, defined on S, by introducing a mesh of curvilinear triangles that conform to the surface of the sphere. The projections of a first degree mesh is shown in Figure 3.3. Details about the construction of first and second degree basis meshes can be found in [29]. A first degree mesh has nodes on the vertices of the triangles only, while a second degree mesh also has nodes on the midpoints of the triangle segments as well as the vertices. Table 3.1 lists the

	1st degree basis		2nd degree basis	
mesh	Nodes	Elements	Nodes	Elements
2	8	12	26	12
4	30	56	114	56
8	122	240	482	0240
16	498	992	1986	992
32	2018	4032	8066	4032

Table 3.1: Mesh sizes and corresponding node and element quantities

mesh size and the corresponding node and element counts contained on a spheroid mesh for a first and second degree basis.

Let $\mathbf{r}_t$ denote the coordinates of the tth mesh point, and let $\psi(\mathbf{r})$ represent basis functions with the kronecker delta property, $\psi_{t_i}(\mathbf{r}_{t_j}) = \delta_{i,j}$. We use Lagrange polynomials as the basis functions. So for first degree basis functions, all mesh points $\mathbf{r}_t$ are vertices of triangles. Second degree basis functions require mesh points to be located at the vertices and on the side edges.

Next, let $w(\mathbf{r}) = w_o(\mathbf{r})$ and $k(\mathbf{r}) = \frac{\partial w_o(\mathbf{r})}{\partial \mathbf{n}_o}$. Then we can interpolate w and k using the Lagrange basis functions as follows:

$$w(\mathbf{r}) \approx \sum_t w_t \psi_t(\mathbf{r}) = \sum_t w(\mathbf{r}_t) \psi_t(\mathbf{r}) \quad \text{and} \quad k(\mathbf{r}) \approx \sum_t k_t \psi_t(\mathbf{r}) = \sum_t k(\mathbf{r}_t) \psi_t(\mathbf{r}). \quad (3.1)$$

3.1.1 Matrix equation

Rewriting the second kind integral equations (2.39) and (2.54) in terms of the unknowns w_t and k_t, we have

$$w(\mathbf{p}) = \sum_t k_t \oint_S \varepsilon_o \left(G_i(\mathbf{r}, \mathbf{p}) - G_o(\mathbf{r}, \mathbf{p}) \right) \psi_t(\mathbf{r}) \, \mathrm{d}S(\mathbf{r})$$

$$+ \sum_t w_t \oint_S \left(\varepsilon_o \frac{\partial G_o(\mathbf{r}, \mathbf{p})}{\partial \mathbf{n}_o} - \varepsilon_i \frac{\partial G_i(\mathbf{r}, \mathbf{p})}{\partial \mathbf{n}_o} \right) \psi_t(\mathbf{r}) \, \mathrm{d}S(\mathbf{r})$$

$$+ \oint_S \left(\varepsilon_o G_i(\mathbf{r}, \mathbf{p}) \frac{\partial H(\mathbf{r}, \mathbf{r}_s)}{\partial \mathbf{n}_o} - \varepsilon_i H(\mathbf{r}, \mathbf{r}_s) \frac{G_i(\mathbf{r}, \mathbf{p})}{\partial \mathbf{n}_o} \right) \mathrm{d}S(\mathbf{r}) \qquad (3.2)$$

$$+ \oint_S \left(\varepsilon_o G_i(\mathbf{r}, \mathbf{p}) \frac{\partial T(\mathbf{r}, \mathbf{r}_s)}{\partial \mathbf{n}_o} - \varepsilon_i T(\mathbf{r}, \mathbf{r}_s) \frac{G_i(\mathbf{r}, \mathbf{p})}{\partial \mathbf{n}_o} \right) \mathrm{d}S(\mathbf{r})$$

$$- \frac{1}{2} H(\mathbf{p}, \mathbf{r}_s) - \frac{1}{2} T(\mathbf{p}, \mathbf{r}_s).$$

$$\left(\frac{1}{2} + \frac{1}{2} \frac{\varepsilon_o}{\varepsilon_i} \right) k(\mathbf{p}) = \sum_t w_t \oint_S \left(\varepsilon_o \frac{\partial^2 G_o(\mathbf{r}, \mathbf{p})}{\partial \mathbf{n}'_o \partial \mathbf{n}_o} - \varepsilon_i \frac{\partial^2 G_i(\mathbf{r}, \mathbf{p})}{\partial \mathbf{n}'_o \partial \mathbf{n}_o} \right) \psi_t(\mathbf{r}) \, \mathrm{d}S(\mathbf{r})$$

$$+ \sum_t k_t \oint_S \varepsilon_o \left(\frac{\partial G_i(\mathbf{r}, \mathbf{p})}{\partial \mathbf{n}'_o} - \frac{\partial G_o(\mathbf{r}, \mathbf{p})}{\partial \mathbf{n}'_o} \right) \psi_t(\mathbf{r}) \, \mathrm{d}S(\mathbf{r})$$

$$+ \oint_S \varepsilon_o \frac{\partial G_i(\mathbf{r}, \mathbf{p})}{\partial \mathbf{n}'_o} \left(\frac{\partial H(\mathbf{r}, \mathbf{r}_s)}{\partial \mathbf{n}_o} + \frac{\partial T(\mathbf{r}, \mathbf{r}_s)}{\partial \mathbf{n}_o} \right) \mathrm{d}S(\mathbf{r})$$

$$- \oint_{S \smallsetminus S_a} \varepsilon_i (H(\mathbf{r}, \mathbf{r}_s) + T(\mathbf{r}, \mathbf{r}_s)) \frac{\partial^2 G_i(\mathbf{r}, \mathbf{p})}{\partial \mathbf{n}'_o \partial \mathbf{n}_o} \, \mathrm{d}S(\mathbf{r})$$

$$+ \oint_{S_a} \varepsilon_i (v(\mathbf{r}) - H(\mathbf{r}, \mathbf{r}_s) - T(\mathbf{r}, \mathbf{r}_s)) \frac{\partial^2 G_i(\mathbf{r}, \mathbf{p})}{\partial \mathbf{n}'_o \partial \mathbf{n}_o} \, \mathrm{d}S(\mathbf{r}) \qquad (3.3)$$

$$+ \oint_\Gamma \varepsilon_i v(\mathbf{r}) \frac{\partial^2 G_i(\mathbf{r}, \mathbf{p})}{\partial \mathbf{n}'_o \partial \mathbf{n}_\Gamma} \, \mathrm{d}S(\mathbf{r}) - \oint_{S_a} \varepsilon_i \frac{\partial G_i(\mathbf{r}, \mathbf{p})}{\partial \mathbf{n}'_o} \frac{\partial v(\mathbf{r})}{\partial \mathbf{n}_o} \, \mathrm{d}S(\mathbf{r})$$

$$- \oint_\Gamma \varepsilon_i \frac{\partial G_i(\mathbf{r}, \mathbf{p})}{\partial \mathbf{n}_o} \frac{\partial v(\mathbf{r})}{\partial \mathbf{n}_\Gamma} \, \mathrm{d}S(\mathbf{r}) + \frac{1}{2} \frac{\partial v(\mathbf{p})}{\partial \mathbf{n}_o}$$

$$- \frac{1}{2} \frac{\varepsilon_o}{\varepsilon_i} \frac{\partial H(\mathbf{p}, \mathbf{r}_s)}{\partial \mathbf{n}_o} - \frac{1}{2} \frac{\varepsilon_o}{\varepsilon_i} \frac{\partial T(\mathbf{p}, \mathbf{r}_s)}{\partial \mathbf{n}_o}$$

For the sake of elegance, let the following quantities be defined.

$$S0 = \oint_S G_i(\mathbf{r},\mathbf{p})\psi_t(\mathbf{r})\,\mathrm{d}S(\mathbf{r}) \qquad S1 = \oint_S G_o(\mathbf{r},\mathbf{p})\psi(\mathbf{r})\,\mathrm{d}S(\mathbf{r})$$

$$D0 = \oint_S \frac{\partial G_i(\mathbf{r},\mathbf{p})}{\partial \mathbf{n}_o}\psi_t(\mathbf{r})\,\mathrm{d}S(\mathbf{r}) \qquad D1 = \oint_S \frac{\partial G_o(\mathbf{r},\mathbf{p})}{\partial \mathbf{n}_o}\psi_t(\mathbf{r})\,\mathrm{d}S(\mathbf{r})$$

$$D2 = \oint_S \frac{\partial G_i(\mathbf{r},\mathbf{p})}{\partial \mathbf{n}_o'}\psi_t(\mathbf{r})\,\mathrm{d}S(\mathbf{r}) \qquad D3 = \oint_S \frac{\partial G_o(\mathbf{r},\mathbf{p})}{\partial \mathbf{n}_o'}\psi_t(\mathbf{r})\,\mathrm{d}S(\mathbf{r})$$

$$T0 = \oint_S \frac{\partial^2 G_i(\mathbf{r},\mathbf{p})}{\partial \mathbf{n}_o'\partial \mathbf{n}_o}\psi_t(\mathbf{r})\,\mathrm{d}S(\mathbf{r}) \qquad T1 = \oint_S \frac{\partial^2 G_o(\mathbf{r},\mathbf{p})}{\partial \mathbf{n}_o'\partial \mathbf{n}_o}\psi_t(\mathbf{r})\,\mathrm{d}S(\mathbf{r})$$

$$J5 = -\oint_\Gamma \varepsilon_i\left(\frac{\partial G_i(\mathbf{r},\mathbf{p})}{\partial \mathbf{n}_o'}\frac{\partial v(\mathbf{r})}{\partial \mathbf{n}_\Gamma}\right)\mathrm{d}S(\mathbf{r}) \qquad J6 = -\oint_{S_a} \varepsilon_i\left(\frac{\partial G_i(\mathbf{r},\mathbf{p})}{\partial \mathbf{n}_o'}\frac{\partial v(\mathbf{r})}{\partial \mathbf{n}_o}\right)\mathrm{d}S(\mathbf{r})$$

$$J7 = \oint_\Gamma \varepsilon_i\left(v(\mathbf{r})\frac{\partial^2 G_i(\mathbf{r},\mathbf{p})}{\partial \mathbf{n}_o'\partial \mathbf{n}_\Gamma}\right)\mathrm{d}S(\mathbf{r}) \qquad L0 = \frac{1}{2}\frac{\partial v_o(\mathbf{p})}{\partial \mathbf{n}_o}$$

$$L1 = -\frac{1}{2}H(\mathbf{p},\mathbf{r}_s) \qquad L2 = -\frac{1}{2}T(\mathbf{p},\mathbf{r}_s)$$

$$L3 = -\frac{1}{2}\frac{\varepsilon_o}{\varepsilon_i}\frac{\partial H(\mathbf{p},\mathbf{r}_k)}{\partial \mathbf{n}_o} \qquad L4 = -\frac{1}{2}\frac{\varepsilon_o}{\varepsilon_i}\frac{\partial T(\mathbf{p},\mathbf{r}_k)}{\partial \mathbf{n}_o}$$

$$J0 = \oint_S \left(\varepsilon_o G_i(\mathbf{r},\mathbf{p})\frac{\partial H(\mathbf{r},\mathbf{r}_s)}{\partial \mathbf{n}_o} - \varepsilon_i H(\mathbf{r},\mathbf{r}_s)\frac{\partial G_i(\mathbf{r},\mathbf{p})}{\partial \mathbf{n}_o}\right)\mathrm{d}S(\mathbf{r})$$

$$J1 = \oint_S \left(\varepsilon_o G_i(\mathbf{r},\mathbf{p})\frac{\partial T(\mathbf{r},\mathbf{r}_s)}{\partial \mathbf{n}_o} - \varepsilon_i T(\mathbf{r},\mathbf{r}_s)\frac{\partial G_i(\mathbf{r},\mathbf{p})}{\partial \mathbf{n}_o}\right)\mathrm{d}S(\mathbf{r})$$

$$J2 = \oint_{S_a} \varepsilon_i(v(\mathbf{r}) - H(\mathbf{r},\mathbf{r}_s) - T(\mathbf{r},\mathbf{r}_s))\frac{\partial^2 G_i(\mathbf{r},\mathbf{p})}{\partial \mathbf{n}_o'\partial \mathbf{n}_o}\mathrm{d}S(\mathbf{r})$$

$$J3 = \oint_S \varepsilon_o\frac{\partial G_i(\mathbf{r},\mathbf{p})}{\partial \mathbf{n}_o'}\left(\frac{\partial H(\mathbf{r},\mathbf{r}_s)}{\partial \mathbf{n}_o} + \frac{\partial T(\mathbf{r},\mathbf{r}_s)}{\partial \mathbf{n}_o}\right)\mathrm{d}S(\mathbf{r}))$$

$$J4 = -\oint_{S\setminus S_a} \varepsilon_i(H(\mathbf{r},\mathbf{r}_s) + T(\mathbf{r},\mathbf{r}_s))\frac{\partial^2 G_i(\mathbf{r},\mathbf{p})}{\partial \mathbf{n}_o'\partial \mathbf{n}_o}\mathrm{d}S(\mathbf{r})$$

Then we can rewrite (2.39) and (2.54) as the following matrix equation:

$$\left[\begin{pmatrix} I & 0 \\ 0 & \left(\frac{1}{2}+\frac{1}{2}\frac{\varepsilon_o}{\varepsilon_i}\right)I \end{pmatrix} + \begin{pmatrix} (\varepsilon_i D0 - \varepsilon_o D1) & -(S0-S1)\varepsilon_o \\ (\varepsilon_i T0 - \varepsilon_o T1) & -(D2-D3)\varepsilon_o \end{pmatrix}\right]\begin{pmatrix} w_o \\ k_o \end{pmatrix} = \begin{pmatrix} J0+J1+L1+L2 \\ J2+J3+J4+J5+J6+J7+L0+L3+L4 \end{pmatrix} \tag{3.4}$$

where $\mathbf{p}$ takes different mesh points $\mathbf{r}_t$ in different rows of the matrix.
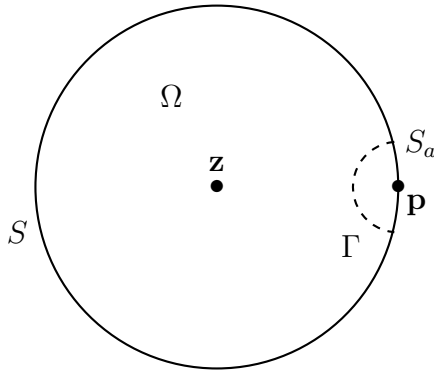
Figure 3.4: The sphere surface S and hemispherical mathematical boundary Γ around singularity location $\mathbf{p}$

In looking at the matrix equation above, the overall goal of introducing the subtraction $w_o = \phi_o - H - T$ becomes clearer: the matrix equation solves for smoother variable w_o and its normal derivative, while the right-hand side vector $\mathbf{b}$ contains integrals that house the bulk of the singular behavior of the the electric potential of the close charge-sphere system. So to find accurate values for the potential and its derivative, emphasis shifts to accurately calculating the auxiliary integrals. Since the integral equations are of the second kind and therefore the coefficient matrix in (3.4) has a low condition number [50], the matrix equation can be solved with a small number of iterations of the GMRES solver. Also, since the auxiliary integrals play such an important role in the accuracy of the solutions, we will focus the rest of this chapter, and all of the next, on describing how the integrals are calculated and ways that they can be done so more efficiently.

3.1.2 Calculation of right-hand-side integrals in matrix equation

Here we describe in more detail what happens when we introduce the interior hemisphere Γ "bubble" at each mesh point location $\mathbf{p}$ where the matrix equation (3.4) is satisfied. The figure is repeated here for convenience in Figure 3.4.

It must be emphasized that in defining the special solution $v(\mathbf{r})$ and introducing

a hemisphere at $\mathbf{p}$, we are actually introducing a mathematical boundary Γ around each mesh point as a result. This means that for every mesh point $\mathbf{p}$, we introduce this hemisphere, or "bubble", and then calculate the corresponding integrals in the matrix equation (3.4).

Attention should also be drawn to the bounds on the integrals $J0 - J7$ that exist in the right-hand side vector $\mathbf{b} = A\mathbf{x}$ portion of the matrix equation (3.4). Each of these integrals have different portions of the structure's surface as its region of integration. For example, while integral $J0$ is evaluated over the entire surface of the sphere S, the integral $J2$ is evaluated over the region S_a, which is the portion of the surface defined by the intersection of the hemisphere Γ with the sphere S. This region S_a is then dependent on the location of the hemisphere Γ, which itself is dependent on the location of the mesh points $\mathbf{p}$. Since the mathematical barrier Γ is used over each mesh points $\mathbf{p}$, we must develop an adaptable way of calculating the RHS integrals over their various domains, as we cycle through all the mesh points.

3.1.3 Normal Gauss-Legendre quadrature

In this paper, we use traditional Gauss-Legendre quadrature to calculate the right-hand side integrals in the matrix equation. Let x_i denote the Gauss points on the standard interval $[-1, 1]$ and let ξ_i denote the weights. Since the integrals are evaluated over regions conducive to spherical coordinates, let ϕ denote the azimuthal angle and θ the polar angle. Then each integral is defined over region $[\theta_{\min}, \theta_{\max}] \times [\phi_{\min}, \phi_{\max}]$, where the radius is constant since evaluation is on the surface. We then employ a standard mapping to scale the integration intervals

$$[\theta_{\min}, \theta_{\max}] \times [\phi_{\min}, \phi_{\max}] \quad \longrightarrow \quad [-1, 1] \times [-1, 1]. \tag{3.5}$$

by means of the following: for $\phi_{\min} \leq \phi \leq \phi_{\max}$,

$$\phi_i \rightarrow (\phi_{max} - \phi_{min})\left(\frac{x_i + 1}{2}\right) + \phi_{min}$$

$$w_i \rightarrow \left(\frac{\phi_{max} - \phi_{min}}{2}\right)\xi_i$$

and for $\theta_{min} \leq \theta \leq \theta_{max}$,

$$\theta_i \rightarrow (\theta_{max} - \theta_{min})\left(\frac{x_i + 1}{2}\right) + \theta_{min}$$

$$\hat{w}_i \rightarrow \left(\frac{\theta_{max} - \theta_{min}}{2}\right)\xi_i.$$

With these mappings, each ordered pair (ϕ_i, θ_j) corresponds to one individual Gauss point. Next, in order to calculate any integral in Cartesian coordinates, we additionally have to perform the change of coordinates for each Gauss point (ϕ_i, θ_j):

$$x_i = r\sin(\theta_j)\cos(\phi_i)$$

$$y_i = r\sin(\theta_j)\sin(\phi_i)$$

$$z_i = r\cos(\theta_j).$$

So then, for any integral with integrand $f(x, y, z)$ and $x = x(r, \phi, \theta)$, $y = y(r, \phi, \theta)$, $z = z(r, \phi, \theta)$, we calculate

$$\int_{\theta_{min}}^{\theta_{max}} \int_{\phi_{min}}^{\phi_{max}} f(r, \phi, \theta)|J(r, \phi, \theta)|\,\mathrm{d}\phi\,\mathrm{d}\theta \approx \sum_{i=1}^{M}\sum_{j=1}^{N} w_i\hat{w}_j f(r, \phi_i, \theta_j)|J(r, \phi_i, \theta_j)|. \quad (3.6)$$

3.1.4 Reference sphere and point rotation

When wishing to evaluate any one of the matrix integrals that are not evaluated over the entire surface S, there are a couple of circumstances that arise. Firstly, an integral on the region S_a, for example, requires that we integrate over a circular region on the
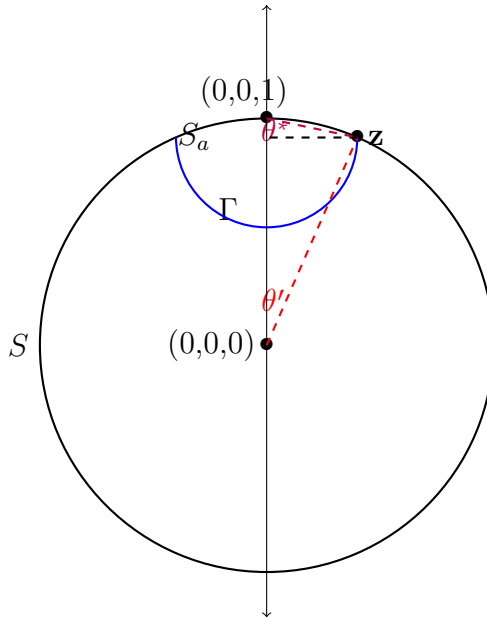
Figure 3.5: Finding necessary angles when integrating over surface of sphere

spheroid. As the boundary of the patch S_a is a constant θ line only if it is centered at the north pole, the bounds of integration are then difficult to find in terms of the polar and azimuthal angles of the sphere. Secondly, even if we could easily find the bounds of integration that determines region S_a, there is a possibility that one of the Gauss points (ϕ_i, θ_j) accidentally has the same location as point $\mathbf{p}$. This would introduce a non-treatable singularity in the integrand, making calculation impossible.

We address these two issues by introducing the concept of a reference sphere, as shown in Figure 3.5. The north pole of the reference sphere is rotated to the location of the mesh point $\mathbf{p}$, where we have a hemisphere of radius a centered at $\mathbf{p}$. There are two angles that will be important on the reference sphere, labeled $\theta^\star$ and θ'. Details on the calculation of $\theta^\star$ and θ' are in Appendix A.

Depending on the regions over which the auxiliary integrals $J0 - J7$ are evaluated, we find the bounds of integration by assuming that the mesh point $\mathbf{p}$ is located at the north pole of the reference sphere. By using the reference sphere, the bounds of integration become constant, easily calculable values. For example, if it was desired

to evaluate an integral over S_a on the reference sphere in Figure 3.5, then the Gauss points need to be distributed over $[0, \theta'] \times [0, 2\pi]$. If instead we wish to evaluate an integral over Γ, then the Gauss points are distributed over $[\theta^*, \pi] \times [0, 2\pi]$ on the reference sphere. Since the bounds of integration on the physical (non-reference) sphere depend on the mesh point $\mathbf{p}$ being the focal point, then we rotate the Gauss points that were already distributed over the reference sphere to the appropriate physical locations. That is, we make the reference sphere north pole position $\mathbf{p}'$ rotate to the orientation of the actual mesh point $\mathbf{p}$, taking the distributed Gauss points along with it. This reference sphere process makes it easier to integrate over the circular patches S_a or the hemisphere Γ.

So then our next concern is the rotation required to map reference point $\mathbf{p}'$, located at the the north pole of the reference sphere, to the mesh point location $\mathbf{p}$. When rotating a point around the surface of the sphere, we only need two transformations: one of angle γ about the x-axis, and another of angle α about the z-axis. This means that we employ two transformation matrices that together will map every previously placed Gauss point. For arbitrary point (x, y, z) and transformed point (x_t, y_t, z_t), the rotation matrices are

$$R_x(\gamma) = \begin{bmatrix} 1 & 0 & 0 \\ 0 & \cos(\gamma) & -\sin(\gamma) \\ 0 & \sin(\gamma) & \cos(\gamma) \end{bmatrix} \quad \text{and} \quad R_z(\alpha) = \begin{bmatrix} \cos(\alpha) & -\sin(\alpha) & 0 \\ \sin(\alpha) & \cos(\alpha) & 0 \\ 0 & 0 & 1 \end{bmatrix}. \quad (3.7)$$

and then we have

$$(x_t, y_t, z_t) = R_z(-\alpha) \times R_x(-\gamma) \times (x, y, z)^T, \quad (3.8)$$

where the operator is standard matrix multiplication and γ and α are readily calculated using trigonometry. Then we have that for arbitrary Gauss point (x_i, y_i, z_i),

which is already under a spherical-to-Cartesian coordinate transformation,

$$x_t = x_i \cos(-\alpha) - y_i \cos(-\gamma) \sin(-\alpha) + z_i \sin(-\alpha) \sin(-\gamma)$$

$$y_t = x_i \sin(-\alpha) + y_i \cos(-\alpha) \cos(-\gamma) - z_i \cos(-\alpha) \sin(-\gamma)$$

$$z_t = y_i \sin(-\gamma) + z_i \cos(-\gamma).$$

Then our boundary integrals, calculated around arbitrary mesh location point $\mathbf{p}$, are now evaluated as follows:

$$\oint f(x, y, z) \, dx \, dy \, dz \approx \sum_{i=1}^{M} \sum_{j=1}^{N} w_i \hat{w}_j f(x_t, y_t, z_t), \tag{3.9}$$

where the bounds of integration for the rotated integrals are the same as in the integrals of the un-rotated reference sphere. Figure 3.6 below shows Gauss points that have been distributed around a complete sphere and then rotated.
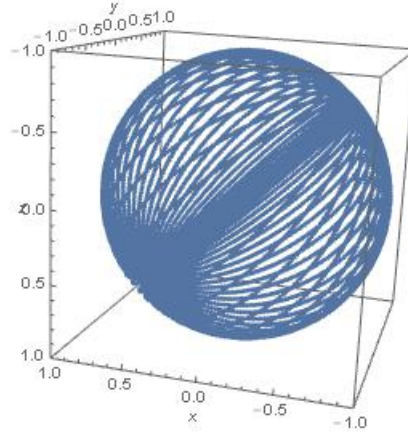
Figure 3.6: Gauss point locations that have been rotated to emanate from point $\mathbf{p}$

3.2 Numerical results for potentials of single dielectric sphere

In this section, we will display numerical results of the subtraction method implemented in the boundary integral equations. Here we will compare the "true solution"

of the total electrostatic potential and its derivative with those that were computed by the the methods presented so far in this paper. Additionally, we will be comparing the values of the reaction field potential, as it is a much smaller quantity and therefore harder to calculate accurately. Since currently our system consists of a dielectric sphere in a homogeneous medium, the true solution is taken to be the Legendre polynomial expansion in [14], taken to a sufficient number of terms for it to converge. So the true solution of the electric potential is

$$\phi(r, \theta) = 4\pi \sum_{n=0}^{\infty} C(r) P_n(\cos(\theta)), \tag{3.10}$$

where $C(r)$ is given by

$$C(r) = \frac{q}{4\pi\varepsilon_o r_s} \left(\frac{r}{r_s}\right)^n - D_n \frac{1}{r^{n+1}}, \tag{3.11}$$

and D_n is the constant given by

$$D_n = \frac{q}{4\pi\varepsilon_o} \frac{a^{2n+1}}{r_s^{n+1}} \gamma \left(1 - \frac{1-\gamma}{1-\gamma+2n}\right), \tag{3.12}$$

where for this definition only, a is the radius of the dielectric sphere. We make note here that the accuracy of the results of the matrix equation (3.4) is influenced by a number of factors. For instance, we have a choice of how big we let the hemisphere Γ be, how many terms M we use in the reaction field approximation in equation (2.9), how many terms n of the reaction field estimation that we wish to include in the function $T(\mathbf{r}, \mathbf{r}_s)$ and how big or small we choose the mesh sizes to be. Henceforth when showing an example, we will also list what parameters we chose for that particular case.

Now let us discuss a couple more specifics as we go forward to the numerical examples. First, recall that the total potential can be decomposed into the potential

from the source charge and the potential from the reaction field

$$\phi(\mathbf{r}) = H(\mathbf{r}, \mathbf{r}_s) + \phi_{\mathrm{rf}}(\mathbf{r}). \tag{3.13}$$

We will be comparing results for both the total potential and the reaction field, both of which we take the true solution to be the Legendre polynomial expansion. Recall that in the numerical calculations, the reaction field is estimated by image charges. Secondly, we should note that we are solving for $w_o(\mathbf{r})$ and $\frac{\partial w_o(\mathbf{r})}{\partial \mathbf{n}}$ in the matrix equation. So in order to compare the true solution of the total potential $\phi(\mathbf{r})$ and its derivative, we use equation (2.17) to isolate ϕ and $\frac{\partial \phi}{\partial \mathbf{n}}$:

$$w_o = \phi_o - H - T \quad \Rightarrow \quad \phi_o = w_o + H + T, \tag{3.14}$$

$$\frac{\partial w_o}{\partial \mathbf{n}} = \frac{\partial \phi_o}{\partial \mathbf{n}} - \frac{\partial H}{\partial \mathbf{n}} - \frac{\partial T}{\partial \mathbf{n}} \quad \Rightarrow \quad \frac{\partial \phi_o}{\partial \mathbf{n}} = \frac{\partial w_o}{\partial \mathbf{n}} + \frac{\partial H}{\partial \mathbf{n}} + \frac{\partial T}{\partial \mathbf{n}}. \tag{3.15}$$

3.2.1   Example 1

This is a familiar case considered in previous works [50]. For a source location $\mathbf{r}_s = (0.5, 2, 0.2)$, $\varepsilon_i = 2$, $\varepsilon_o = 1$, $\lambda_o = \lambda_i = 0$, the errors in the total potential, reaction field potential, and normal derivative of potential are shown in Tables 3.2-3.4. Each table displays errors from using first or second degree basis functions, as well as the errors found by using the different subtraction options.

In this example, we let the reaction field potential be estimated by $M = 16$ image charge locations, with the first $n = 3$ of those terms being included in the function $T(\mathbf{r}, \mathbf{r}_s)$. Further, we took hemisphere Γ to have radius $a = 0.1$ units, and the true solution was calculated by a Legendre polynomial expansion out to 300 terms. In this example, the source $\mathbf{r}_s$ is 1.07 units away from the surface of the sphere.

To showcase the effectiveness of the subtraction method, we have included what the errors are with and without its use. Recall that the matrix equation (3.4) solves

for the variable $w_o = \phi_o - H - T$, where the presence of the functions H and T indicates use of the "subtraction technique." The column in Tables 3.2-3.4 labeled "no subtr." represents the relative errors per mesh size generated if the potential was calculated directly in the matrix equation; that is, if both $H = T = 0$. The columns labeled "H subtr." and "H & T subtr." represent the cases where $T = 0$ and $H \neq T \neq 0$, respectively.

Additionally, the mesh sizes chosen correspond to those used in prior papers [50] and [30]. For example, mesh size "2" corresponds to 8 total mesh points, mesh size "4" corresponds to 30 mesh points, etc. We chose these specific mesh sizes out of convenience of comparing new data/errors to old.

In analyzing tables 3.2-3.4, we see that using second degree basis functions yields the better results overall. This has already been established and shown in previous works [50][30]. Additionally and more importantly, we see that in using either H or both H and T subtractions in the boundary integral equations, relative error is certainly improved over what errors we see without the subtraction at all. This shows that introducing the variable $w_o = \phi_o - H - T$ in the boundary integral equations, and solving for it in the matrix equation (3.4), is effective in reducing the error in the potential ϕ and its normal derivative $\frac{d\phi}{d\mathbf{n}}$. This example is considered a "nice case" for the source charge location, because the source far enough away from the sphere that sufficiently accurate results can be obtained without using the subtraction technique at all, although the subtraction method certainly improved in those already good results.

Let us now focus on comparing the reaction field potentials for this particular case. In general, the reaction field $\phi_{rf} = \phi - H$ is a much smaller quantity (in absolute value) compared to the potential from the source charge H, so getting accurate results for it out of the matrix equation is harder to accomplish. We see in Table 3.3 that the results using the subtraction method proposed in this paper are improved compared

Table 3.2: Relative errors of total potential in Example 1 for mesh sizes 2-32, using first and second degree basis functions, when first using no subtraction de-singularization and then full subtraction de-singularization

| | Relative Errors of Total Potential | | | | | |
| | 1$^{\text{st}}$ degree basis | | | 2$^{\text{nd}}$ degree basis | | |
mesh	no subtr	H subtr	H & T subtr	no subtr	H subtr	H & T subtr
2	1.47×10^{-1}	4.52×10^{-2}	6.47×10^{-3}	1.25×10^{-1}	3.69×10^{-2}	3.96×10^{-3}
4	5.22×10^{-2}	1.51×10^{-2}	1.94×10^{-3}	2.16×10^{-2}	6.17×10^{-3}	4.66×10^{-4}
8	1.39×10^{-2}	4.17×10^{-3}	5.94×10^{-4}	3.35×10^{-3}	8.98×10^{-4}	3.24×10^{-5}
16	5.69×10^{-3}	1.67×10^{-3}	1.94×10^{-4}	2.31×10^{-4}	6.34×10^{-5}	4.78×10^{-6}
32	1.92×10^{-3}	5.56×10^{-4}	5.51×10^{-4}	2.20×10^{-5}	5.90×10^{-6}	2.37×10^{-6}

Table 3.3: Relative errors of reaction field potential in Example 1 for mesh sizes 2-32, using first and second degree basis functions, when first using no subtraction de-singularization and then full subtraction de-singularization

| | Relative Errors of Reaction Field | | | | | |
| | 1$^{\text{st}}$ degree basis | | | 2$^{\text{nd}}$ degree basis | | |
mesh	no subtr	H subtr	H & T subtr	no subtr	H subtr	H & T subtr
2	34.3892	10.5425	1.5096	39.5287	11.5307	1.0329
4	50.716	13.2191	7.32×10^{-1}	28.499	8.0666	5.45×10^{-1}
8	8.3196	2.6429	5.93×10^{-1}	6.37×10^{-1}	1.60×10^{-1}	6.69×10^{-3}
16	1.6258	5.49×10^{-1}	1.58×10^{-1}	6.91×10^{-2}	2.08×10^{-2}	7.47×10^{-3}
32	1.7072	4.98×10^{-1}	1.11×10^{-1}	1.44×10^{-2}	4.54×10^{-3}	5.86×10^{-3}

to results without it, where the potential was solved for directly. The errors for $\frac{\partial \phi}{\partial \mathbf{n}}$ were determined using 150 terms in the Legendre polynomial expansion.

3.2.2 Example 2

In the interest of pushing the capabilities of the subtraction technique and subsequent new boundary integral equations, in this example the source charge is chosen to be 0.01 units away from the surface of the sphere, which is historically a difficult distance in which to accurately calculate the potential and its derivative. In tables 3.5-3.7, we showcase the relative errors in the total potential, reaction field potential, and the normal derivative of potential. As in last example, there are columns that differentiate the use of the different basis functions, as well as the various choices of how the matrix

Table 3.4: Relative errors of normal derivative of potential in Example 1 for mesh sizes 2-32, using first and second degree basis functions, when first using no subtraction de-singularization and then full subtraction de-singularization

| | Relative Errors of Derivative | | | | | |
| | 1st degree basis | | | 2nd degree basis | | |
mesh	no subtr	H subtr	H & T subtr	no subtr	H subtr	H & T subtr
2	34.3892	1.91×10^{-1}	2.74×10^{-2}	39.5287	1.07×10^{-1}	9.67×10^{-3}
4	50.716	1.0092	6.11×10^{-2}	28.499	6.37×10^{-1}	4.03×10^{-2}
8	8.3196	2.15×10^{-1}	4.45×10^{-2}	6.37×10^{-1}	1.22×10^{-1}	1.52×10^{-2}
16	1.6258	2.85×10^{-1}	5.74×10^{-2}	6.91×10^{-2}	7.79×10^{-3}	1.18×10^{-3}
32	1.7072	8.33×10^{-2}	1.49×10^{-2}	1.44×10^{-2}	9.15×10^{-4}	8.25×10^{-4}

equation (3.4) solves for $w_o = \phi_o - H - T$. The potentials calculated in the matrix equation are compared to the true solutions, not shown here, that are all taken to be the Legendre polynomial expansion out to 1500 terms.

In this example, all parameters are the same as in the last example, but with the source very close to the sphere at

$$\mathbf{r}_s = (0.2438162975, 0.9752651902, 0.097526519).$$

For the right-hand side integrals in (3.4) that are evaluated over the entire surface S, we allocate over 3 million Gauss points per integral in order to calculate them to sufficient accuracy. For those right-hand side integrals with smaller integration regions than S, a very high density of Gauss points were chosen for those regions as well. In this instance, a dense spread of Gauss points is needed for accurate calculation as the source charge gets closer to the surface of the sphere.

In Table 3.5, we can see the use of both H and T in $w_o = \phi_o - H - T$ in the BIE's paying off, as we have a significantly lower relative error in the total potential than with having solved for just $w_o = \phi_o$. For example, we have 0.00003 relative error for mesh size 32, second degree basis functions, where the subtraction of H and T were used. This is significantly lower than the 0.36 relative error obtained by solving the BIE's without H and T.

Table 3.5: Relative errors of total potential in Example 2 for mesh sizes 2-32, using first and second degree basis functions, when first using no subtraction de-singularization and then full subtraction de-singularization

	Relative Errors of Total Potential					
	1$^{\text{st}}$ degree basis			2$^{\text{nd}}$ degree basis		
mesh	no subtr	H subtr	H & T subtr	no subtr	H subtr	H & T subtr
2	2.52×10^{-1}	1.15×10^{-1}	2.41×10^{-2}	5.31×10^{-1}	1.17×10^{-1}	2.13×10^{-2}
4	4.82×10^{-1}	1.17×10^{-1}	9.11×20^{-3}	4.41×10^{-1}	1.19×10^{-1}	4.02×10^{-3}
8	4.48×10^{-1}	1.18×10^{-1}	3.05×10^{-3}	4.40×10^{-1}	1.14×10^{-1}	1.21×10^{-3}
16	4.41×10^{-1}	1.15×10^{-1}	9.43×10^{-4}	3.46×10^{-1}	8.70×10^{-2}	3.01×10^{-4}
32	3.65×10^{-1}	9.25×10^{-2}	1.95×10^{-4}	3.66×10^{-1}	9.26×10^{-2}	3.22×10^{-5}

Table 3.6: Relative errors of reaction field potential in Example 2 for mesh sizes 2-32, using first and second degree basis functions, when first using no subtraction de-singularization and then full subtraction de-singularization

	Relative Errors of Reaction Field					
	1$^{\text{st}}$ degree basis			2$^{\text{nd}}$ degree basis		
mesh	no subtr	H subtr	H & T subtr	no subtr	H subtr	H & T subtr
2	5.1824	1.6975	0.3528	43.6461	10.2175	9.87×10^{-1}
4	40.4081	10.1842	1.75×10^{-1}	80.106	21.7792	6.43×10^{-1}
8	80.7679	21.6078	4.48×10^{-1}	300.33	76.6964	$3.24 \times 1^{-{-1}}$
16	302.034	77.8786	2.03×10^{-1}	565.648	141.099	2.23×10^{-1}
32	626.125	158.083	1.23×10^{-1}	1407.16	355.185	5.39×10^{-2}

Also, in Table 3.6, where we are comparing errors in the reaction field, we see that the error only converges as we take finer meshes for the second degree basis functions, with both H and T being used. Again this is because the reaction field is a much smaller quantity than the total potential. So the accuracy gathered for the total potential will always be better than the accuracy gathered for the reaction field, but it is important to demonstrate that the subtraction method is noticeably more effective for calculating this small quantity as well.

Table 3.7: Relative errors of derivative of potential in Example 2 for mesh sizes 2-32, using first and second degree basis functions, when first using no subtraction de-singularization and then full subtraction de-singularization

| | Relative Errors of Derivative | | | | | |
| | 1$^{\text{st}}$ degree basis | | | 2$^{\text{nd}}$ degree basis | | |
mesh	no subtr	H subtr	H & T subtr	no subtr	H subtr	H & T subtr
2	3.23×10^{-1}	1.16×10^{-1}	2.43×10^{-2}	2.49×10^{-1}	1.83×10^{-1}	2.15×10^{-2}
4	2.69×10^{-1}	1.83×10^{-1}	9.17×10^{-3}	2.82×10^{-1}	1.87×10^{-1}	4.84×10^{-3}
8	2.77×10^{-1}	1.86×10^{-1}	3.74×10^{-3}	1.4795	7.01×10^{-1}	1.33×10^{-3}
16	1.4807	7.08×10^{-1}	4.42×10^{-3}	2.4667	9.82×10^{-1}	2.17×10^{-3}
32	2.6608	1.0955	1.94×10^{-3}	10.5346	5.5738	2.70×10^{-3}

CHAPTER 4: Adaptive quadratures for singular right-hand side integrals

In subtracting the $H(\mathbf{r}, \mathbf{r}_s)$ and $T(\mathbf{r}, \mathbf{r}_s)$ functions from the electric potential and re-deriving the boundary integral equations in terms of $w = \phi - H - T$, we shift the most difficult-to-calculate parts of the potential to the right-hand side auxiliary integrals in the BIE's and resulting matrix equation (3.4). Therefore, to get accurate results for the potential, we must be able to calculate those right-hand side integrals extremely accurately. In the case of the examples of the last section, this meant using millions Gauss points on some integrals in order to achieve sufficient accuracy to result in those small relative errors. While this does indeed yield the desired effect, it is computationally expensive and rather wasteful, as such densities of Gauss points on the integrals are only necessary in specific locations. So in this section, we endeavor to reduce the amount of Gauss points required to calculate the auxiliary integrals accurately, while maintaining the accuracy in the potentials seen in the examples in the last section. This will make the subtraction de-singularization technique in the boundary integral equations more efficient.

To begin this process, we observe that singular behavior in the auxiliary integrals $J0 - J7$ is displayed in two regions: around each mesh point location $\mathbf{p}$ and around the projection $\mathbf{r}'_s$ of the source charge $\mathbf{r}_s$ on the sphere . For instance, Figures 4.7, 4.8 shows the graph of the integrand $J0$ where the two "spikes" around those two regions show singular behavior. In order to capture all of that singularity and calculate those integrals accurately, more Gauss points must be placed around those locations. Since the integrand is smooth everywhere else, such a Gauss point density is unnecessary

and, indeed, wasteful. Therefore, we introduce an adaptive integration quadrature, where we partition the integration domain into subdomains, only putting a dense coverage of points where required.
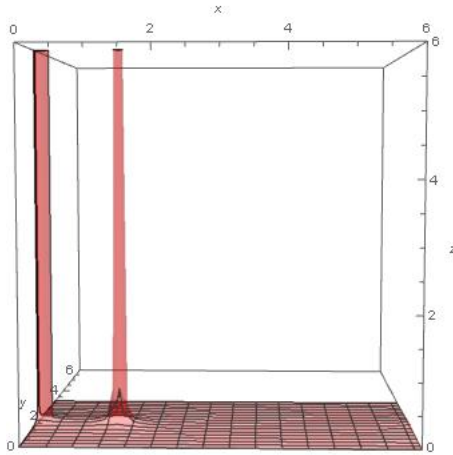
Figure 4.7: Graph of the integrand J0 for mesh point $\mathbf{p} = (1, 0, 0)$ and source $\mathbf{r}_s = (0.2438, 0.9752, 0.0975)$, which is 0.01 units away from the surface of the sphere
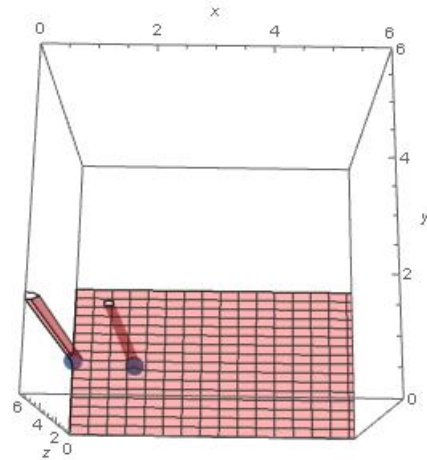
Figure 4.8: Top view of the same graph, with balls indicating where $\mathbf{p}$ and $\mathbf{r}_s$ are

4.1 Subdomain grid

Initially, each of our RHS integrals are calculated as written above in (3.9), written again here for convenience:

$$\oint f(x, y, z) \, dx \, dy \, dz \approx \sum_{i=1}^{M} \sum_{j=1}^{N} w_i \hat{w}_j f(x_t, y_t, z_t). \tag{4.1}$$

For each integral, the Gauss points and weights were calculated to be spread over a set of bounds that would cover the entirety of whatever boundary region the integrals dictated. So for example for integral J0, which is defined over the entire spherical surface area S, the Gauss points would be distributed over the region $[0, \pi] \times [0, 2\pi]$.
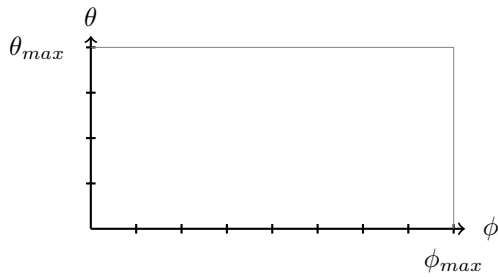
Figure 4.9: Normal integration region
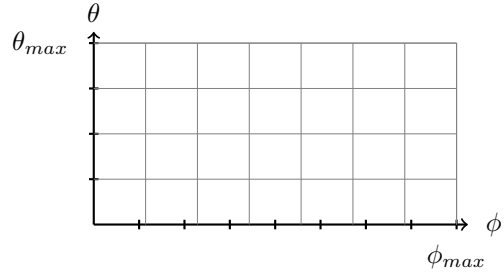
Figure 4.10: Integration region divided into a grid

However, to better allocate Gauss points where needed, we start by taking a standard region that an integral will be calculated over, $\theta_{min} \leq \theta \leq \theta_{max}$ and $\phi_{min} \leq \phi \leq \phi_{max}$, and subdivide this region into blocks of arbitrary size. We note here that ϕ is temporarily used to represent the azimuthal angle in spherical coordinates, not the electrostatic potential $\phi(\mathbf{r})$. So if we wish to have p divisions for $\theta \in [\theta_{min}, \theta_{max}]$, then we divide this direction into p sections of length $(\theta_{max} - \theta_{min})/p$. Similarly, the ϕ axis will be divided into sections of length $(\phi_{max} - \phi_{min})/q$. This creates a grid pattern seen in figure 4.10. For each subdivision or "box", we will use the scaled tensor product Gauss-Legendre quadrature formula.

Now for an arbitrary m, n-box, we can distribute a higher number of Gauss points in that specific box, leaving other boxes with a much lower density. Calculating the integrals using this grid-spaced distribution of Gauss points rather than a high density over the entire domain means that calculation time is reduced. Now that we know how we want to distribute Gauss points, the next step is to find a way to determine specifically what regions over the bounds of an integral that a higher distribution of Gauss points is needed.

4.1.1 Point allocation

We have previously shown that we need more Gauss points in the region around mesh point $\mathbf{p}$ and the projection of the source $\mathbf{r}_s$ onto the sphere. So we want to identify into which m, n boxes these two points on the surface of the sphere fall. For this, we determine what the respective (ϕ', θ') coordinates of these points are and find which m, n makes the following test true:

$$mI_\theta \leq \theta' \leq (m+1)I_\theta$$

$$nI_\phi \leq \phi' \leq (n+1)I_\phi.$$

Knowing into which m, n box the point falls, we assign an increased number of points to that box, the density of which can vary.
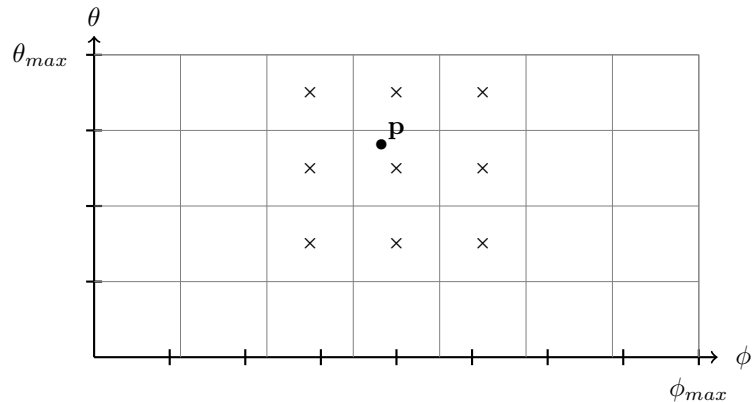
Figure 4.11: Boxes that will have a dense distribution of Gauss points around $\mathbf{p}$

In the event that the point does not fall directly into the center of the m, n-box, which will happen more often than not, not all of the singular region of the integrand around that point is entirely contained in that box. To eliminate this issue, we dictate that all of m, n-box's neighbors will have denser points as well, as shown by the ×'d boxes in the integration region in Figure 4.11 and on the sphere in Figure 4.12. This creates a region large enough to capture all of the integrand's singularity, regardless

of where the point is located in the m, n-box. When the divisions size, p and q, are sufficiently large (but not too large, as the boxes become too small to capture all behavior), then we have a significant portion of the rest of the boundary where we can distribute fewer points, as there is no singular behavior there.
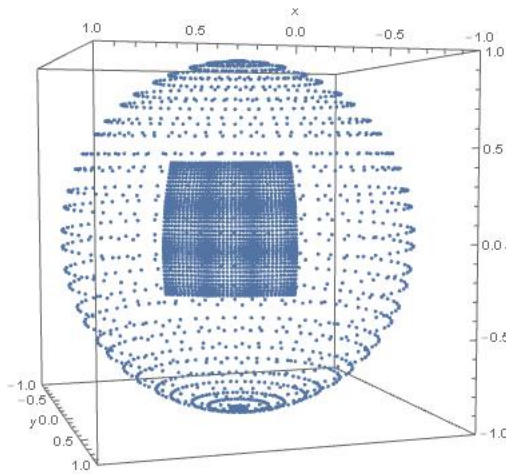
Figure 4.12: The nine boxes with a denser Gauss pt distribution visible

4.1.2 Rotation of patches

Finally, we need to comment on the rotation that is used when distributing Gauss points around mesh point **p**. Recall this rotation was implemented to make it easier to find the bounds over which to evaluate the RHS integrals, specifically the ones that are not over the entire spherical boundary S. Some integrals are defined over boundary S, S_a, or Γ. The entire mathematical boundary that our integrals are calculated over is shown in Figure 4.13.

When using rotation to distribute the Gauss points, we encounter a difficulty when locating the m, n box that a point falls into, as those regions have been moved. The test we discussed in the previous section is only valid for non-rotated points
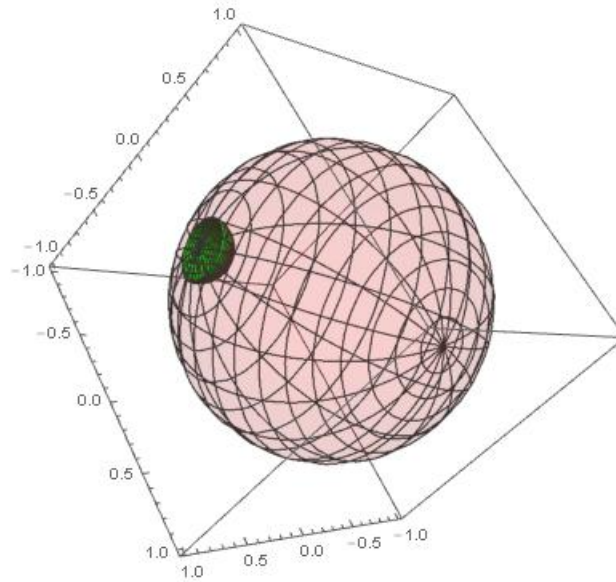
Figure 4.13: Mathematical integration geometry, with "bubble" used and visible; all RHS integrals will be evaluated over specific regions of this geometry

distributed over the box $[0, \pi] \times [0, 2\pi]$. As a result, it becomes necessary to find which now-skewed "box" a point resides. That is, we need to identify which m, n box gets mapped and rotated to contain a point of interest.

Then let us first consider the rotation matrix R, which is the matrix multiplication of the two matrices in (3.7). Then we have

$$R(\alpha, \gamma) = R_z(\alpha) times R_x(\gamma), \tag{4.2}$$

and for any arbitrary $\mathbf{x} = (x_1, x_2, x_3)$, the rotated point is $\hat{\mathbf{x}} = R(\alpha, \gamma)\mathbf{x}^T$. Now, to identify which m, n-box will rotate to contain a point $\mathbf{x}'$, we have to find its coordinates under the inverse mapping, and determine into which m, n box *those* coordinates fall. In other words, we are treating $\mathbf{x}'$ as $\hat{\mathbf{x}}'$ and evaluating

$$\mathbf{x}'' = R^{-1}(\alpha, \gamma)\hat{\mathbf{x}}'. \tag{4.3}$$

We then find the associated polar coordinates of $\mathbf{x}''$ and perform the test to see which m, n-box contains it. So then once the rotation mapping is performed on all Gauss points, that m, n-box will rotate to contain $\mathbf{x}'$.

Finally, it should be noted here that by using the rotation matrix, which, as it is defined, rotates Gauss points to emanate from a mesh point $\mathbf{p}$, then the "patch", or m, n-box that the mesh point $\mathbf{p}$ is in will always be at the north pole. When Gauss locations over the standard interval $[-1, 1] \times [-1, 1]$ get mapped to $[0, \pi] \times [0, 2\pi]$, then the boxes along the top of our divvied grid become "squished," compared to boxes that span over the equator of the sphere. To further ensure that sufficient surface area is covered to capture singular behavior of an integral at $\mathbf{p}$, we dictate that the top two rows of boxes will have a denser Gauss point distribution for the region around the mesh point, as shown in the figure below.
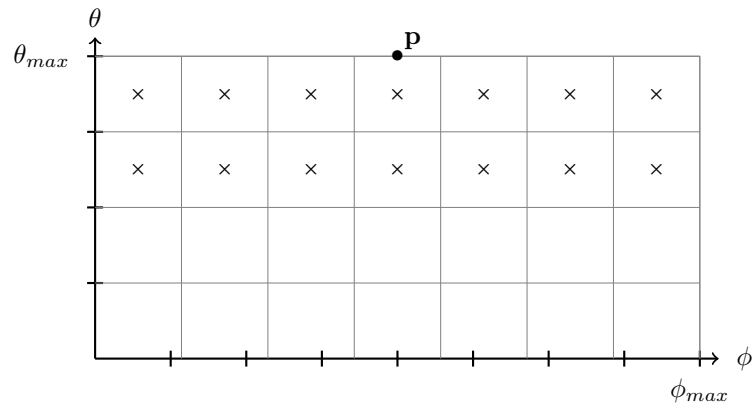
Figure 4.14: Boxes that will have a dense distribution of Gauss points around $\mathbf{p}$. In practice, there will be many more boxes used than in this figure.

This results in one patch on the sphere looking like a circle, while the other patch located around the projection of $\mathbf{r}_s$ looks like a skewed box.
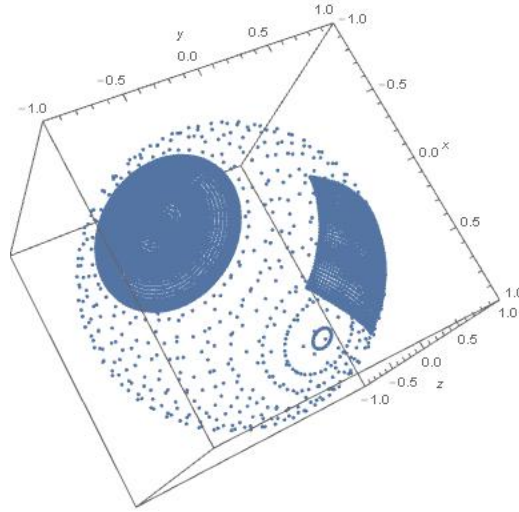
Figure 4.15: Spherical patch around mesh point **p** and rectangular patch around source projection region

Table 4.8: Integrals calculated using patch method

integral	true	d=128, s=8 677888 pts	abs error
J0	0.420119962364	0.42011996239	2.6×10^{-11}
J1	-0.015986142	-0.01598671417	5.7217×10^{-7}
J3	-0.04183241584	-0.04183241586	2×10^{-11}

4.2 Adaptive Numerical results

Now we will demonstrate the effectiveness of this "patch method" adaptive quadrature we have developed. First we will show how the values of the auxiliary integrals in (3.4) improved using this adaptive quadrature. Then we will go on to revisit previous examples in estimating the errors of the potentials. In this, we will show how this adaptive quadrature for the integrals overall improves the accuracy gotten when solving the matrix equation.

Table 4.9: Integrals calculated using traditional $[0, 2\pi] \times [0, \pi]$ point distribution

integral	true	1024*1024 1,048,576 pts	abs error
J0	0.420119962364	0.41999738802	1.225×10^{-4}
J1	-0.015986142	-0.016026949148	4.0807×10^{-5}
J3	-0.04183241584	-0.04175077572	8.164×10^{-5}

4.2.1 Integral accuracy improvement

For mesh point $(0, 0, 1)$ and source location $\mathbf{r}_s = (0.2438, 0.9752, 0.0975)$, we show results that we have gathered for the integrals $J0$, $J1$, $J2$. The top table shows the true value of the integral, gotten through Mathematica, compared to the value we calculated for the integrals in our program. The third column in Table 4.8 are the values we got in our program when using the patch method. The denser patches had Gauss point distributions of 128×128, with the rest of the domain grid having 8×8 distributions. This means that the total number of Gauss points over the entire integral domain is 677888 points. The last column in Table 4.8 is the absolute error between the values in column two (the true value) and column three (the estimated value).

The next table, Table 4.9, we have the true value of the integrals and the estimated value of the integrals without using the patch method in our program. The values in the third column were found by using a traditional all-over 1024×1024 distribution of Gauss points. Notice that we end up using more more Gauss points here, with larger error. We then see that the patch technique is more efficient and improves accuracy compared to without it.

4.2.2 Example 2 with adaptive quadratures

For source location

$$\mathbf{r}_s = (0.2438162975, 0.9752651902, 0.097526519),$$

which is 0.01 units away from the surface of the sphere, we compare our previous results in Example 2 with results found by patch method. The overall parameters are the same as in Example 2: $\varepsilon_i = 2$, $\varepsilon_o = 1$, $\lambda_o = \lambda_i = 0$, $M = 16$, $n = 3$, $a = 0.1$. Additionally, we should note that there are four integrals, $J0$, $J1$, $J3$, $J4$ that are over large domains of the integration geometry. For these four integrals, we employ the patch method technique, using a 10×20 grid. This means that for those four integrals, we divvie the integration region into 200 patches. The other four integrals are evaluated over such a small region, that instead of using the patch method, we just assign a dense spread of Gauss points distributed in the traditional way.

Table 4.10 shows the relative errors gotten for the total potential using a second degree basis for the mesh. Table 4.10 shows the relative errors in the reaction field using a second degree basis. The first columns of the tables are errors that we already saw in Tables 3.5, 3.6, and 3.7. The successive columns in these tables show the relative errors in the respective quantities gotten by using the patch method on the four right-hand side integrals, instead of no method at all. For column two in Tables 4.10 and 4.10, the denser patches had 128×128 Gauss points per patch, and the rest of the patches had 8×8 points per patch. In column three, the denser patches had 64×64 Gauss points per patch.

The goal of these tables are two demonstrate how few total Gauss points we could use and still get the good results that we already had. We can see for both the total potential and the reaction field potential, for this particular example and setup, anything below 210368 total Gauss points on those four integrals would generate

unacceptable errors. Given that the results we had before took over three million total points on those integrals, the savings just between the first and second row is substantial, with very minute differences in relative error.

4.2.3 Example 4

For source location identical to Example 2 at 0.01 units away from the sphere,

$$\mathbf{r}_s = (0.2438162975, 0.9752651902, 0.097526519),$$

with parameters all the same except for $n = 12$ and $M = 64$ (reaction field estimated by 64 images, 12 of those included in $T(\mathbf{r}, \mathbf{r}_s)$), we get the following relative errors using second degree basis functions for the potential and reaction field potential. These results were gathered using the patch method for the four right-hand side integrals, using a $10 \times 20 = 200$ patch grid. The denser patches used 128×128 Gauss points each, while the other patches were of size 8×8. Since this example would take substantially more time to calculate since the function $T(\mathbf{r}, \mathbf{r}_s)$ has more terms, we waited to try it until we had a more efficient way to evaluate the integrals (i.e. the patch method). Notice that with the results here are improved over those gotten with $M = 16$ and $n = 3$.

4.2.4 Example 3

For source location $\mathbf{r}_s = (0.0, 0.0, 1.01)$, we test the accuracy of our methods against those by which variable substitution and quadrature adaption were not used. For $n = 3$, $M = 16$, $a = 0.1$, and a 10×20 quadrature grid with dense patches of size 128×128 and 77×77, and all other patches of size 8×8, we see the following results for the total potential and its derivative. Notice in Figure 4.17, which the subtraction method was not used, the potential calculates to a negative value instead of the
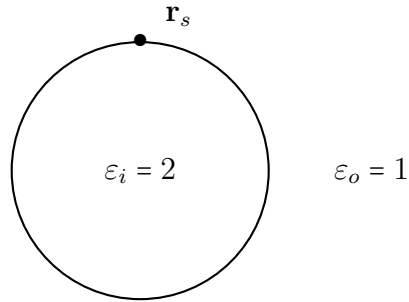
Figure 4.16: To-scale illustration of physical interaction between dielectric sphere and source charge in Example 3
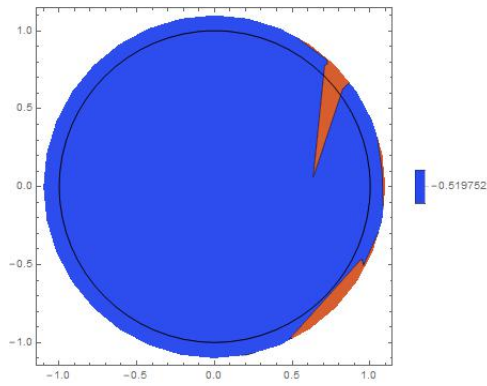
Figure 4.17: Contour plot of potential for deg 1, mesh 32 for the plane z=0 without de-singularization subtraction method
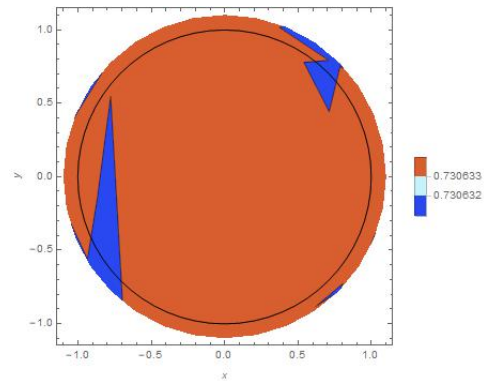
Figure 4.18: Contour plot of potential for deg 1, mesh 32 for the plane z=0 with de-singularization subtraction method

expected positive. Figure 4.18 uses the subtraction method and subsequent RHS integral grid refinement techniques to show a similar, but positive-valued electric potential contour plot.

4.2.5 Example 4 (refined adaptive quadrature)

Based on the way we set up the patch method technique for the right-hand side integrals in the matrix equation (3.4), when we choose a domain grid size of $p \times q$, then a total of $9 + 2q$ patches will have denser Gauss point coverage; nine patches are

around the projection of the source point onto the sphere, $\mathbf{r}'_s$, and $2q$ patches will be around the mesh point $\mathbf{p}$.

When we revisited Example 2 earlier, we used a domain grid size of 10×20, resulting in 200 total patches over which the domain was divided. Out of those 200, 49 of those patches would then have the denser coverage of Gauss points. So in this case, $2q$ equals 40, which is a substantially higher number of patches used around the mesh point $\mathbf{p}$ than the nine used for $\mathbf{r}'_s$. Recall that the extra number of patches around the mesh point is necessary due to the way the patches shrink and are compressed around it. This means that we are actually placing, in this example, four times as many Gauss points in the region around the mesh point than the region about $\mathbf{r}'_s$. Since those specific patches have a very high density of Gauss points distributed over them, this means that perhaps we are using far too many points than are necessary for accuracy.

Here we explore further reducing the total number of Gauss points used to calculate those four right-hand side auxiliary integrals, while preserving the accuracy we have gotten so far. The idea is to use a comparable total number of Gauss points over both regions. So, in the example we've been discussing, if we use M total Gauss points in the nine patches about $\mathbf{r}'_s$, we aim to use close to M number of total points in the 40 patches about the mesh point $\mathbf{p}$. We hope this will greatly reduce the cost of calculation with minimal loss in overall accuracy of the results for the potential.

We revisit Example 4 again. This time we are attempting to reduce the density of Gauss points in the patch around mesh point $\mathbf{p}$ when calculating the auxiliary integrals in the matrix equation (3.4). The tables below contain results previously shown, where $d = 128$, $s = 8$ (dense patches are $d \times d$ and smaller-density patches are $s \times s$). The value d_1 corresponds to the density of the patches around $\mathbf{r}'_s$, and the value d_2 corresponds to the density of the patches around mesh point $\mathbf{p}$. In tables 4.16 through 4.18, the "points used per integral" row indicates how many total Gauss

points were necessary to calculate the four difficult right-hand-side integrals in matrix equation 3.4 for which this "patch method" is meant to improve results. All other integrals were calculated using far fewer Gauss points, as the dense coverage is not needed for those.

4.3 Summary

Thus far, we have tested a variety of ideas to increase the accuracy and efficiency of the electric potential and its normal derivative for an interacting system of *one* dielectric sphere and *one* charge. This specific interaction has been preferable to us until now to demonstrate and compare the accuracy obtained when using our techniques and methods since exact (true) values of the potential can be evaluated using Legendre polynomial expansions [13][14]. However, the boundary integral equations considered so far in this paper also allow for the interaction of multiple spheres and multiple source charges, should such a system be desired. Since the errors shown in our examples have been compared with reliable, accurate methods that already exist, we can be confident that the subtraction de-singularized substitution $w_o = \phi(\mathbf{r}) - H(\mathbf{r}, \mathbf{r}_s) - T(\mathbf{r}, \mathbf{r}_s)$ in the boundary integral equations does indeed work for more general cases.

In addition, the use of a couple of numerical "tricks" has proved most valuable in increasing or maintaining the accuracy of results, while reducing computational cost. In particular, we have implemented the "bubble technique" in the boundary integral equations, and we have used the "patch method" in the C++ code, both of which lighten the burden of computation compared to their absence. The "bubble technique" is effective at mathematically altering the boundary integral equations in such a way that the resulting auxiliary integrals in (3.4) split the burden of singular behavior over several integrals that are much easier to tend to individually. Further, the "patch method" is very effective at allowing for accurate calculation of those

integrals, while using fewer Gauss points and therefore reducing computational cost.

In concluding this portion of our work, we have shown how our methods improve calculation of electric potentials for the interaction of one sphere and one source charge. Naturally, we want to further this investigation into how effective these methods would be in a system of more than one sphere. So the next segment of our work focuses on modeling *systems* of spheres and, to the best of our ability, determining how accurate our techniques are when calculating those electric potentials.

Table 4.10: Relative error of total potential in Example 2 for mesh sizes 2-32, using second degree basis functions and refined adaptive quadrature

		Parameters			
		d=128	d=128, s=8	d=64, s=8	d = 32, s=8
pts. used per int.		3,276,800	812480	210368	59776
mesh	2	2.13×10^{-2}	2.13×10^{-2}	2.12×10^{-2}	2.04×10^{-2}
	4	4.02×10^{-3}	4.02×10^{-3}	4.11×10^{-3}	1.74×10^{-2}
	8	1.21×10^{-3}	1.21×10^{-3}	1.27×10^{-3}	2.17×10^{-2}
	16	3.01×10^{-4}	3.01×10^{-4}	3.97×10^{-4}	2.18×10^{-2}
	32	3.21×10^{-5}	3.21×10^{-5}	2.86×10^{-4}	2.18×10^{-2}

Table 4.11: Relative error of reaction field potential in Example 2 for mesh sizes 2-32, using second degree basis functions and refined adaptive quadrature

		Parameters			
		d=128	d=128, s=8	d=64, s=8	d = 32, s=8
pts. used per int.		3,276,800	812480	210368	59776
mesh	2	$0\ 9.87 \times 10^{-1}$	9.87×10^{-1}	9.87×10^{-1}	9.99×10^{-1}
	4	6.43×10^{-1}	6.43×10^{-1}	6.41×10^{-1}	4.52×10^{-1}
	8	3.24×10^{-1}	3.24×10^{-1}	3.39×10^{-1}	2.006
	16	2.23×10^{-1}	2.23×10^{-1}	2.27×10^{-1}	3.0974
	32	5.39×10^{-2}	5.39×10^{-2}	8.16×10^{-2}	6.5585

Table 4.12: Relative error of normal derivative of potential in Example 2 for mesh sizes 2-32, using second degree basis functions and refined adaptive quadrature

		Parameters			
		d=128	d=128, s=8	d=64, s=8	d = 32, s=8
pts. used per int.		3,276,800	812480	210368	59776
mesh	2	2.15×10^{-2}	2.15×10^{-2}	2.13×10^{-2}	2.06×10^{-2}
	4	4.84×10^{-3}	4.84×10^{-3}	4.84×10^{-3}	1.75×10^{-2}
	8	1.33×10^{-3}	1.33×10^{-3}	1.34×10^{-3}	3.06×10^{-2}
	16	2.17×10^{-3}	2.17×10^{-3}	2.73×10^{-3}	1.74×10^{-1}
	32	2.70×10^{-3}	2.70×10^{-3}	8.05×10^{-3}	8.06×10^{-1}

Table 4.13: Relative error of total potential, reaction field potential, and derivative of potential for mesh sizes 2, 4, 8, 16, 32 in Example 4, using second degree basis

mesh size	2	4	8	16	32
tot. pot.	1.80×10^{-2}	2.67×10^{-3}	7.57×10^{-4}	8.35×10^{-5}	4.75117×10^{-6}
r.f.	8.38×10^{-1}	4.06×10^{-1}	2.40×10^{-1}	5.16×10^{-2}	3.34×10^{-3}
der.	1.81×10^{-2}	3.09×10^{-3}	8.41×10^{-4}	1.12×10^{-3}	2.98×10^{-3}

Table 4.14: Relative error in total potential for mesh sizes 2-32 in Example 3, using no subtraction de-singularization and then full subtraction de-singularization

	Relative Errors of Total Potential			
	1st degree basis		2nd degree basis	
mesh	no subtr	H & T subtr	no subtr	H & T subtr
2	552.394	1.17×10^{-1}	27.762	4.21×10^{-3}
4	140.758	2.82×10^{-2}	6.4480	1.23×10^{-3}
8	35.2121	6.85×10^{-3}	1.7531	3.19×10^{-4}
16	8.5716	1.72×10^{-3}	6.69×10^{-1}	1.01×10^{-4}
32	1.9248	4.60×10^{-4}	2.51×10^{-1}	9.99×10^{-5}

Table 4.15: Relative error in normal derivative of potential for mesh sizes 2-32 in Example 3, using no subtraction de-singularization and then full subtraction de-singularization

	Relative Errors of Derivative of Potential			
	1st degree basis		2nd degree basis	
mesh	no subtr	H & T subtr	no subtr	H & T subtr
2	286.837	1.22×10^{-1}	16.9181	4.93×10^{-3}
4	83.7425	3.33×10^{-2}	10.2608	3.56×10^{-3}
8	53.8031	2.06×10^{-2}	2.1537	8.35×10^{-4}
16	12.3785	4.75×10^{-3}	1.4254	8.13×10^{-4}
32	3.3697	1.69×10^{-3}	8.94×10^{-1}	9.12×10^{-4}

Table 4.16: Relative error of total potential in Example 4 for mesh sizes 2-32, using second degree basis functions and refined adaptive quadrature

		Parameters		
		$d=128,\ s=8$	$d_1=128,\ d_2=77,\ s=8$	$d_1=128,\ d_2=64,\ s=8$
pts per int.		812480	394280	320960
mesh	2	1.80×10^{-2}	1.80×10^{-2}	1.80×10^{-2}
	4	2.67×10^{-3}	2.67×10^{-3}	2.67×10^{-3}
	8	7.57×10^{-4}	7.50×10^{-4}	8.26×10^{-4}
	16	8.35×10^{-5}	8.47×10^{-5}	2.68×10^{-4}
	32	4.76×10^{-6}	5.17×10^{-5}	2.41×10^{-4}

Table 4.17: Relative error of reaction field potential in Example 4 for mesh sizes 2-32, using second degree basis functions and refined adaptive quadrature

		Parameters		
		$d=128,\ s=8$	$d_1=128,\ d_2=77,\ s=8$	$d_1=128,\ d_2=64,\ s=8$
pts per int.		812480	394280	320960
mesh	2	8.38×10^{-1}	8.38×10^{-1}	8.37×10^{-1}
	4	4.06×10^{-1}	4.06×10^{-1}	4.05×10^{-1}
	8	2.40×10^{-1}	2.40×10^{-1}	2.42×10^{-1}
	16	5.16×10^{-2}	5.16×10^{-2}	5.31×10^{-2}
	32	3.34×10^{-3}	3.31×10^{-3}	3.52×10^{-3}

Table 4.18: Relative error of normal derivative of potential in Example 4 for mesh sizes 2-32, using second degree basis functions and refined adaptive quadrature

		Parameters		
		$d=128,\ s=8$	$d_1=128,\ d_2=77,\ s=8$	$d_1=128,\ d_2=64,\ s=8$
pts per int.		812480	394280	320960
mesh	2	1.81×10^{-2}	1.81×10^{-2}	1.81×10^{-2}
	4	3.09×10^{-3}	3.09×10^{-3}	3.09×10^{-3}
	8	8.41×10^{-4}	8.43×10^{-4}	1.85×10^{-3}
	16	1.12×10^{-3}	1.52×10^{-3}	2.02×10^{-3}
	32	2.98×10^{-3}	2.76×10^{-3}	8.60×10^{-3}

CHAPTER 5: Systems of dielectric spheres

Since the tools developed in the previous chapter do indeed increase electric potential accuracy for one dielectric sphere and one charge, it is of interest to extend this idea to more than one dielectric sphere interacting with a charge. However, we must go through this process with the understanding that we no longer have any "exact solution" of the potential of such a system with which to compare our results. Our results must stand on their own, and we will show some convincing examples to support our claim that our methods are effective for such a system.

In this section, we will provide an updated set of boundary integral equations that models more than one sphere interacting with a source charge. Much of these derivations are very similar, or identical, to those already shown, so many of the details have been left out.

5.1 Mapping for the case of more than one sphere

We can use a reference particle centered at the origin, radius 1, with the north pole located at the "top" of the sphere at (0,0,1). Next assume there is a physical dielectric sphere with location $\mathbf{R}_k$ and orientation (ϕ_k, θ_k). The orientation can be obtained by considering how much the north pole is rotated from $(0, 0, 1)$. To map the reference sphere to the physical sphere, we define three mappings. First, we rotate around the $y-$axis by

$$\mathbf{m1}(x, y, z) = (x\cos(\theta_k) + z\sin(\theta_k),\ y,\ z\cos(\theta_k)). \tag{5.1}$$

Then we rotate around the z–axis by

$$\mathbf{m2}(x, y, z) = (x \cos(\phi_k) - y \sin(\phi_k), \ y \cos(\phi_k) + x \sin(\phi_k), \ z). \qquad (5.2)$$

Finally, we shift the center of the particle to its physical location by

$$\mathbf{m3}(x, y, z) = (x, y, z) + \mathbf{R}_k. \qquad (5.3)$$

We now define the mapping $\mathbf{m}_k$ from the reference domain to the physical domain by the composition

$$\mathbf{m}_k(x, y, z) = \mathbf{m3}(\mathbf{m2}(\mathbf{m1}(x, y, z))). \qquad (5.4)$$

The Jacobian of this mapping is 1. The inverse mappings that go from the physical sphere to the reference sphere are given by

$$\begin{aligned}
\mathbf{m1}^{-1}(x, y, z) &= (x, y, z) = (x \cos(\theta_k) - z \sin(\theta_k), \ y, \ z \cos(\theta_k) + x \sin(\theta_k)), \\
\mathbf{m2}^{-1}(x, y, z) &= (x, y, z) = (x \cos(\phi_k) + y \sin(\phi_k), \ y \cos(\phi_k) - x \sin(\phi_k), \ z), \\
\mathbf{m3}^{-1} &= (x, y, z) - \mathbf{R}_k, \\
\mathbf{m}_k^{-1} &= \mathbf{m1}^{-1}(\mathbf{m2}^{-1}(\mathbf{m3}^{-1}(x, y, z))).
\end{aligned} \qquad (5.5)$$

5.2   Integral equations for more than one dielectric sphere

In this section, we derive, modify, and update the boundary integral equations for one sphere into an appropriate set necessary to model a system of spheres.

First, we will discuss our options regarding the use of the image subtraction function $T(\mathbf{r}, \mathbf{r}_s)$ for a system of dielectric spheres. Whether discussing the boundary integral equations of one sphere or a system of them, we always have the choice to set $T(\mathbf{r}, \mathbf{r}_s) = 0$, and the integral equations are still true and easily usable. Recall that $T(\mathbf{r}, \mathbf{r}_s)$ represents the first few terms of an image approximation of the reaction

field ϕ_{rf} of the potential ϕ [14]. In setting $T(\mathbf{r}, \mathbf{r}_s)$ equal to the first few terms in this approximation and including it in the subtraction $w_o(\mathbf{r}) = \phi(\mathbf{r}) - H(\mathbf{r}, \mathbf{r}_s) - T(\mathbf{r}, \mathbf{r}_s)$, we increase the accuracy in approximating ϕ, specifically for the case when a source charge $\mathbf{r}_s$ is very close to the surface of the sphere(s). When $\mathbf{r}_s$ is not close enough to cause singular bahavior in the integrands in the BIE's, the function $T(\mathbf{r}, \mathbf{r}_s)$ is unnecessary to obtain good accuracy.

To use this observation in setting up the boundary integral equations of a system, we incorporate the option to use $T(\mathbf{r}, \mathbf{r}_s)$ on sphere S_j if it is within a tolerance distance δ to the source $\mathbf{r}_s$. If the minimum distance of the sphere to the source is greater than δ, we set $T(\mathbf{r}, \mathbf{r}_s) = 0$ on that sphere, as $T(\mathbf{r}, \mathbf{r}_s)$ is not needed. That is, let j and k be differing indexes for functions $w_o(\mathbf{r})$ and $T(\mathbf{r}, \mathbf{r}_s)$ defined on spheres j and k, and let $\delta > 0$ be a tolerance value for the minimum distance between the surface of any particular sphere S_k in the system and a source charge $\mathbf{r}_s$. We dictate that if $\min(\|S_k - \mathbf{r}_s\|) < \delta$ for sphere S_k, then we will use the function $T_k(\mathbf{r}, \mathbf{r}_s)$ to estimate the reaction field on that specific sphere k.

Now to adapt the BIEs to multiple-sphere interactions, we redefine the function $T(\mathbf{r}, \mathbf{r}_s)$ to be equal to the sum of the T terms over the L total spheres where the function is needed. That is,

$$T(\mathbf{r}, \mathbf{r}_s) = T_1(\mathbf{r}, \mathbf{r}_s) + T_2(\mathbf{r}, \mathbf{r}_s) + \cdots, \quad l = 1, \cdots, L. \tag{5.6}$$

So then

$$w_k(\mathbf{r}) = \begin{cases} \phi_o(\mathbf{r}) - H(\mathbf{r}, \mathbf{r}_s) - T(\mathbf{r}, \mathbf{r}_s) & \mathbf{r} \in \Omega_{o_k}, \\ \phi_i(\mathbf{r}) & \mathbf{r} \in \Omega_{i_k}, \end{cases}, \tag{5.7}$$

where the subtraction of the functions $H(\mathbf{r}, \mathbf{r}_s)$ and $T(\mathbf{r}, \mathbf{r}_s)$ is only done in the exterior region of the union of all spheres. Since the source charge is on the outside, the subtraction is not needed for the interior region of the spheres.

In the boundary integral equations for one sphere, S is the union of all the bound-

aries of one sphere. We expand this to include the boundaries of all dielectric spheres, skipping the more laborious details of the derivations. Let $1 \leq j \leq J$ for J total spheres in the system, and let $1 \leq k \leq J$, where k is not necessarily the same as j. Then the first boundary integral equation of the first kind is

$$\frac{1}{2} w_{o_k}(\mathbf{p}) = \sum_{j=1}^{J} \int_{S_j} \varepsilon_o(\mathbf{r}) \left(w_{o_k}(\mathbf{r}) \frac{\partial G_o(\mathbf{r}, \mathbf{p})}{\partial \mathbf{n}} - G_o(\mathbf{r}, \mathbf{p}) \frac{\partial w_{o_k}(\mathbf{r})}{\partial \mathbf{n}} \right) \mathrm{d}S(\mathbf{r}) \qquad (5.8)$$

and the second integral equation of the first kind is

$$
\begin{aligned}
\frac{1}{2} w_{o_k}(\mathbf{p}) =\ & \sum_{j=1}^{J} \int_{S_j} \left(\varepsilon_o(\mathbf{r}) G_i(\mathbf{r}, \mathbf{p}) \frac{\partial w_{o_j}(\mathbf{r})}{\partial \mathbf{n}} - \varepsilon_o(\mathbf{r}) w_{o_j}(\mathbf{r}) \frac{\partial G_i(\mathbf{r}, \mathbf{p})}{\partial \mathbf{n}} \right) \mathrm{d}S(\mathbf{r}) \\
& + \sum_{j=1}^{J} \int_{S_j} \left(\varepsilon_o(\mathbf{r}) G_i(\mathbf{r}, \mathbf{p}) \frac{\partial H(\mathbf{r}, \mathbf{r}_s)}{\partial \mathbf{n}} - \varepsilon_i(\mathbf{r}) H(\mathbf{r}, \mathbf{r}_s) \frac{\partial G_i(\mathbf{r}, \mathbf{p})}{\partial \mathbf{n}} \right) \mathrm{d}S(\mathbf{r}) \\
& + \sum_{j=1}^{J} \int_{S_j} \left(\varepsilon_o(\mathbf{r}) G_i(\mathbf{r}, \mathbf{p}) \frac{\partial T(\mathbf{r}, \mathbf{r}_s)}{\partial \mathbf{n}} - \varepsilon_i(\mathbf{r}) T(\mathbf{r}, \mathbf{r}_s) \frac{\partial G_i(\mathbf{r}, \mathbf{p})}{\partial \mathbf{n}} \right) \mathrm{d}S(\mathbf{r}) \\
& - \frac{1}{2} H(\mathbf{r}, \mathbf{r}_s) - \frac{1}{2} T(\mathbf{r}, \mathbf{r}_s).
\end{aligned}
\qquad (5.9)
$$

To develop the integral equations of the second kind, we need to take the normal derivatives of the two previous integral equations. The derivative of (5.8) is

$$\frac{1}{2} \frac{w_{o_k}(\mathbf{r})}{\partial \mathbf{n}} = \sum_{j=1}^{J} \int_{S_j} \varepsilon_o(\mathbf{r}) \left(w_{o_k}(\mathbf{r}) \frac{\partial^2 G_o(\mathbf{r}, \mathbf{p})}{\partial \mathbf{n}' \partial \mathbf{n}} - \frac{\partial G_o(\mathbf{r}, \mathbf{p})}{\partial \mathbf{n}'} \frac{w_{o_k}(\mathbf{r})}{\partial \mathbf{n}} \right) \mathrm{d}S(\mathbf{r}) \qquad (5.10)$$

and the derivative of the (5.9) is

$$
\frac{1}{2}\frac{\varepsilon_o(\mathbf{r})}{\varepsilon_i(\mathbf{r})}\frac{\partial w_{o_k}(\mathbf{p})}{\partial \mathbf{n}_{o_k}} = \sum_{j=1}^{J}\int\limits_{S_j}\left(\varepsilon_o(\mathbf{r})\frac{\partial G_i(\mathbf{r},\mathbf{p})}{\partial \mathbf{n}'}\frac{\partial w_{o_j}(\mathbf{r})}{\partial \mathbf{n}} - \varepsilon_i(\mathbf{r})w_{o_j}(\mathbf{r})\frac{\partial^2 G_i(\mathbf{r},\mathbf{p})}{\partial \mathbf{n}'\partial \mathbf{n}}\right)\mathrm{d}S(\mathbf{r})
$$

$$
+ \sum_{j=1}^{J}\int\limits_{S_j}\left(\varepsilon_o(\mathbf{r})\frac{\partial G_i(\mathbf{r},\mathbf{p})}{\partial \mathbf{n}'}\frac{\partial H(\mathbf{r},\mathbf{r}_s)}{\partial \mathbf{n}} - \varepsilon_i(\mathbf{r})H(\mathbf{r},\mathbf{r}_s)\frac{\partial^2 G_i(\mathbf{r},\mathbf{p})}{\partial \mathbf{n}'\partial \mathbf{n}}\right)\mathrm{d}S(\mathbf{r})
$$

$$
+ \sum_{j=1}^{J}\int\limits_{S_j}\left(\varepsilon_o(\mathbf{r})\frac{\partial G_i(\mathbf{r},\mathbf{p})}{\partial \mathbf{n}'}\frac{\partial T(\mathbf{r},\mathbf{r}_s)}{\partial \mathbf{n}} - \varepsilon_i(\mathbf{r})T(\mathbf{r},\mathbf{r}_s)\frac{\partial^2 G_i(\mathbf{r},\mathbf{p})}{\partial \mathbf{n}'\partial \mathbf{n}}\right)\mathrm{d}S(\mathbf{r})
$$

$$
- \frac{1}{2}\frac{\varepsilon_o(\mathbf{r})}{\varepsilon_i(\mathbf{r})}\frac{\partial H(\mathbf{p},\mathbf{r}_s)}{\partial \mathbf{n}_{o_k}} - \frac{1}{2}\frac{\varepsilon_o(\mathbf{r})}{\varepsilon_i(\mathbf{r})}\frac{\partial T(\mathbf{p},\mathbf{r}_s)}{\partial \mathbf{n}_{o_k}},
$$

$$(5.11)$$

where we take $\mathbf{n}_{o_k}$ to be the outward unit normal corresponding to sphere k, on which $\mathbf{p}$ lies. Adding the two equations of the first kind, (5.8) and (5.9), gives the first integral equation of the second kind, and adding the derivatives of the two first kind equations, (5.10) and (5.11), gives the second equation of the second kind.

$$
w_{o_k}(\mathbf{p}) = \sum_{j=1}^{J}\int\limits_{S_j}\varepsilon_o(\mathbf{r})\left(G_i(\mathbf{r},\mathbf{p}) - G_o(\mathbf{r},\mathbf{r}_s)\right)\frac{\partial w_{o_j}(\mathbf{r})}{\partial \mathbf{n}_o}\mathrm{d}S(\mathbf{r})
$$

$$
+ \sum_{j=1}^{J}\int\limits_{S_j}\left(\varepsilon_o(\mathbf{r})G_i(\mathbf{r},\mathbf{p})\frac{\partial H(\mathbf{r},\mathbf{r}_s)}{\partial \mathbf{n}_o} - \varepsilon_i(\mathbf{r})H(\mathbf{r},\mathbf{r}_s)\frac{\partial G_i(\mathbf{r},\mathbf{p})}{\partial \mathbf{n}_o}\right)\mathrm{d}S(\mathbf{r})
$$

$$
+ \sum_{j=1}^{J}\int\limits_{S_j}\left(\varepsilon_o(\mathbf{r})G_i(\mathbf{r},\mathbf{p})\frac{\partial T(\mathbf{r},\mathbf{r}_s)}{\partial \mathbf{n}_o} - \varepsilon_i(\mathbf{r})T(\mathbf{r},\mathbf{r}_s)\frac{\partial G_i(\mathbf{r},\mathbf{p})}{\partial \mathbf{n}_o}\right)\mathrm{d}S(\mathbf{r})
$$

$$
- \frac{1}{2}H(\mathbf{r},\mathbf{r}_s) - \frac{1}{2}T(\mathbf{r},\mathbf{r}_s)
$$

$$(5.12)$$

and

$$\left(\frac{1}{2} + \frac{1}{2}\frac{\varepsilon_o(\mathbf{r})}{\varepsilon_i(\mathbf{r})}\right)\frac{\partial w_{o_k}(\mathbf{p})}{\partial \mathbf{n}_{o_k}} = \sum_{j=1}^{J}\int_{S_j}\left(\varepsilon_o(\mathbf{r})\frac{\partial^2 G_o(\mathbf{r},\mathbf{p})}{\partial \mathbf{n}'_o \partial \mathbf{n}_o} - \varepsilon_i(\mathbf{r})\frac{\partial^2 G_i(\mathbf{r},\mathbf{p})}{\partial \mathbf{n}'_o \partial \mathbf{n}_o}\right)w_{o_j}(\mathbf{r})\,\mathrm{d}S(\mathbf{r})$$

$$+ \sum_{j=1}^{J}\int_{S_j}\left(\varepsilon_o(\mathbf{r})\frac{\partial G_i(\mathbf{r},\mathbf{p})}{\partial \mathbf{n}'_o} - \varepsilon_o(\mathbf{r})\frac{\partial G_o(\mathbf{r},\mathbf{p})}{\partial \mathbf{n}'_o}\right)\frac{\partial w_{o_j}(\mathbf{r})}{\partial \mathbf{n}_o}\,\mathrm{d}S(\mathbf{r})$$

$$- \sum_{j=1}^{J}\mathrm{p.f.}\int_{S_j}\varepsilon_i(\mathbf{r})\left(H(\mathbf{r},\mathbf{r}_s) + T(\mathbf{r},\mathbf{r}_s)\right)\frac{\partial^2 G_i(\mathbf{r},\mathbf{p})}{\partial \mathbf{n}'_o \partial \mathbf{n}_o}\,\mathrm{d}S(\mathbf{r})$$

$$+ \sum_{j=1}^{J}\int_{S_j}\varepsilon_o(\mathbf{r})\left(\frac{\partial H(\mathbf{r},\mathbf{r}_s)}{\partial \mathbf{n}_o} + \frac{\partial T(\mathbf{r},\mathbf{r}_s)}{\partial \mathbf{n}_o}\right)\frac{\partial G_i(\mathbf{r},\mathbf{p})}{\partial \mathbf{n}'_o}\,\mathrm{d}S(\mathbf{r})$$

$$- \frac{1}{2}\frac{\varepsilon_o(\mathbf{r})}{\varepsilon_i(\mathbf{r})}\frac{\partial H(\mathbf{r},\mathbf{r}_s)}{\partial \mathbf{n}_{o_k}} - \frac{1}{2}\frac{\varepsilon_o(\mathbf{r})}{\varepsilon_i(\mathbf{r})}\frac{\partial T(\mathbf{r},\mathbf{r}_s)}{\partial \mathbf{n}_{o_k}}.$$

$$(5.13)$$

Before going further, we should note here that equation (5.13) does not yet include the use of the "bubble technique" we developed to regularize the finite part integrals. In addition, we have the option to pick and choose when and on which sphere(s) the bubble method and image subtraction method are used. As a reminder, the so-called "bubble technique" is used to regularize the integral

$$-\mathrm{p.f.}\oint_{S}\varepsilon_o(H(\mathbf{r},\mathbf{r}_s) + T(\mathbf{r},\mathbf{r}_s))\frac{\partial^2 G_i(\mathbf{r},\mathbf{p})}{\partial \mathbf{n}'\partial \mathbf{n}}\,\mathrm{d}S(\mathbf{r}). \qquad (5.14)$$

Its integrand is hypersingular, and therefore difficult to accurately calculate, when mesh point $\mathbf{p}$ is close to watch point $\mathbf{r}$. This difficulty is mitigated by using the identity (2.51), which distributes the computational load over a more manageable set of integrals. As a result, for the integral equations of one sphere, this identity was used for every row in the matrix equation (3.4).

However, when discussing the boundary integral equations of a *system* of spheres, this integral will be calculated J times. This means that any given mesh point $\mathbf{p}$ will not be located on every sphere S_j being integrated over in the sum of J finite part

integrals, but $\mathbf{p}$ will always be on *one* of them. In the case where $\mathbf{p}$ and $\mathbf{r}$ are located on different spheres for the integral ξ_j, the second derivative of the Green's function in ξ does not display singular behavior, and therefore the subsequent exchange of integrals through the identity (2.51) is not necessary. So we then only use the identity (2.51) for the particular integral ξ_j in the sum that corresponds to the same sphere on which $\mathbf{p}$ is located, but not the other integrals in the sum. Incorporating this idea into (5.13), it is now modified to be:

$$
\begin{aligned}
\left(\frac{1}{2} + \frac{1}{2}\frac{\varepsilon_o(\mathbf{r})}{\varepsilon_i(\mathbf{r})} \right) \frac{\partial w_{o_k}(\mathbf{p})}{\partial \mathbf{n}_{o_k}} = {} & \sum_{j=1}^{J} \int_{S_j} \left(\varepsilon_o(\mathbf{r}) \frac{\partial^2 G_o(\mathbf{r},\mathbf{p})}{\partial \mathbf{n}_o' \partial \mathbf{n}_o} - \varepsilon_i(\mathbf{r}) \frac{\partial^2 G_i(\mathbf{r},\mathbf{p})}{\partial \mathbf{n}_o' \partial \mathbf{n}_o} \right) w_{o_j}(\mathbf{r}) \, dS(\mathbf{r}) \\
& + \sum_{j=1}^{J} \int_{S_j} \left(\varepsilon_o(\mathbf{r}) \frac{\partial G_i(\mathbf{r},\mathbf{p})}{\partial \mathbf{n}_o'} - \varepsilon_o(\mathbf{r}) \frac{\partial G_o(\mathbf{r},\mathbf{p})}{\partial \mathbf{n}_o'} \right) \frac{\partial w_{o_j}(\mathbf{r})}{\partial \mathbf{n}_o} \, dS(\mathbf{r}) \\
& - \sum_{j=1}^{J} \mathrm{p.f.} \int_{S_j} \varepsilon_i(\mathbf{r}) \left(H(\mathbf{r},\mathbf{r}_s) + T(\mathbf{r},\mathbf{r}_s) \right) \frac{\partial^2 G_i(\mathbf{r},\mathbf{p})}{\partial \mathbf{n}_o' \partial \mathbf{n}_o} \, dS(\mathbf{r}) \\
& + \sum_{j=1}^{J} \int_{S_j} \varepsilon_o(\mathbf{r}) \left(\frac{\partial H(\mathbf{r},\mathbf{r}_s)}{\partial \mathbf{n}_o} + \frac{\partial T(\mathbf{r},\mathbf{r}_s)}{\partial \mathbf{n}_o} \right) \frac{\partial G_i(\mathbf{r},\mathbf{p})}{\partial \mathbf{n}_o'} \, dS(\mathbf{r}) \\
& - \int_{S_k \backslash S_{a_k}} \varepsilon_i(\mathbf{r}) \left(H(\mathbf{r},\mathbf{r}_s) + T(\mathbf{r},\mathbf{r}_s) \right) \frac{\partial^2 G_i(\mathbf{r},\mathbf{p})}{\partial \mathbf{n}_o' \partial \mathbf{n}_o} \, dS(\mathbf{r}) \\
& + \int_{S_{a_k}} \varepsilon_i(\mathbf{r}) \left(v(\mathbf{r}) - H(\mathbf{r},\mathbf{r}_s) - T(\mathbf{r},\mathbf{r}_s) \right) \frac{\partial^2 G_i(\mathbf{r},\mathbf{r}_s)}{\partial \mathbf{n}_o' \partial \mathbf{n}_o} \, dS(\mathbf{r}) \\
& - \int_{S_{a_k}} \varepsilon_i(\mathbf{r}) \frac{\partial G_i(\mathbf{r},\mathbf{p})}{\partial \mathbf{n}_o'} \frac{\partial v(\mathbf{r})}{\partial \mathbf{n}_o} \, dS(\mathbf{r}) \\
& - \int_{\Gamma_k} \varepsilon_i(\mathbf{r}) \frac{\partial G_i(\mathbf{r},\mathbf{p})}{\partial \mathbf{n}_o'} \frac{\partial v(\mathbf{r})}{\partial \mathbf{n}_\Gamma} \, dS(\mathbf{r}) \\
& + \int_{\Gamma_k} \varepsilon_i(\mathbf{r}) v(\mathbf{r}) \frac{\partial^2 G_i(\mathbf{r},\mathbf{p})}{\partial \mathbf{n}_o' \partial \mathbf{n}_\Gamma} \, dS(\mathbf{r}) + \frac{1}{2} \frac{\partial v(\mathbf{p})}{\partial \mathbf{n}_{o_k}} \\
& - \frac{1}{2} \frac{\varepsilon_o(\mathbf{r})}{\varepsilon_i(\mathbf{r})} \frac{\partial H(\mathbf{r},\mathbf{r}_s)}{\partial \mathbf{n}_{o_k}} - \frac{1}{2} \frac{\varepsilon_o(\mathbf{r})}{\varepsilon_i(\mathbf{r})} \frac{\partial T(\mathbf{r},\mathbf{r}_s)}{\partial \mathbf{n}_{o_k}}
\end{aligned}
$$

$$(5.15)$$

One last adjustment to equations (5.12) and (5.15) must be completed before we can say that our new derivations are finished. Since we are defining multiple spheres to be our integration domain, we must use the mappings in the previous section to ensure that points from a reference sphere centered at the origin get mapped to the appropriate physical location(s). So that means that points $\mathbf{p}$ and $\mathbf{r}$ in (5.12) and (5.15) are understood to already be under the mapping (5.4). More precisely, let $\hat{\mathbf{r}}$ and $\hat{\mathbf{p}}$ be the points on the reference sphere that correspond to $\mathbf{r}$ and $\mathbf{p}$ via the mappings. Then in (5.12) and (5.15), $\mathbf{p} = \mathbf{m}_k(\hat{\mathbf{p}})$ and $\mathbf{r} = \mathbf{m}_k(\hat{\mathbf{r}})$.

Further, it should be noted that the layered Green's function is only defined for the reference dielectric sphere (one centered at the origin). Since we eventually want to prepare for using these BIE's for Janus particle systems, where the superimposed mathematical hemispherical boundary of the spheres have different dielectric constant values, we want to address this particular restriction of the layered Green's functions sooner than later. Ultimately we will need to map from the physical location back to the reference sphere location in order to make use of the layered Green's functions. This inverse mapping need not be applied to all the integrals in the BIE, as those that do not contain basis functions do not contain layered Green's functions, since there are no layers outside of the boundary of the spheres. These extra integrals can therefore be calculated normally. So for the integrals in (5.12) and (5.15) that will contain basis functions, we need the variable of integration to be passed to the Green's functions as $\hat{\mathbf{r}}$, not $m_j(\mathbf{r})$. So to make the layered Green's functions useful for both Janus particles and dielectric spheres, we will apply the mapping m_j^{-1} to all arguments of the Green's functions in the integrals that will contain basis functions.

Finally, our system of boundary integral equations for a system of dielectric

spheres can be written out as follows:

$$w_{o_k}(\mathbf{p}) = \sum_{j=1}^{J} \int_{S_j} \varepsilon_o(\hat{\mathbf{r}}) \left(G_i(\hat{\mathbf{r}}, m_j^{-1}(m_k(\hat{\mathbf{p}}))) - G_o(\hat{\mathbf{r}}, m_j^{-1}(m_k(\hat{\mathbf{p}}))) \right) \frac{\partial w_{o_j}(\hat{\mathbf{r}})}{\partial \mathbf{n}_o} \, \mathrm{d}S(\hat{\mathbf{r}})$$

$$+ \sum_{j=1}^{J} \int_{S_j} \left(\varepsilon_o(\mathbf{r}) G_i(\mathbf{r}, \mathbf{p}) \frac{\partial H(\mathbf{r}, \mathbf{r}_s)}{\partial \mathbf{n}_o} - \varepsilon_i(\mathbf{r}) H(\mathbf{r}, \mathbf{r}_s) \frac{\partial G_i(\mathbf{r}, \mathbf{p})}{\partial \mathbf{n}_o} \right) \mathrm{d}S(\mathbf{r})$$

$$+ \sum_{j=1}^{J} \int_{S_j} \left(\varepsilon_o(\mathbf{r}) G_i(\mathbf{r}, \mathbf{p}) \frac{\partial T(\mathbf{r}, \mathbf{r}_s)}{\partial \mathbf{n}_o} - \varepsilon_i(\mathbf{r}) T(\mathbf{r}, \mathbf{r}_s) \frac{\partial G_i(\mathbf{r}, \mathbf{p})}{\partial \mathbf{n}_o} \right) \mathrm{d}S(\mathbf{r}) \tag{5.16}$$

$$- \frac{1}{2} H(\mathbf{r}, \mathbf{r}_s) - \frac{1}{2} T(\mathbf{r}, \mathbf{r}_s)$$

and

$$\left(\frac{1}{2} + \frac{1}{2} \frac{\varepsilon_o(\mathbf{r})}{\varepsilon_i(\hat{\mathbf{r}})} \right) \frac{\partial w_{o_k}(\mathbf{p})}{\partial \mathbf{n}_{o_k}} = \sum_{j=1}^{J} \int_{S_j} \left(\varepsilon_o(\hat{\mathbf{r}}) \frac{\partial^2 G_o(\hat{\mathbf{r}}, m_j^{-1}(m_k(\hat{\mathbf{p}})))}{\partial \mathbf{n}_o' \partial \mathbf{n}_o} - \varepsilon_i(\mathbf{r}) \frac{\partial^2 G_i(\hat{\mathbf{r}}, m_j^{-1}(m_k(\hat{\mathbf{p}})))}{\partial \mathbf{n}_o' \partial \mathbf{n}_o} \right) w_{o_j}(\hat{\mathbf{r}}) \, \mathrm{d}S(\hat{\mathbf{r}})$$

$$+ \sum_{j=1}^{J} \int_{S_j} \left(\varepsilon_o(\hat{\mathbf{r}}) \frac{\partial G_i(\hat{\mathbf{r}}, m_j^{-1}(m_k(\hat{\mathbf{p}})))}{\partial \mathbf{n}_o'} - \varepsilon_o(\mathbf{r}) \frac{\partial G_o(\hat{\mathbf{r}}, m_j^{-1}(m_k(\hat{\mathbf{p}})))}{\partial \mathbf{n}_o'} \right) \frac{\partial w_{o_j}(\hat{\mathbf{r}})}{\partial \mathbf{n}_o} \, \mathrm{d}S(\hat{\mathbf{r}})$$

$$- \sum_{j=1}^{J} \mathrm{p.f.} \int_{S_j} \varepsilon_i(\mathbf{r}) \left(H(\mathbf{r}, \mathbf{r}_s) + T(\mathbf{r}, \mathbf{r}_s) \right) \frac{\partial^2 G_i(\mathbf{r}, \mathbf{p})}{\partial \mathbf{n}_o' \partial \mathbf{n}_o} \, \mathrm{d}S(\mathbf{r})$$

$$+ \sum_{j=1}^{J} \int_{S_j} \varepsilon_o(\mathbf{r}) \left(\frac{\partial H(\mathbf{r}, \mathbf{r}_s)}{\partial \mathbf{n}_o} + \frac{\partial T(\mathbf{r}, \mathbf{r}_s)}{\partial \mathbf{n}_o} \right) \frac{\partial G_i(\mathbf{r}, \mathbf{p})}{\partial \mathbf{n}_o'} \, \mathrm{d}S(\mathbf{r})$$

$$- \int_{S_k \backslash S_{a_k}} \varepsilon_i(\mathbf{r}) \left(H(\mathbf{r}, \mathbf{r}_s) + T(\mathbf{r}, \mathbf{r}_s) \right) \frac{\partial^2 G_i(\mathbf{r}, \mathbf{p})}{\partial \mathbf{n}_o' \partial \mathbf{n}_o} \, \mathrm{d}S(\mathbf{r}) \tag{5.17}$$

$$+ \int_{S_{a_k}} \varepsilon_i(\mathbf{r}) \left(v(\mathbf{r}) - H(\mathbf{r}, \mathbf{r}_s) - T(\mathbf{r}, \mathbf{r}_s) \right) \frac{\partial^2 G_i(\mathbf{r}, \mathbf{r}_s)}{\partial \mathbf{n}_o' \partial \mathbf{n}_o} \, \mathrm{d}S(\mathbf{r})$$

$$- \int_{S_{a_k}} \varepsilon_i(\mathbf{r}) \frac{\partial G_i(\mathbf{r}, \mathbf{p})}{\partial \mathbf{n}_o'} \frac{\partial v(\mathbf{r})}{\partial \mathbf{n}_o} \, \mathrm{d}S(\mathbf{r})$$

$$- \int_{\Gamma_k} \varepsilon_i(\mathbf{r}) \frac{\partial G_i(\mathbf{r}, \mathbf{p})}{\partial \mathbf{n}_o'} \frac{\partial v(\mathbf{r})}{\partial \mathbf{n}_\Gamma} \, \mathrm{d}S(\mathbf{r})$$

$$+ \int_{\Gamma_k} \varepsilon_i(\mathbf{r}) v(\mathbf{r}) \frac{\partial^2 G_i(\mathbf{r}, \mathbf{p})}{\partial \mathbf{n}_o' \partial \mathbf{n}_\Gamma} \, \mathrm{d}S(\mathbf{r}) + \frac{1}{2} \frac{\partial v(\mathbf{p})}{\partial \mathbf{n}_{o_k}}$$

$$- \frac{1}{2} \frac{\varepsilon_o(\mathbf{r})}{\varepsilon_i(\mathbf{r})} \frac{\partial H_l(\mathbf{r}, \mathbf{r}_s)}{\partial \mathbf{n}_{o_k}} - \frac{1}{2} \frac{\varepsilon_o(\mathbf{r})}{\varepsilon_i(\mathbf{r})} \frac{\partial T(\mathbf{r}, \mathbf{r}_s)}{\partial \mathbf{n}_{o_k}}$$

Let the following quantities be defined as we have defined them previously, and let all other integrals simply be described as "right-hand side integrals." Consider these definitions to be flexible, in that the Green's function can either be layered or not (hence the lack of mappings in the definitions). Then we have the following matrix

equation for this system of boundary integral equations:

$$S0 = \oint_S G_i(\mathbf{r},\mathbf{p})\psi_t(\mathbf{r})\,dS(\mathbf{r}) \qquad S1 = \oint_S G_o(\mathbf{r},\mathbf{p})\psi(\mathbf{r})\,dS(\mathbf{r})$$

$$D0 = \oint_S \frac{\partial G_i(\mathbf{r},\mathbf{p})}{\partial \mathbf{n}_o}\psi_t(\mathbf{r})\,dS(\mathbf{r}) \qquad D1 = \oint_S \frac{\partial G_o(\mathbf{r},\mathbf{p})}{\partial \mathbf{n}_o}\psi_t(\mathbf{r})\,dS(\mathbf{r})$$

$$D2 = \oint_S \frac{\partial G_i(\mathbf{r},\mathbf{p})}{\partial \mathbf{n}'_o}\psi_t(\mathbf{r})\,dS(\mathbf{r}) \qquad D3 = \oint_S \frac{\partial G_o(\mathbf{r},\mathbf{p})}{\partial \mathbf{n}'_o}\psi_t(\mathbf{r})\,dS(\mathbf{r})$$

$$T0 = \oint_S \frac{\partial^2 G_i(\mathbf{r},\mathbf{p})}{\partial \mathbf{n}'_o \partial \mathbf{n}_o}\psi_t(\mathbf{r})\,dS(\mathbf{r}) \qquad T1 = \oint_S \frac{\partial^2 G_o(\mathbf{r},\mathbf{p})}{\partial \mathbf{n}'_o \partial \mathbf{n}_o}\psi_t(\mathbf{r})\,dS(\mathbf{r})$$

$$\left[\begin{pmatrix} I & 0 \\ 0 & \left(\frac{1}{2} + \frac{1}{2}\frac{\varepsilon_o}{\varepsilon_i}\right)I \end{pmatrix} + \begin{pmatrix} (\varepsilon_i D0 - \varepsilon_o D1) & -(S0 - S1)\varepsilon_o \\ (\varepsilon_i T0 - \varepsilon_o T1) & -(D2 - D3)\varepsilon_o \end{pmatrix}\right]\begin{pmatrix} w_o \\ k_o \end{pmatrix} = \begin{pmatrix} \text{top RHS} \\ \text{bot. RHS} \end{pmatrix},$$

$$(5.18)$$

where $\mathbf{p}$ takes different mesh points $\mathbf{r}_t$ in different rows of the matrix.

5.3 Numerical results as compared to previous single-sphere computation

We now put these new boundary integral equations for a system of spheres to the test. In the following examples, we revisit examples already seen, but with the addition of a secondary dielectric sphere located a certain distance away from the first. We will try different scenarios, changing the distance and dielectric constants of the secondary sphere, and investigating the effect this has on the first sphere. Since we definitively have a solution for the electric potential on *one* of the spheres, we compare the results gotten from previous examples with a single sphere to those potentials on the first sphere in the system. This will help us appropriately gauge if the BIE's and coding look to be behaving as they should. Since we do not have an analytic solution of the electric potential in a system, this is the next best way to test our results.

Additionally, when the second sphere in the system is completely invisible, where its dielectric constants are identical to those of the exterior medium, not only can we

verify results on the first sphere, but we can also use the slightly different Legendre polynomial expansion below to verify that the potential is being calculated correctly on the second sphere:

$$\phi(r,\theta) = 4\pi \sum_{n=0}^{\infty} C(r) P_n(\cos(\theta)), \tag{5.19}$$

where $C(r)$ is given by

$$C(r) = \frac{q}{4\pi\varepsilon_o r_s} \left(\frac{r_s}{r}\right)^n - D_n \frac{1}{r^{n+1}}, \tag{5.20}$$

and D_n is the constant given by

$$D_n = \frac{q}{4\pi\varepsilon_o} \frac{a^{2n+1}}{r_s^{n+1}} \gamma \left(1 - \frac{1-\gamma}{1-\gamma+2n}\right), \tag{5.21}$$

for when $\mathbf{r}$ is out beyond $\mathbf{r}_s$.

5.3.1 Example 1.2

For this example, we consider the same parameters as listed under Example 1, with some additions. That is, for the single-sphere case, we considered the case where there was one source charge located at $\mathbf{r}_s = (0.5, 2, 0.2)$, which is approximately 1.07 units away from the sphere. We let the reaction field potential be estimated by $M = 16$ image charge locations, with the first $n = 3$ of those terms being included in the function $T(\mathbf{r}, \mathbf{r}_s)$. Further, we took hemisphere Γ to have radius $a = 0.1$ units, $\varepsilon_{1_i} = 2$ and $\varepsilon_{1_o} = 1$, and the true solution was calculated by a Legendre polynomial expansion out to 300 terms.

Now we use these errors for the single-sphere as a guide with which to compare a two-sphere dielectric system. We let the source charge be at the same location. We set the first sphere to be located at the origin of a grid and then placed the second one 3 units away with center at $(5, 0, 0)$. Its dielectric constants were $\varepsilon_{2_i} = \varepsilon_{2_o} = 1$ so that
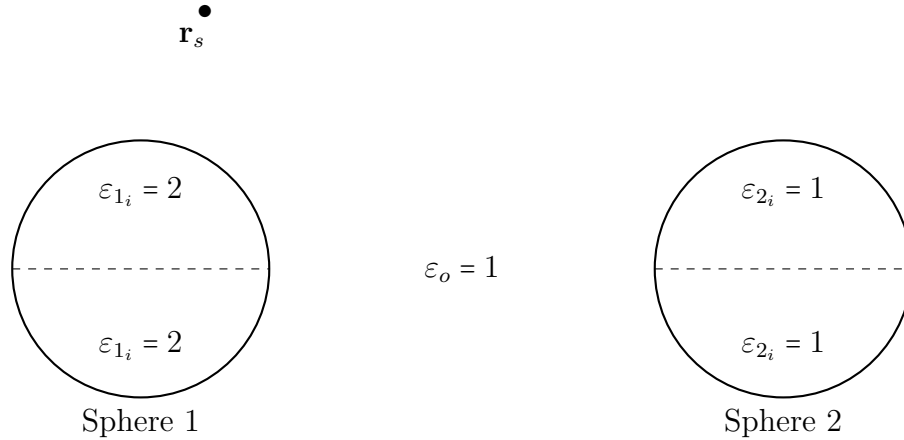
Figure 5.19: Example 1.2 illustration of physical interaction for familiar non-challenging computational example, where source charge is far away and Sphere Two has the same dielectric properties of background medium

Table 5.19: Example 1.2, Sphere 1 mesh point total potential relative errors for mesh sizes 2-32

	Two-sphere system		One sphere (old)	
	1st Degree	2nd Degree	1st Degree	2nd Degree
Mesh	Rel. Error	Rel. Error	Rel. Error	Rel. Error
2	6.47×10^{-3}	3.96×10^{-3}	6.46×10^{-3}	3.95×10^{-3}
4	1.94×10^{-3}	4.67×10^{-4}	1.93×10^{-3}	4.66×10^{-4}
8	5.94×10^{-4}	3.24×10^{-5}	5.94×10^{-4}	3.23×10^{-5}
16	1.94×10^{-4}	3.93×10^{-6}	1.94×10^{-4}	4.78×10^{-6}
32	5.51×10^{-5}	1.94×10^{-6}	5.51×10^{-5}	2.37×10^{-6}

any electric potential results for mesh points on the first sphere should match those of the single-sphere case, as the second sphere is a "fake." As Table 5.19 shows, the results of the electrostatic potential for Sphere 1 in the two-sphere system match those of the one-sphere system quite nicely. Any improvement in the new data compared to the old can be attributed to the "patch method" technique being implemented for the new data.

Additionally, since Sphere 2 in this system is "fake," or invisible, we would like to demonstrate that the potentials evaluated on that sphere are accurate. To that end,

Table 5.20: Example 1.2, Sphere 2 mesh point total potential relative errors for mesh sizes 2-32

| | Sphere 2 potentials | |
| | 1st Degree | 2nd Degree |
Mesh	Rel. Error	Rel. Error
2	3.42×10^{-3}	1.28×10^{-3}
4	1.20×10^{-4}	5.70×10^{-5}
8	3.37×10^{-5}	1.64×10^{-6}
16	7.94×10^{-6}	1.81×10^{-7}
32	1.99×10^{-6}	9.00×10^{-8}

we use equation 5.19 to compare with our results, since the mesh points on Sphere 2 are basically acting like watch points $\mathbf{r}$ outside of Sphere 1. As we can see in Table 5.20, the potentials for the mesh points on the second sphere are very accurate. This ensures that the implementation of solving for the potential for systems is correct.

5.3.2 Example 2.2

In this example, we revisit Example 2 from earlier. Here everything is the same as it was in Example 2, except that now we have added a second "fake" dielectric sphere 3 units away. The source charge is located at $\mathbf{r}_s = (0.2438162975, 0.9752651902, 0.097526519)$, which is 0.01 units away from the surface of Sphere 1. We have that $\lambda_o = \lambda_{1_i} = \lambda_{2_i} = 0$, $M = 16$, $n = 3$, $a = 0.1$, and the true solution for the mesh points on Sphere 1 is found by using 1500 terms of the Legendre polynomial expansion. We see that the total potential errors are very good for both Sphere 1 and Sphere 2. In this we show that the subtraction method is implemented correctly and working well for systems.

5.3.3 Example 2.3

In this example, we revisit Example 2 again. This time, everything is the same as it was in Example 2, except that now we have added a second dielectric sphere 3 units away, whose dielectric constants are only 0.01 units off from Example 2.2. We have

Figure 5.20: Example 2.2 illustration of physical interaction between dielectric spheres and a source charge located 0.01 units away from Sphere One's surface when Sphere Two has the same dielectric properties of background medium

Table 5.21: Example 2.2, Sphere 1 mesh point total potential absolute errors for mesh sizes 2-32

	Two-sphere system		One sphere (old)	
	1st Degree	2nd Degree	1st Degree	2nd Degree
Mesh	Abs. Error	Abs. Error	Abs. Error	Abs. Error
2	2.07×10^{-2}	1.57×10^{-2}	2.07×10^{-2}	1.57×10^{-2}
4	6.70×10^{-3}	9.20×10^{-3}	6.70×10^{-3}	9.21×10^{-3}
8	7.07×10^{-3}	2.00×10^{-3}	7.07×10^{-3}	2.00×10^{-3}
16	3.58×10^{-3}	9.56×10^{-4}	3.37×10^{-3}	9.55×10^{-4}
32	1.08×10^{-3}	3.19×10^{-4}	1.01×10^{-3}	2.35×10^{-4}

Table 5.22: Example 2.2, Sphere 1 mesh point total potential relative errors for mesh sizes 2-32

	Two-sphere system		One sphere (old)	
	1st Degree	2nd Degree	1st Degree	2nd Degree
Mesh	Rel. Error	Rel. Error	Rel. Error	Rel. Error
2	2.41×10^{-2}	2.14×10^{-2}	2.41×10^{-2}	2.14×10^{-2}
4	9.12×10^{-3}	4.03×10^{-3}	9.12×10^{-3}	4.03×10^{-3}
8	3.06×10^{-3}	1.20×10^{-3}	3.06×10^{-3}	1.21×10^{-3}
16	9.43×10^{-4}	3.01×10^{-4}	9.43×10^{-4}	3.01×10^{-4}
32	2.22×10^{-4}	7.34×10^{-5}	1.95×10^{-4}	3.22×10^{-5}

that $\lambda_o = \lambda_{1_i} = \lambda_{2_i} = 0$, $M = 16$, $n = 3$, $a = 0.1$, $\mathbf{r}_s = (0.2438162975, 0.9752651902, 0.097526519)$, and the true solution for the mesh points on Sphere 1 is found by using 1500 terms

Table 5.23: Example 2.2, Sphere 2 mesh point total potential relative errors for mesh sizes 2-32

	Sphere 2 potential errors	
	1st Degree	2nd Degree
Mesh	Rel. Error	Rel. Error
2	2.25×10^{-2}	1.21×10^{-2}
4	3.42×10^{-3}	3.29×10^{-3}
8	1.69×10^{-3}	1.52×10^{-4}
16	3.24×10^{-4}	1.13×10^{-4}
32	1.02×10^{-5}	1.34×10^{-5}

of the Legendre polynomial expansion.

Figure 5.21: Example 2.3 illustration of physical interaction where a source charge is located 0.01 units away from Sphere One, and Sphere Two has slightly perturbed dielectric constants

We compare the relative errors obtained from the one-sphere case to the relative errors on the first sphere in the system, with the perturbation present. The results between the single sphere case and the system should only differ by $\mathcal{O}(0.01)$. Table 5.24 shows this to be the case. For the relative errors in the system, the true solution is again taken to be the Legendre polynomial expansion, which completely neglects addressing the perturbation in its calculations. So the errors are found by comparing the results to a true solution without a perturbation.

Table 5.24: Example 2.3, Sphere 1 total potential absolute errors for mesh points, mesh sizes 2-32

| | Two-sphere system | | One sphere (old) | |
| | 1st Degree | 2nd Degree | 1st Degree | 2nd Degree |
Mesh	Abs. Error	Abs. Error	Abs. Error	Abs. Error
2	2.07×10^{-2}	1.614×10^{-2}	2.07×10^{-2}	1.57×10^{-2}
4	6.72×10^{-3}	8.49×10^{-3}	6.70×10^{-3}	9.21×10^{-3}
8	7.04×10^{-3}	2.84×10^{-3}	7.07×10^{-3}	2.00×10^{-3}
16	3.54×10^{-3}	1.68×10^{-3}	3.37×10^{-3}	9.55×10^{-4}
32	1.05×10^{-3}	1.10×10^{-3}	1.01×10^{-3}	2.35×10^{-4}

5.3.4   Example 2.4

In this example, we revisit Example 2 again. This time, everything is the same as it was in Example 2, except that now we have added a second "dielectric" sphere 3 units away, and have perturbed the first sphere's dielectric constants in the top and bottom to differ by 0.01. We have that $\lambda_o = \lambda_{1_i} = \lambda_{2_i} = 0$, $M = 16$, $n = 3$, $a = 0.1$, $\mathbf{r}_s = (0.2438162975, 0.9752651902, 0.097526519)$, and the true solution for the mesh points on Sphere 1 is found by using 1500 terms of the Legendre polynomial expansion.
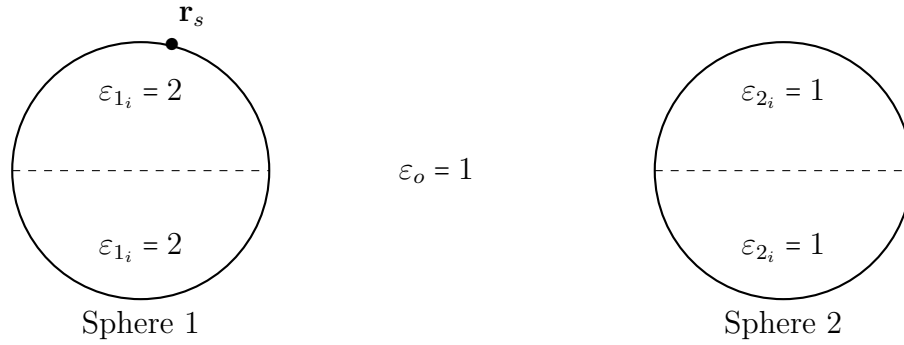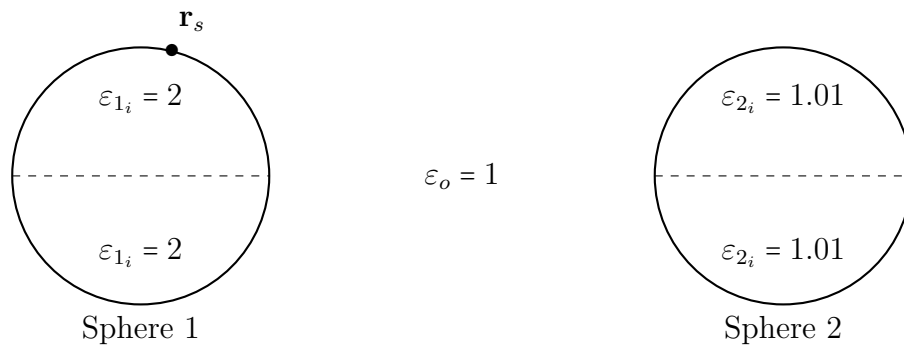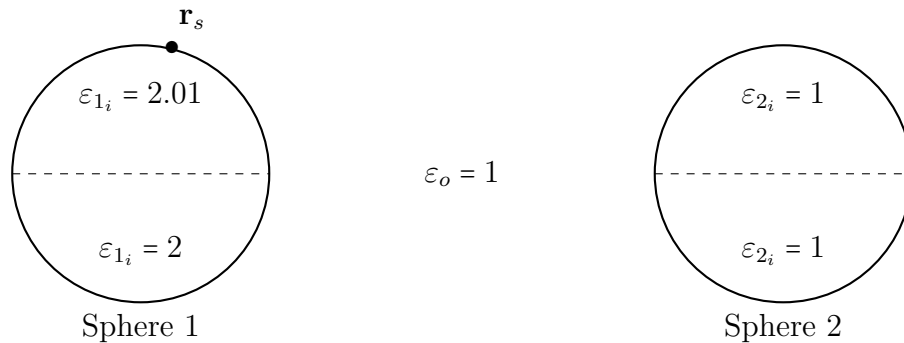

Figure 5.22: Example 2.4 illustration of physical interaction where a source charge is located 0.01 units away from Sphere One, and Sphere One has slightly perturbed dielectric constants

We compare the relative errors obtained from the one-sphere case to the relative

errors on the first sphere in the system, with the perturbation present. The results between the single sphere case and the system should only differ by $\mathcal{O}(0.01)$, as we see in Tables 5.25 and ref2.4Sphere2. For the relative errors in the system, the true solution is again taken to be the Legendre polynomial expansion, which completely neglects addressing the perturbation in its calculations. So the errors are found by comparing the results to a true solution without a perturbation.

Table 5.25: Example 2.4, Sphere 1 total potential absolute errors for mesh points, mesh sizes 2-32

| | Two-sphere system | | One sphere (old) | |
| | 1st Degree | 2nd Degree | 1st Degree | 2nd Degree |
Mesh	Abs. Error	Abs. Error	Abs. Error	Abs. Error
2	1.98×10^{-2}	1.74×10^{-2}	2.07×10^{-2}	1.57×10^{-2}
4	7.54×10^{-3}	4.06×10^{-3}	6.70×10^{-3}	9.21×10^{-3}
8	2.46×10^{-3}	1.01×10^{-2}	7.07×10^{-3}	2.00×10^{-3}
16	6.92×10^{-3}	3.62×10^{-2}	3.37×10^{-3}	9.55×10^{-4}
32	3.40×10^{-2}	3.51×10^{-2}	1.01×10^{-3}	2.35×10^{-4}

Table 5.26: Example 2.4, Sphere 2 total potential absolute errors for mesh points, mesh sizes 2-32

| | Sphere 2 potential errors | |
| | 1st Degree | 2nd Degree |
Mesh	Rel. Error	Rel. Error
2	5.44×10^{-3}	3.39×10^{-3}
4	1.15×10^{-3}	5.01×10^{-4}
8	8.71×10^{-5}	3.89×10^{-4}
16	2.69×10^{-4}	4.42×10^{-4}
32	3.99×10^{-4}	3.99×10^{-4}

5.3.5 Example 2.5

In this example, we revisit Example 2 once more. This time, everything is the same as it was in Example 2, except that now we have added a second, fake dielectric sphere 0.1 units away. We have that $\lambda_o = \lambda_{1_i} = \lambda_{2_i} = 0$, $M = 16$, $n = 3$, $a = 0.1$,

$\mathbf{r}_s = (0.2438162975, 0.9752651902, 0.097526519)$, and the true solution for the mesh

points on Sphere 1 is found by using 1500 terms of the Legendre polynomial expansion.

As we see in Tables 5.27 and 5.28, the total potential absolute errors are unaffected

by the close proximity of Sphere 2 and are identical to those already seen in Example

2.2.

Figure 5.23: Example 2.5 illustration of physical interaction where a source charge
is located 0.01 units away from Sphere One, Sphere One is "fake," with Sphere Two
close to Sphere One

Table 5.27: Example 2.5, Sphere 1 total potential absolute errors for mesh points,
mesh sizes 2-32

	Two-sphere system		One sphere (old)	
	1st Degree	2nd Degree	1st Degree	2nd Degree
Mesh	Abs. Error	Abs. Error	Abs. Error	Abs. Error
2	2.07×10^{-2}	1.57×10^{-2}	2.07×10^{-2}	1.57×10^{-2}
4	6.70×10^{-3}	9.20×10^{-3}	6.70×10^{-3}	9.21×10^{-3}
8	7.07×10^{-3}	2.01×10^{-3}	7.07×10^{-3}	2.00×10^{-3}
16	3.58×10^{-3}	9.57×10^{-4}	3.37×10^{-3}	9.55×10^{-4}
32	1.08×10^{-3}	3.19×10^{-4}	1.01×10^{-3}	2.35×10^{-4}

5.3.6 Example 2.6

In this example, we revisit Example 2 once more. Everything is the same as it was in

Example 2, except that now we have added a second dielectric sphere 0.1 units away,

Table 5.28: Example 2.5, Sphere 2 total potential absolute errors for mesh points, mesh sizes 2-32

| | Sphere 2 potential errors | |
| | 1st Degree | 2nd Degree |
Mesh	Rel. Error	Rel. Error
2	1.93×10^{-2}	1.11×10^{-2}
4	2.89×10^{-3}	2.50×10^{-3}
8	1.57×10^{-3}	3.41×10^{-4}
16	1.98×10^{-4}	8.77×10^{-5}
32	5.86×10^{-5}	1.47×10^{-5}

with perturbed dielectric constants. We have that $\lambda_o = \lambda_{1_i} = \lambda_{2_i} = 0$, $M = 16$, $n = 3$, $a = 0.1$, $\mathbf{r}_s = (0.2438162975, 0.9752651902, 0.097526519)$, and the true solution for the mesh points on Sphere 1 is found by using 1500 terms of the Legendre polynomial expansion. Again we see in Table 5.29 that the resulting perturbation in the results of the electric potential is of the expected $\mathcal{O}(|0.01|)$ compared to those errors in Table 5.27.
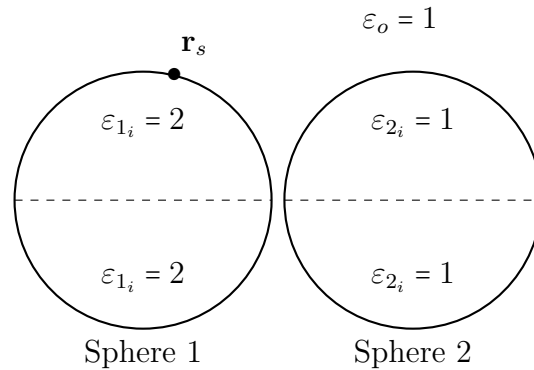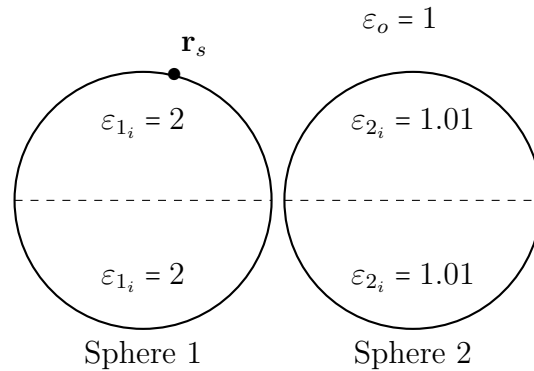

Figure 5.24: Example 2.6 illustration of physical interaction where a source charge is located 0.01 units away from Sphere One, Sphere Two close to Sphere One and has perturbed dielectric constants

Table 5.29: Example 2.6, Sphere 1 total potential absolute errors for mesh points, mesh sizes 2-32

	Two-sphere system		CPU time in seconds	
	1st Degree	2nd Degree	1st Degree	2nd Degree
Mesh	Abs. Error	Abs. Error	seconds	seconds
2	2.04×10^{-2}	1.73×10^{-2}	54	180
4	6.96×10^{-3}	7.58×10^{-3}	210	797
8	6.85×10^{-3}	4.07×10^{-3}	857	3578
16	3.37×10^{-3}	2.74×10^{-3}	3714	15952
32	8.54×10^{-4}	2.68×10^{-3}	18615	93195

5.3.7   Example 5

In this example, we investigate an entirely new interaction arrangement. We have that $\lambda_o = \lambda_{1_i} = \lambda_{2_i} = 0$, $M = 16$, $n = 3$, $a = 0.1$, $\mathbf{r}_s = (1.05, 0, 0.2)$ (approximately 0.069 units away), and the true solution for the mesh points on sphere 1 is found by using 1500 terms of the Legendre polynomial expansion. The second, fake sphere is located 0.1 units away from the first, and the source charge is located midway between those two dielectric spheres, at approximately 0.07 units distance. Since the Legendre polynomial analytic solution is again applicable to this interaction, we can verify the accuracy of the electrostatic potential in Tables 5.30 and 5.31
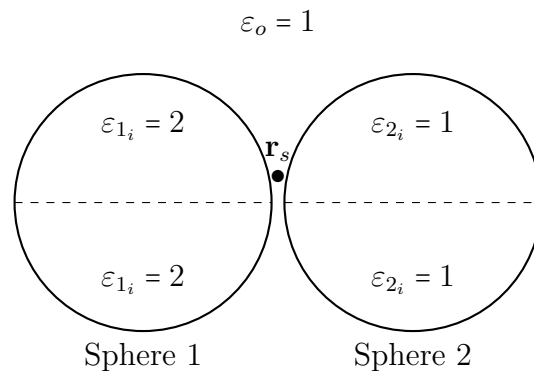

Figure 5.25: Example 5 illustration of physical interaction, where source is located 0.07 units away from either sphere, the spheres are located 0.01 units away from each other, and Sphere Two is "fake."

Table 5.30: Example 5, Sphere 1 mesh point total potential absolute errors for mesh sizes 2-32

| | Two-sphere system | | CPU time in seconds | |
| | 1st Degree | 2nd Degree | 1st Degree | 2nd Degree |
Mesh	Abs. Error	Abs. Error	seconds	seconds
2	3.67×10^{-2}	1.99×10^{-3}	73	232
4	1.10×10^{-2}	1.84×10^{-3}	269	1010
8	3.11×10^{-3}	2.26×10^{-3}	1087	4359
16	1.19×10^{-3}	6.10×10^{-4}	4601	19236
32	7.63×10^{-4}	5.13×10^{-5}	21089	97852

Table 5.31: Example 5, Sphere 2 mesh point total potential absolute errors for mesh sizes 2-32

| | Sphere 2 potential errors | |
| | 1st Degree | 2nd Degree |
Mesh	Rel. Error	Rel. Error
2	3.45×10^{-2}	1.40×10^{-3}
4	9.91×10^{-3}	1.42×10^{-3}
8	1.83×10^{-3}	1.62×10^{-3}
16	7.17×10^{-4}	3.26×10^{-4}
32	4.26×10^{-4}	1.24×10^{-5}

5.3.8 Example 6

In this example, the two spheres are 0.02 units apart. Sphere 1 is located at $(0,0,0)$ and Sphere 2 is located at $(2.02,0,0)$, with the source charge in the middle at $(1.01,0,0)$. Figure 5.27 shows the potential calculated when the subtraction method (resulting in RHS integrals) is not used. On the other hand, Figure 5.28 shows the potential calculated when the subtraction method and subsequent RHS integral grid refinement is used. We see that the potential is symmetric. Due to the unavailability of an analytic solution for this interaction, we will only show the numerical convergence of the computed solution. In Table 5.32, we see convergence in the relative error of the potential on the mesh points for mesh sizes 2-16, when we use mesh size 32 as a reference.

$$\varepsilon_o = 1$$

$\varepsilon_{1_i} = 2$ $\mathbf{r}_s$ $\varepsilon_{2_i} = 2$

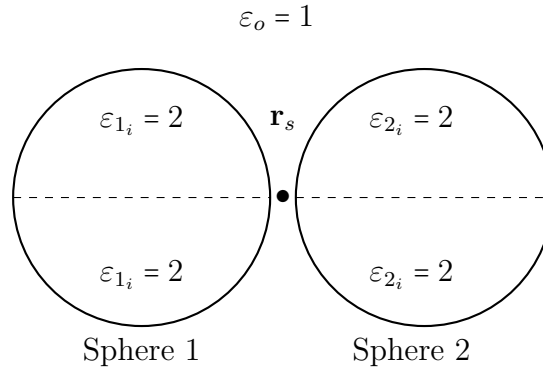$\varepsilon_{1_i} = 2$ $\varepsilon_{2_i} = 2$

Sphere 1 Sphere 2

Figure 5.26: Example 6 illustration of physical interaction, where both spheres have dielectric constants of 2 and are located 0.02 units away from each other, with source charge in the middle at 0.01 units' distance

Table 5.32: Relative error of total potential in Example 6 for mesh sizes 2-16 when mesh size 32 is used as the reference solution

Deg 1 mesh	Rel. error
2	2.62×10^0
4	7.39×10^{-1}
8	2.38×10^{-1}
16	5.9×10^{-2}

5.4 Summary

There are numerous tests and examples shown at the end of this section. The purpose of these tests is to demonstrate the accuracy and convergence of the results compared to those from a single-sphere system. The "fake" sphere in these examples is meant to make our algorithm treat the system as a pair of spheres, while the results should mimic those gotten as if there were only one. The slight variations in each example presented here are to highlight that perturbations in the dielectric values do not drastically change the results and that our methods to treat the singular behavior induced by proximity are effective for systems. In the next chapter we will re-derive the boundary integral equations to represent systems of Janus particles. This will require slightly different treatment of the Hadamard finite part integral than that for
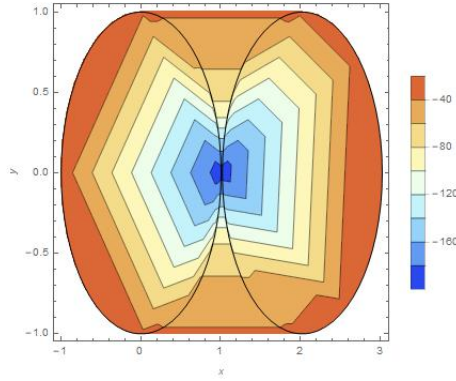
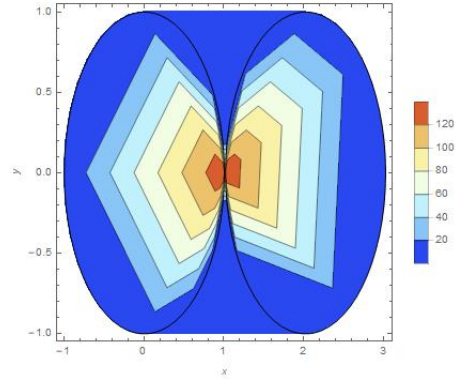Figure 5.27: Example 6 contour plot of potential for deg 1, mesh 32 for the plane z=0 without subtraction

Figure 5.28: Example 6 contour plot of potential for deg 1, mesh 32 for the plane z=0 with subtraction

systems of dielectric spheres in homogeneous media.

CHAPTER 6: Systems of Janus particles

The next step in our journey through boundary integral techniques and systems of objects leads us to consider not just a system of dielectric spheres, but a system of Janus particles. The computational framework of Janus particles is similar to that of dielectric spheres; however, Janus particles do require more care in numerical calculation due to their layered structure. The behavior and properties of the corresponding layered Green's function that exists for the interior of the particle requires that the boundary integral equations be derived in a different fashion. We seek to benefit from the same techniques that were implemented for dielectric spheres (the so-called "subtraction substitution," "bubble technique," and "patch method"), but we will have to alter the functions that are included in the subtraction substitution and how the bubble technique is used when adapting to Janus particle systems.

Further, in continuing our work in this direction, it should be noted that we have no analytic values of the electric potential generated by Janus particles with which to test our results for accuracy. Since we have observed stable and accurate computation for dielectric spheres, we will extend this to study the qualitative behavior of a system of Janus particles. As ultimately the only numerical change implemented in the BIEs is in the definitions of Green's functions and what is included in the subtraction substitution, there should be no new difficulty and we expect no different behavior in the computational stability and accuracy.

6.1 Definitions and setup

Consider a sphere in an infinite, homogeneous medium. For region Ω_j, we denote dielectric constants by ε_j and the inverse Debye Huckel lengths by λ_j. Here, Ω_o and Ω_i represents the domain inside and outside the spheroid, respectively. Similarly, the indices on the dielectric constants and inverse Debye-Huckel lengths indicate values inside and outside the sphere. Assume that there are is a charge with magnitude q_s at $\mathbf{r}_s$ located outside the sphere. For convenience, we let $q_s = 1$.
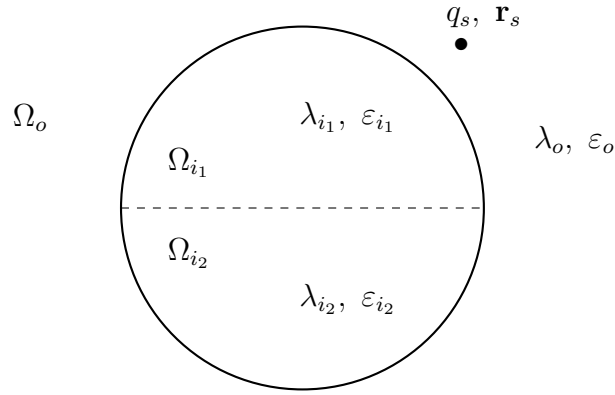
Figure 6.29: Janus particle and source charge interaction, showing layered interior domains Ω_{i_1} and Ω_{i_2} and corresponding dielectric and ionic properties

The potential field $\phi(\mathbf{r})$ at arbitrary position $\mathbf{r}$ satisfies the Poisson-Boltzmann equation

$$\nabla^2\phi(\mathbf{r}) - \lambda^2(\mathbf{r})\phi(\mathbf{r}) = -\frac{4\pi}{\varepsilon(\mathbf{r})}q_s\delta(\mathbf{r} - \mathbf{r}_s) \tag{6.1}$$

with boundary conditions

$$[\phi(\mathbf{r})] = 0 \text{ and } \left[\varepsilon(\mathbf{r})\frac{\partial\phi(\mathbf{r})}{\partial\mathbf{n}}\right] = 0, \tag{6.2}$$

where δ is the Dirac delta function and $[\cdot]$ is the jump across a boundary. Here, we

have that

$$\varepsilon(\mathbf{r}) = \begin{cases} \varepsilon_{i_1} & \mathbf{r} \in \Omega_{i_1} \\ \varepsilon_{i_2} & \mathbf{r} \in \Omega_{i_2} \\ \varepsilon_o & \mathbf{r} \in \Omega_o \end{cases}, \tag{6.3}$$

and

$$\lambda(\mathbf{r}) = \begin{cases} \lambda_{i_1} & \mathbf{r} \in \Omega_{i_1} \\ \lambda_{i_2} & \mathbf{r} \in \Omega_{i_2} \\ \lambda_o & \mathbf{r} \in \Omega_o \end{cases}. \tag{6.4}$$

Let the fundamental solution for (6.1) be given by G, where

$$G(\mathbf{r}, \mathbf{r}') = \frac{e^{-\lambda(\mathbf{r})|\mathbf{r} - \mathbf{r}'|}}{4\pi\varepsilon(\mathbf{r})|\mathbf{r} - \mathbf{r}'|}. \tag{6.5}$$

Then G satisfies the PDE

$$\varepsilon(\mathbf{r})\left[\nabla^2 G(\mathbf{r}, \mathbf{r}') - \lambda^2(\mathbf{r})G(\mathbf{r}, \mathbf{r}')\right] = -\delta(\mathbf{r} - \mathbf{r}') \tag{6.6}$$

with boundary conditions

$$[G(\mathbf{r}, \mathbf{r}')] = 0, \quad \left[\varepsilon(\mathbf{r})\frac{\partial G}{\partial \mathbf{n}}(\mathbf{r}, \mathbf{r}')\right] = 0. \tag{6.7}$$

In general, the potential $\phi(\mathbf{r})$ can be decomposed into two parts: the potential due to the source charge and the reaction field potential $\phi_{\mathrm{rf}}(\mathbf{r})$ that reflects the polarization of the material outside the sphere, Ω_o. That is,

$$\phi(\mathbf{r}) = \frac{q_s e^{-\lambda(\mathbf{r})|\mathbf{r} - \mathbf{r}_s|}}{\varepsilon(\mathbf{r})|\mathbf{r} - \mathbf{r}_s|} + \phi_{\mathrm{rf}}(\mathbf{r}). \tag{6.8}$$

For the Kelvin image location $\mathbf{x}_1$ and Jacobi-Gauss-Radau locations $\mathbf{x}_{m=2}^{M-1}$, we esti-

mate the reaction field potential using image charges [14]

$$\phi_{\text{rf}}(\mathbf{r}) \approx \sum_{m=1}^{M} \frac{q_m e^{-\lambda(\mathbf{r})|\mathbf{r}-\mathbf{x}_m|}}{\varepsilon(\mathbf{r})|\mathbf{r}-\mathbf{x}_m|}, \tag{6.9}$$

where M is a pre-determined number of image charge locations. The higher the chosen value of M, the more accurate the estimation of the reaction field potential becomes.

For practical applications where multiple spheres and charges are present, the electric potential $\phi(\mathbf{r})$ has no analytical solution and image approximations as above, and numerical methods will be needed to find approximations. When requiring that the particles and source charge(s) interact in close proximity (<0.2 units), singular behavior is observed in the layered Green's functions and requires treatment. In order to achieve better accuracy in numerical approximation of the potential, we first define a "de-singularized" solution variable such that the potential due to the source charge in (2.8) as well as the dominant part of the field from the image charges (6.9) are explicitly removed from the potential. For this purpose, we first define a function H by

$$H(\mathbf{r}, \mathbf{r}_s) = 4\pi q_s G_o(\mathbf{r}, \mathbf{r}_s), \tag{6.10}$$

where

$$G_o(\mathbf{r}, \mathbf{r}') = \frac{e^{-\lambda_o(\mathbf{r})|\mathbf{r}-\mathbf{r}'|}}{4\pi\varepsilon_o(\mathbf{r})|\mathbf{r}-\mathbf{r}'|} \tag{6.11}$$

and where H satisfies the P-B equation

$$\varepsilon_{out}[\nabla^2 H(\mathbf{r}, \mathbf{r}_s) - \lambda_o^2 H(\mathbf{r}, \mathbf{r}_s)] = -\rho(\mathbf{r}), \tag{6.12}$$

and, for the sphere Ω,

$$\rho(\mathbf{r}) = \begin{cases} 4\pi q_s \delta(\mathbf{r} - \mathbf{r}_s) & \text{if } \mathbf{r} \in \Omega_o \\ 0 & \text{if } \mathbf{r} \in \Omega_i \end{cases}. \tag{6.13}$$

Secondly, define $T(\mathbf{r}, \mathbf{r}_s)$ equal to the sum of $n < M$ screened Coulomb potential terms,

$$T(\mathbf{r}, \mathbf{r}_s) = \sum_{j=1}^{n} \frac{q_j e^{-\lambda_o |\mathbf{r} - \mathbf{x}_j|}}{\varepsilon_o |\mathbf{r} - \mathbf{x}_j|}, \tag{6.14}$$

where, for each image location $\mathbf{x}_j$ and corresponding charge value q_j, $T(\mathbf{r}, \mathbf{r}_s)$ satisfies the P-B equation

$$\varepsilon_o [\nabla^2 T(\mathbf{r}, \mathbf{r}_s) - \lambda_o^2 T(\mathbf{r}, \mathbf{r}_s)] = -\nu(\mathbf{r}), \tag{6.15}$$

and, for sphere Ω,

$$\nu(\mathbf{r}) = \begin{cases} 0 & \text{if } \mathbf{r} \in \Omega_o \\ 4\pi \sum_{j=1}^{n} \delta(\mathbf{r} - \mathbf{x}_j) & \text{if } \mathbf{r} \in \Omega_i \end{cases}. \tag{6.16}$$

6.2 Boundary integral equations for systems of Janus particles

Since we are defining the substitution variable $w(\mathbf{r})$ the same as we had for a system of dielectric spheres, and we wish for the corresponding matrix equation of BIE's to solve for $w_o(\mathbf{r})$ like we had before, the derivation of the boundary integral equations for Janus particles will be identical. Thus, we will omit the laborious parts of the derivations and simply re-write the resulting boundary integral equations of the second kind here:

$$w_{o_k}(\mathbf{p}) = \sum_{j=1}^{J} \int_{S_j} \varepsilon_o(\mathbf{r}) \left(G_i(\mathbf{r},\mathbf{p}) - G_o(\mathbf{r},\mathbf{r}_s) \right) \frac{\partial w_{o_j}(\mathbf{r})}{\partial \mathbf{n}_o} \, dS(\mathbf{r})$$

$$+ \sum_{j=1}^{J} \int_{S_j} \left(\varepsilon_o(\mathbf{r}) G_i(\mathbf{r},\mathbf{p}) \frac{\partial H(\mathbf{r},\mathbf{r}_s)}{\partial \mathbf{n}_o} - \varepsilon_i(\mathbf{r}) H(\mathbf{r},\mathbf{r}_s) \frac{\partial G_i(\mathbf{r},\mathbf{p})}{\partial \mathbf{n}_o} \right) dS(\mathbf{r})$$

$$+ \sum_{j=1}^{J} \int_{S_j} \left(\varepsilon_o(\mathbf{r}) G_i(\mathbf{r},\mathbf{p}) \frac{\partial T(\mathbf{r},\mathbf{r}_s)}{\partial \mathbf{n}_o} - \varepsilon_i(\mathbf{r}) T(\mathbf{r},\mathbf{r}_s) \frac{\partial G_i(\mathbf{r},\mathbf{p})}{\partial \mathbf{n}_o} \right) dS(\mathbf{r})$$

$$- \frac{1}{2} H(\mathbf{r},\mathbf{r}_s) - \frac{1}{2} T(\mathbf{r},\mathbf{r}_s) \tag{6.17}$$

and

$$\left(\frac{1}{2} + \frac{1}{2} \frac{\varepsilon_o(\mathbf{r})}{\varepsilon_i(\mathbf{r})} \right) \frac{\partial w_{o_k}(\mathbf{p})}{\partial \mathbf{n}_{o_k}} = \sum_{j=1}^{J} \int_{S_j} \left(\varepsilon_o(\mathbf{r}) \frac{\partial^2 G_o(\mathbf{r},\mathbf{p})}{\partial \mathbf{n}_o' \partial \mathbf{n}_o} - \varepsilon_i(\mathbf{r}) \frac{\partial^2 G_i(\mathbf{r},\mathbf{p})}{\partial \mathbf{n}_o' \partial \mathbf{n}_o} \right) w_{o_j}(\mathbf{r}) \, dS(\mathbf{r})$$

$$+ \sum_{j=1}^{J} \int_{S_j} \left(\varepsilon_o(\mathbf{r}) \frac{\partial G_i(\mathbf{r},\mathbf{p})}{\partial \mathbf{n}_o'} - \varepsilon_o(\mathbf{r}) \frac{\partial G_o(\mathbf{r},\mathbf{p})}{\partial \mathbf{n}_o'} \right) \frac{\partial w_{o_l}(\mathbf{r})}{\partial \mathbf{n}_o} \, dS(\mathbf{r})$$

$$- \sum_{j=1}^{J} \text{p.f.} \int_{S_j} \varepsilon_i(\mathbf{r}) \left(H(\mathbf{r},\mathbf{r}_s) + T(\mathbf{r},\mathbf{r}_s) \right) \frac{\partial^2 G_i(\mathbf{r},\mathbf{p})}{\partial \mathbf{n}_o' \partial \mathbf{n}_o} \, dS(\mathbf{r})$$

$$+ \sum_{j=1}^{J} \int_{S_j} \varepsilon_o(\mathbf{r}) \left(\frac{\partial H(\mathbf{r},\mathbf{r}_s)}{\partial \mathbf{n}_o} + \frac{\partial T(\mathbf{r},\mathbf{r}_s)}{\partial \mathbf{n}_o} \right) \frac{\partial G_i(\mathbf{r},\mathbf{p})}{\partial \mathbf{n}_o'} \, dS(\mathbf{r})$$

$$- \frac{1}{2} \frac{\varepsilon_o(\mathbf{r})}{\varepsilon_i(\mathbf{r})} \frac{\partial H(\mathbf{r},\mathbf{r}_s)}{\partial \mathbf{n}_{o_k}} - \frac{1}{2} \frac{\varepsilon_o(\mathbf{r})}{\varepsilon_i(\mathbf{r})} \frac{\partial T(\mathbf{r},\mathbf{r}_s)}{\partial \mathbf{n}_{o_k}}, \tag{6.18}$$

where J is the total number of Janus particles in the system and k indicates a sphere that is not necessarily the same as sphere j.

6.2.1 Special solution $v(\mathbf{r})$ and useful identity

In the boundary integral equation (6.18), just like for the dielectric sphere system, there is a set of integrals with hypersingular integrands that could use some assistance becoming less computationally cumbersome. To accomplish this, we again rely on

deriving a mathematical identity that we will apply. Let

$$\xi = -\text{p.f.} \oint \varepsilon_i(\mathbf{r})(H(\mathbf{r}, \mathbf{r}_s) + T(\mathbf{r}, \mathbf{r}_s)) \frac{\partial^2 G_i(\mathbf{r}, \mathbf{p})}{\partial \mathbf{n}'_o \partial \mathbf{n}_o} \tag{6.19}$$

denote the hypersingular ($\mathcal{O}(|\mathbf{r} - \mathbf{p}|^{-3})$) integral to be regularized. Since we are considering a system of Janus particles, this integral ξ will be calculated a total of J times, once for every particle in the system. However, as is the case in the dielectric sphere systems in Chapter 5, since $\mathbf{p}$ is fixed in (6.18), the integral ξ will only be hypersingular on one of the J, not all of them. So in practice, we only need to apply to one of the J integrals the mathematical boundary integral equation identity that we are about to derive.

Let us introduce a mathematical boundary on our sphere-particle physical setup and boundary. Construct a hemisphere of radius a and center it at the point $\mathbf{p}$ along the outside of the surface of our sphere. The hemispherical surface is denoted by Γ and the intersection of the hemisphere and the boundary of Ω is denoted by $S_a \equiv S_a(\mathbf{p})$. We call the region enclosed by this hemisphere Ω_p. For some $\mathbf{z} \in \Omega_i$, and for some constant C, let us construct some special solution for the potential of a charge at $\mathbf{z}$:

$$v(\mathbf{r}) = \frac{e^{-\lambda(\mathbf{r})|\mathbf{r} - \mathbf{z}|}}{\varepsilon(\mathbf{r})|\mathbf{r} - \mathbf{z}|} C. \tag{6.20}$$

For ease of calculating the constant C, we generally take $\mathbf{z}$ to be located in the center of the sphere, and the exact formula for C can be seen in the appendix. We now have that V satisfies
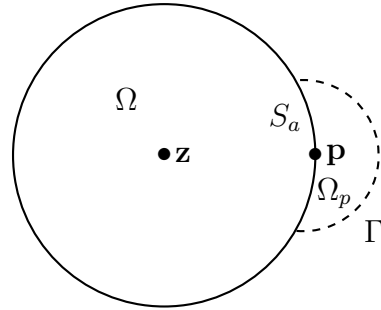

Figure 6.30: Janus particle and outward bubble for identity boundary integral equation derivation

the PDE

$$\varepsilon_o(\mathbf{r})(\nabla^2 v(\mathbf{r}) - \lambda_o^2(\mathbf{r})v(\mathbf{r})) = -C \cdot 4\pi\delta(\mathbf{r} - \mathbf{z}).$$

(6.21)

Then the PDE for $v(\mathbf{r})$ in Ω_p is given by

$$\varepsilon_o(\nabla^2 v(\mathbf{r}) - \lambda_o^2 v(\mathbf{r})) = 0.$$

(6.22)

We wish to derive the boundary integral equations for v on the domain Ω_p. The two PDE's for $\mathbf{r}'$ outside the sphere Ω are:

$$\varepsilon_o(\nabla^2 v(\mathbf{r}) - \lambda_o^2 v(\mathbf{r})) = 0$$

(6.23)

$$\varepsilon_o(\nabla^2 G_o(\mathbf{r},\mathbf{r}') - \lambda_o^2 G_o(\mathbf{r},\mathbf{r}')) = -\delta(\mathbf{r} - \mathbf{r}'),$$

(6.24)

so multiplying (6.23) by $G_o(\mathbf{r},\mathbf{r}')$ and (6.24) by $v(\mathbf{r})$, and taking their difference, we get

$$\varepsilon_o(G_o(\mathbf{r},\mathbf{r}')\nabla^2 v(\mathbf{r}) - v(\mathbf{r})\nabla^2 G_o(\mathbf{r},\mathbf{r}')) = v(\mathbf{r})\delta(\mathbf{r} - \mathbf{r}').$$

(6.25)

Integrating over $\Omega_p \cup B(\mathbf{r}',\rho)$ and using Green's identity yields

$$\oint_{\partial(\mathbb{R}^3 \setminus (\Omega_p \cup B(\mathbf{r}',\rho)))} \varepsilon_o\left(G_o(\mathbf{r},\mathbf{r}')\frac{\partial v(\mathbf{r})}{\partial \mathbf{n}} - v(\mathbf{r})\frac{\partial G_o(\mathbf{r},\mathbf{r}')}{\partial \mathbf{n}}\right) dS(\mathbf{r}) = 0,$$

which, using a previous argument, becomes

$$v(\mathbf{r}') = \oint_{S_a \cup \Gamma} \varepsilon_i\left(G_o(\mathbf{r},\mathbf{r}')\frac{\partial v(\mathbf{r})}{\partial \mathbf{n}} - v(\mathbf{r})\frac{\partial G_o(\mathbf{r},\mathbf{r}')}{\partial \mathbf{n}}\right) dS(\mathbf{r}).$$

(6.26)

Once again we introduce the notation $\mathbf{n}_o = -\mathbf{n}_i$, where $\mathbf{n}_i$ is the unit normal on the surface of the sphere, at point $\mathbf{p}$, pointing into domain Ω. Furthermore, we denote $\mathbf{n}_\Gamma$

as the outward unit normal on Γ. Instituting this new notation, (6.26) becomes

$$
\begin{aligned}
v(\mathbf{r}') = &\oint_{S_a} \varepsilon_o \left(G_o(\mathbf{r}, \mathbf{r}') \frac{\partial v(\mathbf{r})}{\partial \mathbf{n}_i} - v(\mathbf{r}) \frac{\partial G_o(\mathbf{r}, \mathbf{r}')}{\partial \mathbf{n}_i} \right) \mathrm{d}S(\mathbf{r}) \\
&+ \oint_{\Gamma} \varepsilon_o \left(G_o(\mathbf{r}, \mathbf{r}') \frac{\partial v(\mathbf{r})}{\partial \mathbf{n}_{\Gamma}} - v(\mathbf{r}) \frac{\partial G_o(\mathbf{r}, \mathbf{r}')}{\partial \mathbf{n}_{\Gamma}} \right) \mathrm{d}S(\mathbf{r})
\end{aligned}
\tag{6.27}
$$

Taking the normal derivative of (6.27) with respect to $\mathbf{r}'$

$$
\begin{aligned}
\frac{\partial v(\mathbf{r}')}{\partial \mathbf{n}_o'} = &\oint_{S_a} \varepsilon_o \left(\frac{\partial G_o(\mathbf{r}, \mathbf{r}')}{\partial \mathbf{n}_o'} \frac{\partial v(\mathbf{r})}{\partial \mathbf{n}_i} - v(\mathbf{r}) \frac{\partial^2 G_o(\mathbf{r}, \mathbf{r}')}{\partial \mathbf{n}_o' \partial \mathbf{n}_i} \right) \mathrm{d}S(\mathbf{r}) \\
&+ \oint_{\Gamma} \varepsilon_o \left(\frac{\partial G_o(\mathbf{r}, \mathbf{r}')}{\partial \mathbf{n}_o'} \frac{\partial v(\mathbf{r})}{\partial \mathbf{n}_{\Gamma}} - v(\mathbf{r}) \frac{\partial^2 G_o(\mathbf{r}, \mathbf{r}')}{\partial \mathbf{n}_o' \partial \mathbf{n}_{\Gamma}} \right) \mathrm{d}S(\mathbf{r}),
\end{aligned}
\tag{6.28}
$$

and taking the limit as $\mathbf{r}'$ approaches $\mathbf{p}$ in S from the inside yields the following identity:

$$
\begin{aligned}
\frac{1}{2} \frac{\partial v(\mathbf{p})}{\partial \mathbf{n}_o} + &\oint_{S_a} \varepsilon_o \left(\frac{\partial G_o(\mathbf{r}, \mathbf{p})}{\partial \mathbf{n}_o'} \frac{\partial v(\mathbf{r})}{\partial \mathbf{n}_o} - v(\mathbf{r}) \frac{\partial^2 G_o(\mathbf{r}, \mathbf{p})}{\partial \mathbf{n}_o' \partial \mathbf{n}_o} \right) \mathrm{d}S(\mathbf{r}) \\
&- \oint_{\Gamma} \varepsilon_o \left(\frac{\partial G_o(\mathbf{r}, \mathbf{p})}{\partial \mathbf{n}_o'} \frac{\partial v(\mathbf{r})}{\partial \mathbf{n}_{\Gamma}} - v(\mathbf{r}) \frac{\partial^2 G_o(\mathbf{r}, \mathbf{p})}{\partial \mathbf{n}_o' \partial \mathbf{n}_{\Gamma}} \right) \mathrm{d}S(\mathbf{r}) = 0.
\end{aligned}
\tag{6.29}
$$

6.2.2 Modified boundary integral equations

Notice that equation (6.29) has been mathematically derived to be in terms of the outside Green's functions. However, the integral ξ that needs regularized is written in terms of the interior Green's functions. Since the identity (6.29) is indeed derived over a mathematical boundary Γ, not a physical one, we can actually impose whatever dielectric properties over that region that we please. So far it has been convenient to impose the same dielectric properties of the region Ω_p as that of its background. But for this case, we will need to alter that arrangement and dictate that the dielectric

properties of Ω_p are the same as those in Ω. Thus notationally we will alter the Green's functions in the identity 6.29 to be $G_i(\mathbf{r}, \mathbf{r}')$ instead of $G_o(\mathbf{r}, \mathbf{r}')$.

Further, since we are modeling a system of Janus particles with the boundary integral equations, we end up needing to use *layered* Green's functions, whose dielectric properties obviously differ based on where in/on the particle a point lies. This means that for arbitrary point $\mathbf{r}$ in the identity (6.29), the Green's functions defined over the region Ω_p will also be layered and will take on whatever dielectric properties that will make the identity useful for regularization.

We now treat (6.29) as the value zero and subtract it from the appropriate integral in the boundary integral equations. But first let us split the arbitrary hypersingular integral up over the union $(S \smallsetminus S_a) \cup S_a$ and use the above identity

$$\xi = -\oint_{(S \smallsetminus S_a)} \varepsilon_i(\mathbf{r})(H(\mathbf{r}, \mathbf{r}_s) + T(\mathbf{r}, \mathbf{r}_s)) \frac{\partial^2 G_i(\mathbf{r}, \mathbf{p})}{\partial \mathbf{n}'_o \partial \mathbf{n}_o} \, dS(\mathbf{r})$$
$$- \oint_{S_a} \varepsilon_i(\mathbf{r})(H(\mathbf{r}, \mathbf{r}_s) + T(\mathbf{r}, \mathbf{r}_s)) \frac{\partial^2 G_i(\mathbf{r}, \mathbf{p})}{\partial \mathbf{n}'_o \partial \mathbf{n}_o} \, dS(\mathbf{r}). \tag{6.30}$$

Subtract 0 from ξ:

$$\xi - 0 = -\oint_{(S \smallsetminus S_a)} \varepsilon_i(\mathbf{r})(H(\mathbf{r}, \mathbf{r}_s) + T(\mathbf{r}, \mathbf{r}_s)) \frac{\partial^2 G_i(\mathbf{r}, \mathbf{p})}{\partial \mathbf{n}'_o \partial \mathbf{n}_o} \, dS(\mathbf{r})$$
$$+ \oint_{S_a} \varepsilon_i(\mathbf{r}) \left(v(\mathbf{r}) - H(\mathbf{r}, \mathbf{r}_s) - T(\mathbf{r}, \mathbf{r}_s) \right) \frac{\partial^2 G_i(\mathbf{r}, \mathbf{p})}{\partial \mathbf{n}'_o \partial \mathbf{n}_o} \, dS(\mathbf{r})$$
$$- \oint_{S_a} \varepsilon_i(\mathbf{r}) \left(\frac{\partial G_i(\mathbf{r}, \mathbf{p})}{\partial \mathbf{n}'_o} \frac{\partial v(\mathbf{r})}{\partial \mathbf{n}_o} \right) dS(\mathbf{r}) + \oint_{\Gamma} \varepsilon_i(\mathbf{r}) \left(\frac{\partial G_i(\mathbf{r}, \mathbf{p})}{\partial \mathbf{n}'_o} \frac{\partial v(\mathbf{r})}{\partial \mathbf{n}_\Gamma} \right) dS(\mathbf{r})$$
$$- \oint_{\Gamma} \varepsilon_i(\mathbf{r}) \left(v(\mathbf{r}) \frac{\partial^2 G_i(\mathbf{r}, \mathbf{p})}{\partial \mathbf{n}'_o \partial \mathbf{n}_\Gamma} \right) dS(\mathbf{r}) - \frac{1}{2} \frac{\partial v(\mathbf{p})}{\partial \mathbf{n}_o}. $$

$$\tag{6.31}$$

Again, it can be shown (in the Appendix) that the function $v(\mathbf{r}) - H(\mathbf{r}, \mathbf{r}_s) - T(\mathbf{r}, \mathbf{r}_s)$

is of order $\mathcal{O}(|\mathbf{r} - \mathbf{p}|^{-3})$. All of the values and integrals in (6.31) are therefore more readily calculable than the integral ξ by itself, as the singular behavior of the Green's functions is reduced and distributed over several more manageable integration regions.

Applying the same mapping conventions established in the last chapter and the same summing notation used in (6.18) and (6.17), we have the following resulting boundary integral equations for a system of Janus particles:

$$
\begin{aligned}
w_{o_k}(\mathbf{p}) = {}& \sum_{j=1}^{J} \int_{S_j} \varepsilon_o(\hat{\mathbf{r}}) \left(G_i(\hat{\mathbf{r}}, m_j^{-1}(m_k(\hat{\mathbf{p}}))) - G_o(\hat{\mathbf{r}}, m_j^{-1}(m_k(\hat{\mathbf{p}}))) \right) \frac{\partial w_{o_j}(\hat{\mathbf{r}})}{\partial \mathbf{n}_o} \, dS(\hat{\mathbf{r}}) \\
& + \sum_{j=1}^{J} \int_{S_j} \left(\varepsilon_o(\mathbf{r}) G_i(\mathbf{r}, \mathbf{p}) \frac{\partial H(\mathbf{r}, \mathbf{r}_s)}{\partial \mathbf{n}_o} - \varepsilon_i(\mathbf{r}) H(\mathbf{r}, \mathbf{r}_s) \frac{\partial G_i(\mathbf{r}, \mathbf{p})}{\partial \mathbf{n}_o} \right) dS(\mathbf{r}) \\
& + \sum_{j=1}^{J} \int_{S_k} \left(\varepsilon_o(\mathbf{r}) G_i(\mathbf{r}, \mathbf{p}) \frac{\partial T(\mathbf{r}, \mathbf{r}_s)}{\partial \mathbf{n}_o} - \varepsilon_i(\mathbf{r}) T(\mathbf{r}, \mathbf{r}_s) \frac{\partial G_i(\mathbf{r}, \mathbf{p})}{\partial \mathbf{n}_o} \right) dS(\mathbf{r}) \\
& - \frac{1}{2} H(\mathbf{r}, \mathbf{r}_s) - \frac{1}{2} T(\mathbf{r}, \mathbf{r}_s)
\end{aligned}
\tag{6.32}
$$

and

$$
\begin{aligned}
\left(\frac{1}{2} + \frac{1}{2} \frac{\varepsilon_o(\mathbf{r})}{\varepsilon_i(\hat{\mathbf{r}})} \right) & \frac{\partial w_{o_k}(\mathbf{p})}{\partial \mathbf{n}_{o_k}} \\
= {}& \sum_{j=1}^{J} \int_{S_j} \left(\varepsilon_o(\hat{\mathbf{r}}) \frac{\partial^2 G_o(\hat{\mathbf{r}}, m_j^{-1}(m_k(\hat{\mathbf{p}})))}{\partial \mathbf{n}_o' \partial \mathbf{n}_o} - \varepsilon_i(\mathbf{r}) \frac{\partial^2 G_i(\hat{\mathbf{r}}, m_j^{-1}(m_k(\hat{\mathbf{p}})))}{\partial \mathbf{n}_o' \partial \mathbf{n}_o} \right) w_{o_j}(\hat{\mathbf{r}}) \, dS(\hat{\mathbf{r}}) \\
& + \sum_{j=1}^{J} \int_{S_j} \left(\varepsilon_o(\hat{\mathbf{r}}) \frac{\partial G_i(\hat{\mathbf{r}}, m_j^{-1}(m_k(\hat{\mathbf{p}})))}{\partial \mathbf{n}_o'} - \varepsilon_o(\mathbf{r}) \frac{\partial G_o(\hat{\mathbf{r}}, m_j^{-1}(m_k(\hat{\mathbf{p}})))}{\partial \mathbf{n}_o'} \right) \frac{\partial w_{o_j}(\hat{\mathbf{r}})}{\partial \mathbf{n}_o} \, dS(\hat{\mathbf{r}}) \\
& - \sum_{j=1}^{J} \text{p.f.} \int_{S_j} \varepsilon_i(\mathbf{r}) \left(H(\mathbf{r}, \mathbf{r}_s) + T(\mathbf{r}, \mathbf{r}_s) \right) \frac{\partial^2 G_i(\mathbf{r}, \mathbf{p})}{\partial \mathbf{n}_o' \partial \mathbf{n}_o} \, dS(\mathbf{r}) \\
& + \sum_{j=1}^{J} \int_{S_k} \varepsilon_o(\mathbf{r}) \left(\frac{\partial H(\mathbf{r}, \mathbf{r}_s)}{\partial \mathbf{n}_o} + \frac{\partial T(\mathbf{r}, \mathbf{r}_s)}{\partial \mathbf{n}_o} \right) \frac{\partial G_i(\mathbf{r}, \mathbf{p})}{\partial \mathbf{n}_o'} \, dS(\mathbf{r}) \\
& - \int_{S_k \setminus S_{a_k}} \varepsilon_i(\mathbf{r}) \left(H(\mathbf{r}, \mathbf{r}_s) + T(\mathbf{r}, \mathbf{r}_s) \right) \frac{\partial^2 G_i(\mathbf{r}, \mathbf{p})}{\partial \mathbf{n}_o' \partial \mathbf{n}_o} \, dS(\mathbf{r}) \\
& + \int_{S_{a_k}} \varepsilon_i(\mathbf{r}) \left(v(\mathbf{r}) - H(\mathbf{r}, \mathbf{r}_s) - T(\mathbf{r}, \mathbf{r}_s) \right) \frac{\partial^2 G_i(\mathbf{r}, \mathbf{r}_s)}{\partial \mathbf{n}_o' \partial \mathbf{n}_o} \, dS(\mathbf{r}) \\
& - \int_{S_{a_k}} \varepsilon_i(\mathbf{r}) \frac{\partial G_i(\mathbf{r}, \mathbf{p})}{\partial \mathbf{n}_o'} \frac{\partial v(\mathbf{r})}{\partial \mathbf{n}_o} \, dS(\mathbf{r})
\end{aligned}
$$

$$+ \int_{\Gamma_k} \varepsilon_i(\mathbf{r}) \frac{\partial G_i(\mathbf{r},\mathbf{p})}{\partial \mathbf{n}'_o} \frac{\partial v(\mathbf{r})}{\partial \mathbf{n}_\Gamma} \, \mathrm{d}S(\mathbf{r})$$

$$- \int_{\Gamma_k} \varepsilon_i(\mathbf{r}) v(\mathbf{r}) \frac{\partial^2 G_i(\mathbf{r},\mathbf{p})}{\partial \mathbf{n}'_o \partial \mathbf{n}_\Gamma} \, \mathrm{d}S(\mathbf{r})$$

$$- \frac{1}{2} \frac{\varepsilon_o(\mathbf{r})}{\varepsilon_i(\mathbf{r})} \frac{\partial H(\mathbf{r},\mathbf{r}_s)}{\partial \mathbf{n}_{o_k}} - \frac{1}{2} \frac{\varepsilon_o(\mathbf{r})}{\varepsilon_i(\mathbf{r})} \frac{\partial T(\mathbf{r},\mathbf{r}_s)}{\partial \mathbf{n}_o} - \frac{1}{2} \frac{\partial v_l(\mathbf{p})}{\partial \mathbf{n}_{o_k}}, \tag{6.33}$$

where we take $\mathbf{n}_{o_k}$ to be the outward unit normal corresponding to sphere k, on which $\mathbf{p}$ lies.

Let the following quantities be defined as we have defined them previously, and let all other integrals simply be described as "right-hand side integrals." Consider these definitions to be flexible, in that the Green's function can either be layered or not (hence the lack of mappings in the definitions). Then we have the following matrix equation for this system of boundary integral equations:

$$S0 = \oint_S G_i(\mathbf{r},\mathbf{p}) \psi_t(\mathbf{r}) \, \mathrm{d}S(\mathbf{r}) \quad S1 = \oint_S G_o(\mathbf{r},\mathbf{p}) \psi(\mathbf{r}) \, \mathrm{d}S(\mathbf{r})$$

$$D0 = \oint_S \frac{\partial G_i(\mathbf{r},\mathbf{p})}{\partial \mathbf{n}_o} \psi_t(\mathbf{r}) \, \mathrm{d}S(\mathbf{r}) \quad D1 = \oint_S \frac{\partial G_o(\mathbf{r},\mathbf{p})}{\partial \mathbf{n}_o} \psi_t(\mathbf{r}) \, \mathrm{d}S(\mathbf{r})$$

$$D2 = \oint_S \frac{\partial G_i(\mathbf{r},\mathbf{p})}{\partial \mathbf{n}'_o} \psi_t(\mathbf{r}) \, \mathrm{d}S(\mathbf{r}) \quad D3 = \oint_S \frac{\partial G_o(\mathbf{r},\mathbf{p})}{\partial \mathbf{n}'_o} \psi_t(\mathbf{r}) \, \mathrm{d}S(\mathbf{r})$$

$$T0 = \oint_S \frac{\partial^2 G_i(\mathbf{r},\mathbf{p})}{\partial \mathbf{n}'_o \partial \mathbf{n}_o} \psi_t(\mathbf{r}) \, \mathrm{d}S(\mathbf{r}) \quad T1 = \oint_S \frac{\partial^2 G_o(\mathbf{r},\mathbf{p})}{\partial \mathbf{n}'_o \partial \mathbf{n}_o} \psi_t(\mathbf{r}) \, \mathrm{d}S(\mathbf{r})$$

$$\left[\begin{pmatrix} I & 0 \\ 0 & \left(\frac{1}{2} + \frac{1}{2}\frac{\varepsilon_o}{\varepsilon_i}\right) I \end{pmatrix} + \begin{pmatrix} (\varepsilon_i D0 - \varepsilon_o D1) & -(S0 - S1)\varepsilon_o \\ (\varepsilon_i T0 - \varepsilon_o T1) & -(D2 - D3)\varepsilon_o \end{pmatrix} \right] \begin{pmatrix} w_o \\ k_o \end{pmatrix} \tag{6.34}$$

$$= \begin{pmatrix} \text{top RHS integrals} \\ \text{bottom RHS integrals} \end{pmatrix},$$

where $\mathbf{p}$ takes different mesh points $\mathbf{r}_t$ in different rows of the matrix.

6.3   Numerical results for systems of Janus particles

In this section we explore examples involving the interactions of systems of Janus particles. Since an analytic solution of the potential does not exist except for very limited Janus particle systems [21, 2], we show that the potential is reasonable and, more importantly, improved in value using the subtraction de-singularization technique and regularization methods compared to the results without their use. We also note here that since an analytic expression of the reaction field estimate using image charges is currently not accessible for Janus particles, we use the definition of the reaction field estimate for dielectric spheres instead. While not completely accurate, we show that the results are nevertheless improved in several numerical tests. In addition, the closer the dielectric constants of the two halves of the Janus particle are to each other, the more accurate the dielectric sphere definition of the reaction field is, resulting in less error in the potential than otherwise.

6.3.1   Example 1.3

Here we revisit Example 1.2. That is, we consider the case where there is one source charge located at a familiar location in past examples $\mathbf{r}_s = (0.5, 2, 0.2)$ and two spheres spaced three units apart, one whose interior dielectric constant is two and the other whose interior dielectric constant matches that of the exterior medium. The second sphere whose interior and exterior dielectric constants are equal has the effect of making it numerically present but physically invisible. This makes it easy to compare the numerical solutions for the potential on the first sphere to those obtained for the case when modeling only the one sphere. Notice that in this example, the first sphere is not actually a Janus particle, but a dielectric sphere.

In this example, we will re-calculate Example 1.2, but force the boundary integral equations to use the Janus particle setup and therefore the layered Green's functions for the interior of the sphere. In this way we will determine if the layered Green's
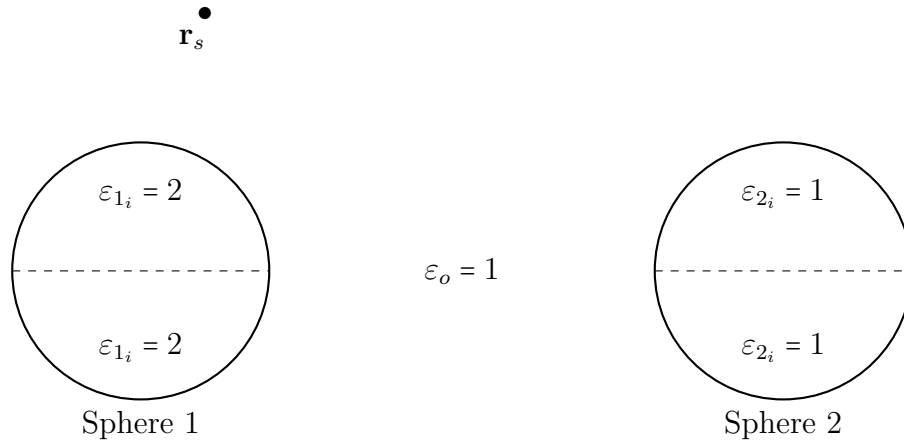
Figure 6.31: To-scale illustration of physical interaction in Example 1.3

functions maintain the level of accuracy gotten when they were not used and make sure that the boundary integral equations have been correctly derived for the Janus particle configuration. Just like before, we have taken the true solution for this example to be the Legendre polynomial expansion evaluated out to 300 terms. The errors in the tables are the errors for the potential at the mesh points of the first sphere only. We compare these errors to those we already saw for Example 1.2. As we can see in Table 6.33, the results match up almost perfectly. This is significant from a debugging standpoint, since we altered the BIE's to use an out-bubble instead of an in-bubble and then changed the interior Green's functions. So now we can be sure that the boundary integral equations have been implemented correctly.

6.3.2 Example 7

Let us take for this example two spheres set three units apart with a source charge located at $\mathbf{r}_s = (1, 1, 1)$. This source charge is approximately 0.73 units away from the surface of the first sphere, so it is not especially close in proximity. Since the source charge and second sphere are sufficiently far away, there is not singular behavior demonstrated in the Green's function kernel, making this example an easy candidate

Table 6.33: Total potential relative errors for mesh points on first sphere in Example 1.3 compared to those in Example 1.2

| | Two-sphere system | | One sphere (old) | |
| | 1st Degree | 2nd Degree | 1st Degree | 2nd Degree |
Mesh	Rel. Error	Rel. Error	Rel. Error	Rel. Error
2	6.47×10^{-3}	3.96×10^{-3}	6.46×10^{-3}	3.96×10^{-3}
4	1.94×10^{-3}	4.67×10^{-4}	1.94×10^{-3}	4.67×10^{-4}
8	5.94×10^{-4}	3.25×10^{-5}	5.94×10^{-4}	3.24×10^{-5}
16	1.94×10^{-4}	3.93×10^{-6}	1.94×10^{-4}	3.93×10^{-6}
32	5.51×10^{-5}	1.94×10^{-6}	5.51×10^{-5}	1.94×10^{-6}

for comparison purposes. In this example, the first sphere is a Janus particle, with the two dielectric constant equal to 18 and the lower dielectric constant equal to 3.9. All Debye-Hückel lengths $\lambda = 0$. The second sphere is actually a dielectric sphere, with its interior dielectric constant equal to that of the exterior medium.

Since singular behavior is not observed in this example, the potential can be easily calculated without any of the processing means developed in this paper. That means that this example is a perfect one to test the results of the methods proposed in this section - if the results for the subtraction method are very close to those without its implementation, then we show that at the very least the subtraction method has been implemented correctly in the code.

This specific example, without the second sphere, has actually been studied and published before [50]. Figure 6.33 shows the electric potential on the plane $z = 0$, using the results for a basis degree 1, mesh size 32 grid. The same parameters were used for the case of the subtraction de-singularization method and grid refinement methods developed in this paper, shown in Figure 6.34 . We see that the potential in these figures are very similar, almost exactly the same, and we therefore show that our derivations and code are working correctly (since this is an easy case that is without the necessity of singularity treatment).
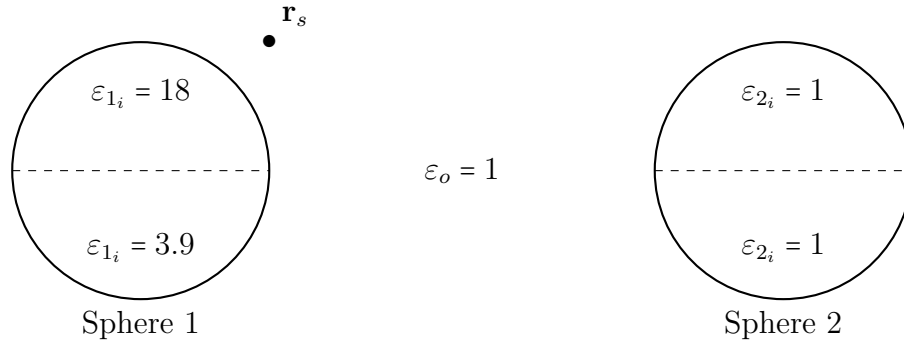
Figure 6.32: To-scale illustration of physical interaction in Example 7, the first particle is a Janus particle and the second sphere is an invisible dielectric sphere
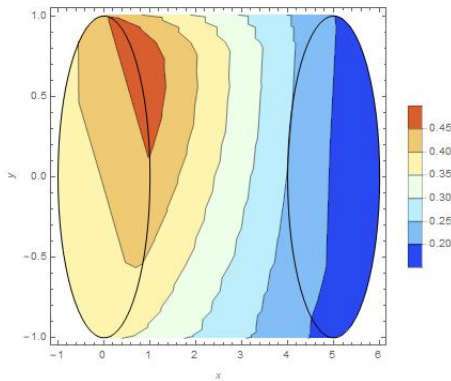

Figure 6.33: Example 7, Contour plot of potential for deg 1, mesh 32 for the plane z=0 without subtraction de-singularization
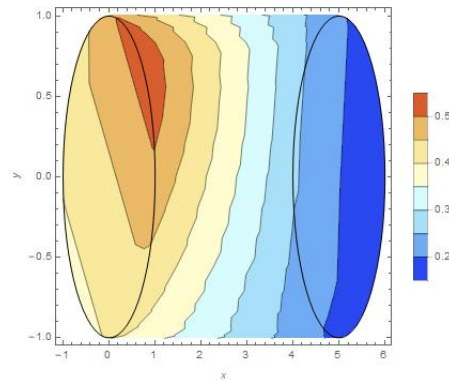

Figure 6.34: Example 7, Contour plot of potential for deg 1, mesh 32 for the plane z=0 with subtraction de-singularization

6.3.3 Example 8

This example sees two Janus particles located 0.1 units apart at centers $(0,0,0)$ and $(2.1,0,0)$, shown in Figure 6.35. The source charge is at $(1.05,0,0.2)$, which is approximately 0.069 units away from the particles, and each Janus particle has different dielectric constants in their northern and southern hemispheres of 3.0 and 2.5, respectively. All Debye-Hückel lengths $\lambda = 0$. The source charge is located sufficiently close to both particles to cause enough singular behavior that the methods developed in this paper will prove necessary.
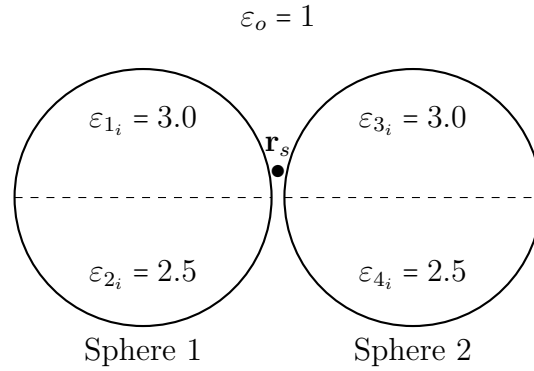
Figure 6.35: To-scale illustration of physical interaction in Example 8, where both particles have identical dielectric values in their hemispheres and the source charge is in the middle between them

We expect that the potential should reflect the symmetry shown in Figures 6.36 and 6.37, where we have sliced the system with the plane $z = 0$. The potential evaluated without the subtraction method (left) in Figure 6.36 shows negative potential values. The subtraction method and subsequent processing methods give the potential contour plot on the right, Figure 6.37, which shows stable, convergent and positive potential values for the system.
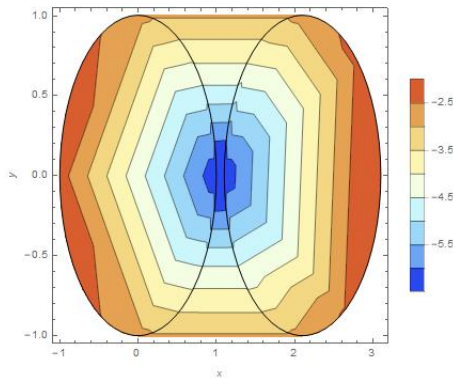

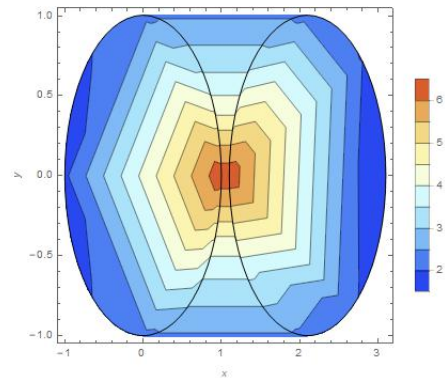Figure 6.36: Contour plot of potential for deg 1, mesh 32 for the plane z=0 without subtraction, Example 8

Figure 6.37: Contour plot of potential for deg 1, mesh 32 for the plane z=0 with subtraction, Example 8

$$\varepsilon_o = 1$$

$\mathbf{r}_s$

$\varepsilon_{1_i} = 18.0$

$\varepsilon_{3_i} = 1.0$

$\varepsilon_{2_i} = 3.9$

$\varepsilon_{4_i} = 1.0$
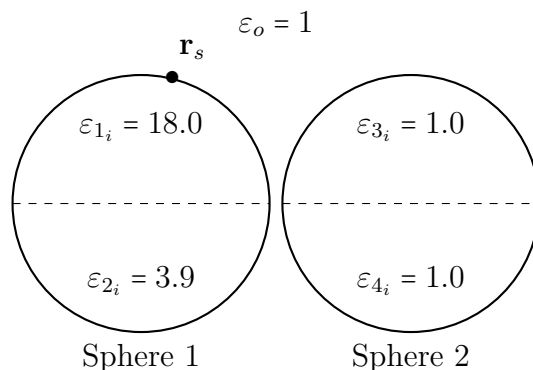
Sphere 1   Sphere 2

Figure 6.38: To-scale illustration of physical interaction in Example 9, where the source charge is located 0.01 units away from Janus Particle One and the second particle is "fake."

6.3.4   Example 9

This example sees two Janus particles located 0.02 units apart at centers (0,0,0) and (2.02,0,0). The source charge is at (0.2438162975, 0.9752651902, 0.097526519), which is 0.01 units away from sphere 1. Janus particle 1 has different dielectric constants in its northern and southern hemispheres of 18.0 and 3.9, respectively. And the second Janus particle is "fake." All Debye-Hückel lengths $\lambda = 0$. Comparing the contour plots in Figures 6.39 and 6.40 shows that the value of the potential is less singular in Figure 6.40, demonstrating that the subtraction method is improving the results.

6.3.5   Example 10

This example sees two Janus particles located 0.02 units apart at centers (0,0,0) and (2.02,0,0). The source charge is at (0.2438, 0.9752, 0.0975), which is 0.01 units away from sphere 1. Janus particle 1 has different dielectric constants in its northern and southern hemispheres of 3.0 and 2.5, respectively. And the second Janus particle is "fake." All Debye-Hückel lengths $\lambda = 0$. Comparing the contour plots in Figures 6.42 and 6.43 shows that the value of the potential is less singular in Figure 6.43, demonstrating that the subtraction method is improving the outcome of the results.

Figure 6.39: Contour plot of potential for deg 1, mesh 32 for the plane z=0 without subtraction, Example 9

Figure 6.40: Contour plot of potential for deg 1, mesh 32 for the plane z=0 with subtraction, Example 9

Figure 6.41: To-scale illustration of physical interaction in Example 10, where the source charge is located 0.01 units away from Janus Particle One and the second particle is "fake."
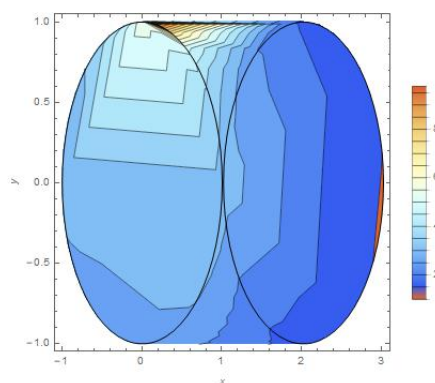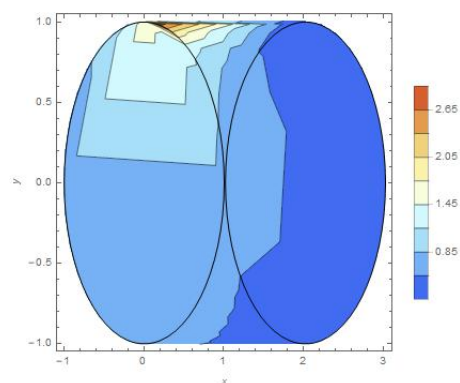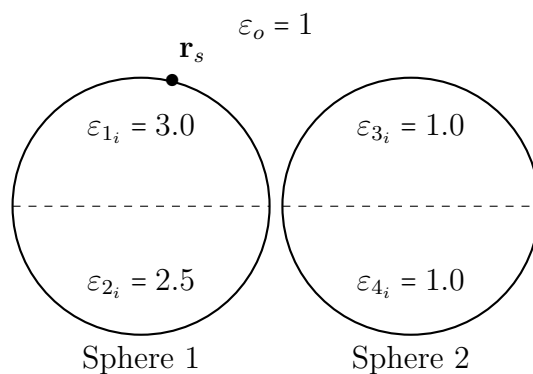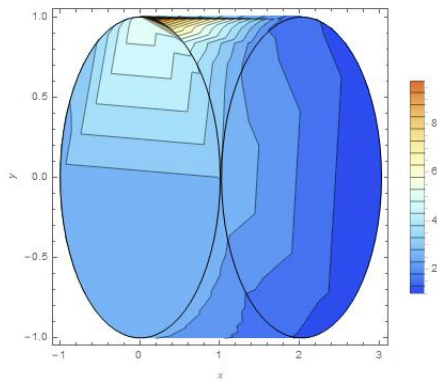
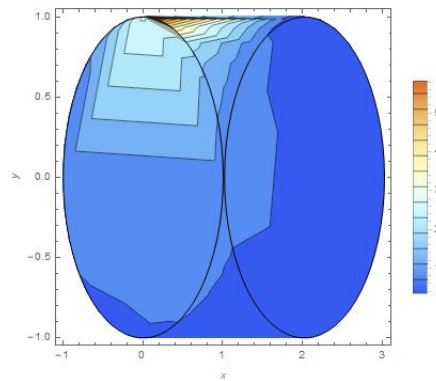Figure 6.42: Contour plot of potential for deg 1, mesh 32 for the plane z=0 without subtraction, Example 10

Figure 6.43: Contour plot of potential for deg 1, mesh 32 for the plane z=0 with subtraction, Example 10

CHAPTER 7: Conclusion

This dissertation has emphasized mathematical methods to overcome computational difficulty introduced by the singular potential due to the close proximity between charges and dielectric spheres. Such effort is much needed when considering the physical interactions on which we sought to accurately model. The first part of the conclusion will recount the physical implications of the mathematics presented here, while the second part of the conclusion will summarize the mathematical techniques implemented. The third part of the conclusion will outline possible future work.

7.1   Physical Models

The inspiration for this work was the desire to model the electric potential field for dielectric spheres and Janus particles closely interacting with each other and a source charge. Once we acquired the capability to model more than one particle, we took a step towards modeling and approximating the potential for colloidal materials, where multiple such particles interact. The electric potential around the particles influences how the particles will move and build. However, when discussing particles and materials in this context, we need the ability to calculate the potential for when the particles are very close together, as is natural for this physical case. When using boundary integral techniques, there has been a limitation to how close together objects and points can get, due to the singular nature of the fundamental solution used to derive the equations.

The model first introduced in chapter one was the interaction of one dielectric

sphere and one source charge in homogeneous media. Chapters two through four were spent deriving the boundary integral equations for that system and subsequent mathematical manipulations required to boost the accuracy of the electric potential results. This is a simple system whose electric potential can be easily calculated using Legendre polynomial expansions. We used this true solution as a comparison tool to refine our mathematical methods for the context of boundary integral equations.

Once we showed that we could get accurate results for this simple system, we could move on to larger systems, confident our methods would best serve us when a true solution was no longer available. Chapter six discussed such larger systems, where several examples of two dielectric spheres and a source charge in homogeneous media were shown. The inclusion of examples where the two-sphere system was "reduced" to the results of a one-sphere system by making the second sphere fake was meant to demonstrate that the electric potential results were still trustworthy for such larger systems. Chapter six saw us dabble in systems of Janus particles, where the dielectric properties throughout each particle are not the same.

7.2   Mathematical Methods

The derivation of hypersingular boundary integral equations for our systems meant that we already took advantage of methods previously developed to treat the singular behavior of the electric potential [50, 30]. However, in the context of source charges and other particles coming within a certain distance of each other, such methods are still insufficient at stopping the singular behavior from ruining the results gotten by solving the matrix equation. Thus, we developed and implemented multiple techniques to treat the boundary integral equations in a manner where such issues are drastically reduced.

Our first step was to re-derive the boundary integral equations using a change of variables. This change of variables resulted in the matrix equation of the boundary

integral equations containing several right-hand-side integrals, which do not contain basis functions, and which contain the bulk of the singular behavior that affects the matrix solver. Thus the matrix equation is solved in terms of the new variable and gives accurate solutions, so long as those right-hand integrals are calculated accurately. Emphasis then shifted to developing means to do so.

Treatment of the right-hand-side integrals began with introducing a hemispherical mathematical boundary and deriving a mathematical identity with which to treat the Hadamard finite part integral. This identity essentially separates the burden of the one integral into several, more manageable ones. Further, each right-hand-side integral was calculated using an adaptive Gauss quadrature, which increased accuracy of results while reducing the computational burden that traditional Gauss quadrature would impose. Each of these mathematical techniques worked together to get highly accurate results using boundary integral equations for close-body interactions.

7.3 Future Work

There are a number of aspects in which this work may be expanded and continued. Systems of a mix of dielectric spheres and Janus particles, the rotation of systems of Janus particles, systems containing more than two or three particles, and systems containing more than one source charge are more direct and immediate ideas that may be explored and implemented fairly easily using the de-singularization methods discussed in this work.

Further, another area that is largely unexplored in this dissertation is inhomogeneous media. While the mathematical framework for inhomogeneous media is discussed, we have yet to demonstrate an example due to the the reaction field term $T(\mathbf{r}, \mathbf{r}_s)$ being defined for homogeneous media only [14]. Further research must be done to derive a reaction field estimate using image charges for dielectric spheres in the presence of inhomogeneous media. While this has been done for the case when

the source charge is inside the sphere [18], it would need to be done for the case that the source is outside the sphere to be of use for the systems in this work.

Along this same vein, in order to have more accurate representations of the electrostatic potential for systems of Janus particles, we must have a reaction field estimate term $T(\mathbf{r}, \mathbf{r}_s)$ that is accurate for Janus particles. The Janus particle examples shown in this work used the dielectric sphere definition of the reaction field estimate, and while that provides improvement over the use of nothing at all, it is still technically inaccurate. As a result, further research must be done to derive a reaction field estimate using image charges in the presence of Janus particles. With this, the successful implementation and accuracy of the subtraction de-singularization technique discussed in this work is assured.

PUBLICATIONS

C. Retz, W. Cai. Accurate and Efficient Calculation of Singular Electrostatic Potentials in Charge-Dielectric Sphere Systems. *Pure and Applied Mathematics Quarterly*, To Appear, 2018.

REFERENCES

[1] *Mathematica 10.1.* Wolfram Research Inc., 2015.

[2] S. Alexander, P.M. Chaikin, P. Grant, G.J. Morales, P. Pincus. Charge renormalization, osmotic pressure, and bulk modulus of colloidal crystals: Theory. *The Journal of Chemical Physics,* Vol 80., 1984.

[3] K.E. Atkinson. A survey of numerical methods for the solution of Fredholm integral equations of the second kind. *SIAM,* 1976.

[4] C.T.H. Baker. *The Numerical Treatment of Integral Equations.* Oxford University Press, 1977.

[5] P.K. Banerjee, R. Butterfield. *Boundary Element Methods in Engineering Science.* McGraw-Hill, London, 1981.

[6] K. Barros, E. Luijten. Dielectric Effects in the Self-Assembly of Binary Colloidal Aggregates. *Physical Review Letters.* PRL 113, 017801, 2014.

[7] A.A. Becker. *The Boundary Element Method in Engineering: A Complete Course.* McGraw-Hill, 1992.

[8] C.A. Brebbia, J Dominguez. *Boundary Elements: An Introductory Course,* 2nd Ed. Computational Mechanics Publications, 1992.

[9] C.A. Brebbia, J. Dominguez. Boundary element methods for potential problems. *Applied Mathematical Modelling,* Vol. 1, pages 372-378, 1977.

[10] C.A. Brebbia. *The Boundary Element Method for Engineers.* Wiley, New York, 1978.

[11] C.A. Brebbia, J.C.F. Telles, L.C. Wrobel. *Boundary Element Techniques, Theory and Applications in Engineering.*, Springer-Verlag, Berlin, Heidelberg, 1984.

[12] C.A. Brebbia. *Progress in Boundary Element Methods*, Vol. 1. Oxford University Press, 1981.

[13] W. Cai. *Computational Methods for Electromagnetic Phenomena, First Ed.* Cambridge University Press, New York, 2013.

[14] W. Cai, S. Deng, D. Jacobs. Extending the fast multipole method to charges inside or outside a dielectric sphere. *Journal of Computational Physics* 223: 846-864, 2007.

[15] A. H.-D. Cheng, D.T. Cheng. Heritage and early history of the boundary element method. *Engineering Analysis with Boundary Elements*, Vol. **9**, Issue (3), pages 268–302, 2005.

[16] P.G. Ciarlet. *The Finite Element Method for Elliptic Problems.* North Holland Publishing, Amsterdam, 1978.

[17] M.E. Davis, J.A. McCammon. Solving the finite difference linearized Poisson-Boltzmann equation: A comparison of relaxation and conjugate gradient methods. *Journal of Computational Chemistry,* Vol. 10, Issue 3, pages 386-391, 1989.

[18] S. Deng, W. Cai. Extending the fast multipole method for charges inside a dielectric sphere in an ionic solvent: High-order image approximations for reaction fields. *Journal of Computational Physics*, pages 1246-1266, 2007.

[19] F. Fogolari, A. A. Brigo, H. Molinari. The Poisson-Boltzmann equation for biomolecular electrostatics: a tool for structural biology. *J. Mol. Recognit.*, pages 377-392, 2002.

[20] W. Gautschi. Algorithm 726: ORTHPOL - a package of routines for generating orthogonal polynomials and Gauss-type quadrature rules. *ACM Transactions on Mathematical Software,* Vol. 20, Issue 1, pages 21-62, 1994.

[21] J. de Graaf, N. Boom, M. Dijkstra, R. van Roij. Electrostatic interactions between Janus particles. *The Journal of Chemical Physics* Vol 137, 2012.

[22] T.L. Hill. *An Introduction to Statistical Thermodynamics.* Dover, New York, 1987.

[23] M. Holst, N. Baker, F. Wang. Adaptive multilevel finite element solution of the Poisson–Boltzmann equation I. Algorithms and examples. *Journal of Computational Chemistry,* Vol. 21, Issue 15, pages 1319-1342, 2000.

[24] B.H. Honig, W.L. Bubbell, R.F. Flewelling. Electrostatic interactions in membranes and proteins. *Annual Review of Biophysics and Biophysical Chemistry,* Vol. 15, pages 163-193, 1986.

[25] M.A. Jaswon , A.R. Ponter. An integral equation solution of the torsion problem. *Proceedings of the Royal Society A,* Volume 273, Issue 1353, pages 237-246, 1963.

[26] M.A. Jaswon. Integral equation methods in potential theory. I. *Proceedings of the Royal Society A* Volume 275, Issue 1360, pages 23-32, 1963.

[27] A.H. Juffer, E.F.F. Botta, B.A.M. van Keulen, A. van der Ploeg, H.J.C. Berendsen. The electric Potential of a macromolecule in a solvent: a fundamental approach. *Journal of Computational Physics* Vol 97, pages 144-171, 1991.

[28] J.C. Lachat , J.O. Watson. Effective numerical treatment of boundary integral equations: a formulation for three-dimensional elastostatics. *Int. J. Numer. Meth. Eng.*, Vol 10: pages 991-1005, 1976.

[29] H. Lin, H. Tang, W. Cai. Accuracy and efficiency in computing electrostatic potential for an ion channel model in layered dielectric/electrolyte media. *Journal of Computational Physics*. 448-512, 2013.

[30] H.M. Lin, Z.L. Xu, H.Z. Tang, W. Cai. Image Approximations to Electrostatic Potentials in Layered Electrolytes/Dielectrics and an Ion-Channel Model. *The Journal of Scientific Computing.* DOI 10.1007/s10915-011-9567-2, 2011.

[31] B. Lu, X. Cheng, J. Huang, J.A. McCammon. Order N algorithm for computation of electrostatic interactions in biomolecular systems. *Proceedings of the National Academy of Sciences of the United States of America* Vol 103, pages 19314-19319, 2006.

[32] B. Lu, Y. C. Zhou, M. J. Holst, J. A. McCammon. Recent progress in numerical methods for the Poisson-Boltzmann equation in biophysical applications. *Communications in Computational Physics*, Vol 3., pages 973-1009, 2008.

[33] B. Lu, D. Zhang, J.A. McCammon. Computation of electrostatic forces between solvated molecules determined by the Poisson–Boltzmann equation using a boundary element method. *The Journal of Chemical Physics,* Vol. 122, Issue 21, 10.1063/1.1924448, 2005.

[34] S.G. Mikhlin, *Linear Integral Equations*, Hindustan Publ., Dehli, 1960.

[35] C. Müller. *Foundations of the Mathematical Theory of Electromagnetic Waves.* Springer-Verlag, 1969.

[36] J.C. Nédélec. *Acoustic and Electromagnetic Equations: Integral Representations for Harmonic Problems.* Springer-Verlag, New York, 2001.

[37] C.W. Outhwaite, L.B. Bhuiyan. An improved modified Poisson-Boltzmann equation in electric-double-layer theory. *Jounal of the Chemical Society, Faraday Transactions2: Molecular and Chemical Physics,* Vol. 79, pages 707-718, 1983.

[38] F.J. Rizzo. An integral equation approach to boundary value problems of classical electrostatics. *Quarterly of Applied Mathematics*, Vol. 25, pages 83-95, 1967.

[39] V. Rokhlin. Solution of acoustic scattering problem by means of second kind of integral equations. *Wave Motion*, pages 257-272, 1983.

[40] Y. Saad, M.H. Schultz. GMRES: A generalized minimal residual algorithm for solving nonsymmetric linear systems. *SIAM Journal on Scientific and Statistical Computing,* Vol. 7, Issue 3, pages 856-869, 1986.

[41] R.P. Sheridan, R.M. Levy, F.R. Salemme. Alpha-Helix dipole model and electrostatic stabilization of 4-alpha-helical proteins. *Proceedings of the National Academy of Sciences of the Unites States of America,* Vol. 79, Issue 15, pages 4545-4549, 1982.

[42] W. C. Still, A. Tempczyk, R. R. Hawkley, T. Hendrickson. Semianalytical treatment of solvation for molecular mechanics and dynamics. *Journal of the American Chemical Society*, pages 6127-6129, 1990.

[43] A.H. Stroud, D. Secrest. *Gaussian Quadrature Formulas,* Prentice-Hall, New Jersey, 1966.

[44] G.T. Symm. Integral equation methods in potential theory, II. *Proceedings of the Royal Society A* Volume 275, Issue 1360, pages 33–46, 1963.

[45] W.L.K. Thomson. *Reprint of Papers on Electrostatics and Magnetism,* 2nd Ed. London: Macmillan, 1884.

[46] E.J.W. Verwey, J.T.G. Overbeek. *Theory of the Stability of Lyophobic Colloids.* Elsevier, New York, 1948.

[47] A. Walther, A.H.E. Müller. Janus Particles: Synthesis, Self-Assembly, Physical Properties and Applications. *Chemical Reviews.* 5194-5261, 2013.

[48] Z. L. Xu, W. Cai. Fast analytical methods for macroscopic electrostatic models in biomolecular simulations. *SIAM Review*, pages 683-720, 2011.

[49] C.H. Yan, W. Cai, X. Zeng. A parallel method for solving Laplace equations with Dirichlet data using local boundary integral equations and random walks. *SIAM Journal of Scientific Computing.* Vol 35, No. 4: B868-B889, 2013.

[50] B. Zinser, W. Cai. A well-conditioned hypersingular boundary element method for electrostatic potentials in the presence of inhomogeneities within layered media. *Communication in Computational Physics.* Vol 19, No. 4: 970-997, 2016.

APPENDIX A: ANGLES TO USE IN INTEGRAL DOMAINS
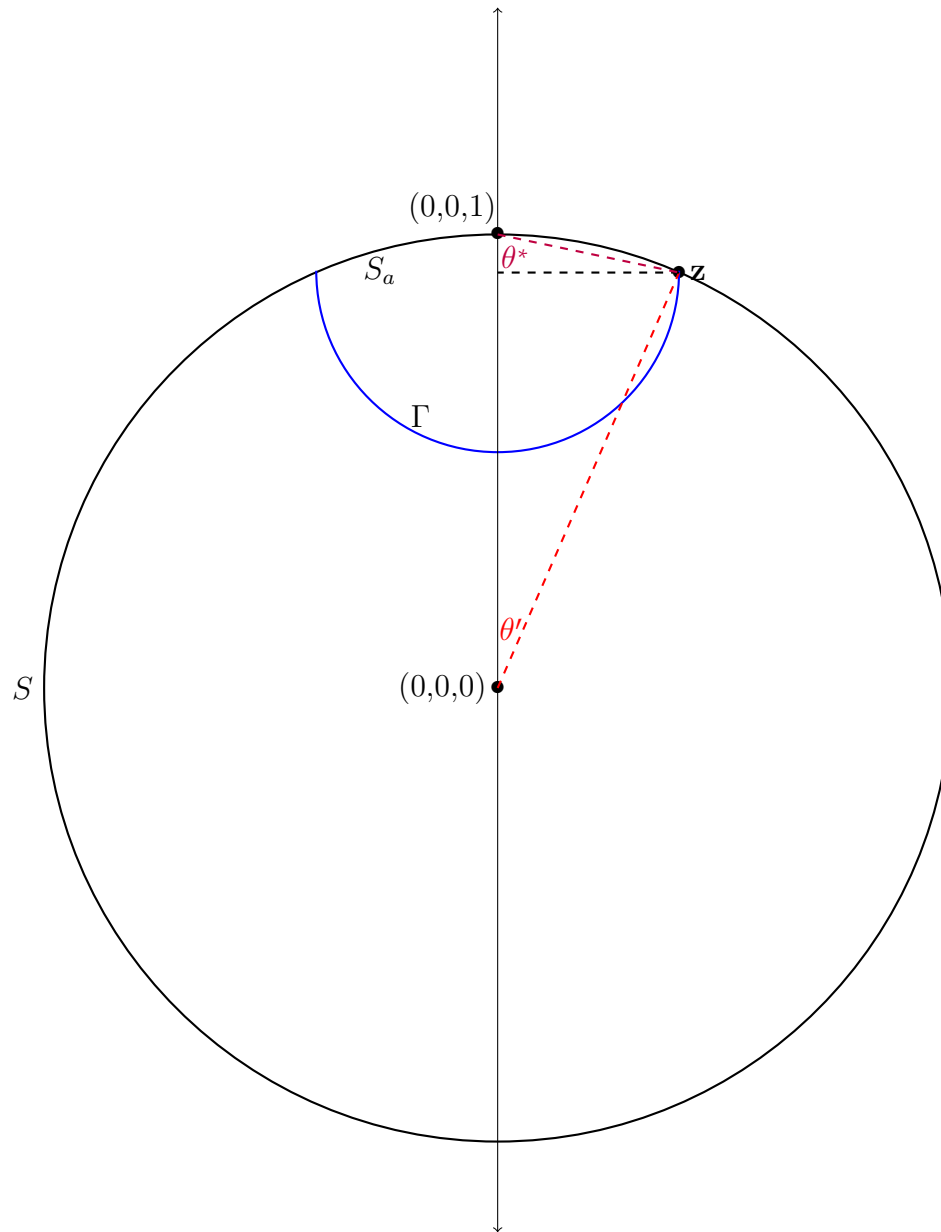
Figure A.44: Finding necessary angles when integrating over surface of sphere

We need to find z, the value where the hemisphere Γ intersects the sphere S. To do that, we consider the intersection of the two spheres. Since the singularity $\mathbf{p}$ is at the north pole, z will be the same value for the whole circle C that will be the curve of intersection of the two spheres. The equation for the larger sphere S (of radius

one) is given by

$$x^2 + y^2 + z^2 = 1.$$

The equation for a sphere of radius a centered at the point $(0, 1)$ is given by

$$x^2 + y^2 + (z - 1)^2 = a^2.$$

Subtracting these two equations gives

$$z^2 - (z - 1)^2 = 1 - a^2$$

Solving this equation for z, we get $z = \dfrac{2 - a^2}{2}$. Now we need to determine the bounds of integration of Θ for both the sphere and the hemisphere.

We see from the figure that $z* = 1 - z = a\cos(\theta^*)$ and $z = \cos(\theta')$. From both of these equations we can solve for θ^* and θ'. So, for example, integrating over the surface of the hemisphere means integrating over Θ from $\pi - \theta^*$ to π. Furthermore, integrating over the surface of the sphere S, omitting region S_a, means integrating over Θ from θ' to π.

APPENDIX B: MATRIX EQUATION FOR FIRST KIND BIE'S

Here we write the matrix equation for the boundary integral equations of the first kind. Using the same notation and integral designations as we did for the second kind matrix equation, we have that the first kind equations (2.34) and (2.29) form the following system:

$$
\left[\begin{pmatrix} \frac{1}{2}I & 0 \\ \frac{1}{2}I & 0 \end{pmatrix} + \begin{pmatrix} -\varepsilon_o D1 & S1\varepsilon_o \\ -\varepsilon_i D0 & S0\varepsilon_o \end{pmatrix} \right] \begin{pmatrix} w_o \\ k_o \end{pmatrix} = \begin{pmatrix} 0 \\ J0 + J1 + L1 + L2 \end{pmatrix}
$$

APPENDIX C: Value of constant C for special solution $v(\mathbf{r})$

A crucial step in the regularization of the hyper-singular integral is the use of $v(\mathbf{r}) - H(\mathbf{r}, \mathbf{r}_s) - T(\mathbf{r}, \mathbf{r}_s)$ as being of order $\mathcal{O}(|\mathbf{r} - \mathbf{p}|)$. This reduced the integral from being hypersingular to being strongly singular. Requiring that $f(\mathbf{r}) = v(\mathbf{r}) - H(\mathbf{r}, \mathbf{r}_s) - T(\mathbf{r}, \mathbf{r}_s) = 0$ at the mesh point $\mathbf{p}$ and using a Taylor expansion

$$f(\mathbf{r}) = f(\mathbf{p}) + f'(\mathbf{p})(\mathbf{r} - \mathbf{p}) = 0 + f'(\mathbf{p})(\mathbf{r} - \mathbf{p}), \tag{C.1}$$

we show the required order. Now we must derive the value of the constant C, which will be shown here. From the definitions, we have that

$$v(\mathbf{r}) = C\frac{e^{-\lambda_i|\mathbf{r}-\mathbf{z}|}}{\varepsilon_i|\mathbf{r}-\mathbf{z}|} \tag{C.2}$$

$$H(\mathbf{r}) = 4\pi G_o(\mathbf{r}, \mathbf{r}_s) = \frac{e^{-\lambda_o|\mathbf{r}-\mathbf{r}_s|}}{\varepsilon_o|\mathbf{r}-\mathbf{r}_s|} \tag{C.3}$$

$$T(\mathbf{r}, \mathbf{r}_s) = \frac{q_k e^{-\lambda_o|\mathbf{r}-\mathbf{r}_k|}}{\varepsilon_o|\mathbf{r}-\mathbf{r}_k|} + \frac{q_1 e^{-\lambda_o|\mathbf{r}-\mathbf{x}_1|}}{\varepsilon_o|\mathbf{r}-\mathbf{x}_1|} + \frac{q_2 e^{-\lambda_o|\mathbf{r}-\mathbf{x}_2|}}{\varepsilon_o|\mathbf{r}-\mathbf{x}_2|} + \cdots \tag{C.4}$$

We require that

$$
\begin{aligned}
v(\mathbf{p}) &= H(\mathbf{p}, \mathbf{r}_s) + T(\mathbf{p}, \mathbf{r}_s) + \cdots \\
C\frac{e^{-\lambda_i|\mathbf{p}-\mathbf{z}|}}{\varepsilon_i|\mathbf{p}-\mathbf{z}|} &= \frac{e^{-\lambda_o|\mathbf{p}-\mathbf{r}_s|}}{\varepsilon_o|\mathbf{p}-\mathbf{r}_s|} + \frac{q_k e^{-\lambda_o|\mathbf{p}-\mathbf{r}_k|}}{\varepsilon_o|\mathbf{p}-\mathbf{r}_k|} + \frac{q_1 e^{-\lambda_o|\mathbf{r}-\mathbf{x}_1|}}{\varepsilon_o|\mathbf{p}-\mathbf{x}_1|} + \frac{q_2 e^{-\lambda_o|\mathbf{r}-\mathbf{x}_2|}}{\varepsilon_o|\mathbf{p}-\mathbf{x}_2|} + \cdots \\
C &= \left(\frac{e^{-\lambda_o|\mathbf{p}-\mathbf{r}_s|}}{\varepsilon_o|\mathbf{p}-\mathbf{r}_s|} + \frac{q_k e^{-\lambda_o|\mathbf{p}-\mathbf{r}_k|}}{\varepsilon_o|\mathbf{p}-\mathbf{r}_k|} + \frac{q_1 e^{-\lambda_o|\mathbf{r}-\mathbf{x}_1|}}{\varepsilon_o|\mathbf{p}-\mathbf{x}_1|} + \frac{q_2 e^{-\lambda_o|\mathbf{r}-\mathbf{x}_2|}}{\varepsilon_o|\mathbf{p}-\mathbf{x}_2|}\right)\frac{\varepsilon_i|\mathbf{p}-\mathbf{z}|}{e^{-\lambda_i|\mathbf{p}-\mathbf{z}|}} + \cdots \\
C &= \frac{\varepsilon_i|\mathbf{p}-\mathbf{z}|}{\varepsilon_o|\mathbf{p}-\mathbf{r}_s|}e^{\lambda_i|\mathbf{p}-\mathbf{z}|-\lambda_o|\mathbf{p}-\mathbf{r}_s|} + \frac{q_k\varepsilon_i|\mathbf{p}-\mathbf{z}|}{\varepsilon_o|\mathbf{p}-\mathbf{r}_k|}e^{\lambda_i|\mathbf{p}-\mathbf{z}|-\lambda_o|\mathbf{p}-\mathbf{r}_k|} + \frac{q_1\varepsilon_i|\mathbf{p}-\mathbf{z}|}{\varepsilon_o|\mathbf{p}-\mathbf{x}_1|}e^{\lambda_i|\mathbf{p}-\mathbf{z}|-\lambda_o|\mathbf{p}-\mathbf{x}_1|} \\
&\quad + \frac{q_2\varepsilon_i|\mathbf{p}-\mathbf{z}|}{\varepsilon_o|\mathbf{p}-\mathbf{x}_2|}e^{\lambda_i|\mathbf{p}-\mathbf{z}|-\lambda_o|\mathbf{p}-\mathbf{x}_2|} + \cdots
\end{aligned}
\tag{C.5}
$$

APPENDIX D: TRUE SOLUTION OF POTENTIAL

The true solution for the potential on the outside of the dielectric sphere, for a source charge located outside on the polar axis, was taken to be the Legendre polynomial expansion given below, taken to a case-by-case sufficient number of terms. For $r = r(x, y, z)$, $\theta = \theta(x, y, z)$, a equalling the radius of the sphere, $\gamma = \frac{\varepsilon_i - \varepsilon_o}{\varepsilon_i + \varepsilon_o}$, and $P_n(\cos(\theta))$ being the nth Legendre polynomial:

$$\phi(r, \theta) = 4\pi \sum_{n=0}^{\infty} C(r) P_n(\cos(\theta)), \tag{D.6}$$

where $C(r)$ is given by

$$C(r) = \frac{q}{4\pi\varepsilon_o r_s} \left(\frac{r}{r_s}\right)^n - D_n \frac{1}{r^{n+1}}, \tag{D.7}$$

and D_n is the constant given by

$$D_n = \frac{q}{4\pi\varepsilon_o} \frac{a^{2n+1}}{r_s^{n+1}} \gamma \left(1 - \frac{1 - \gamma}{1 - \gamma + 2n}\right) \tag{D.8}$$

The normal derivative of (D.6) is

$$\frac{\partial \phi}{\partial \mathbf{n}} = \left(\frac{\partial \phi}{\partial x}, \frac{\partial \phi}{\partial y}, \frac{\partial \phi}{\partial z}\right) \cdot \mathbf{n},$$

where, by product rule,

$$\frac{\partial \phi}{\partial x_i} = 4\pi \sum_{n=0}^{\infty} \left(\frac{\partial C(r)}{\partial x_i} P_n(\cos(\theta)) + C(r) P_n'(\cos(\theta)) \frac{\partial}{\partial x_i}(\cos(\theta))\right). \tag{D.9}$$

The various pieces of (D.9) that are functions are further described here. We write

$$|\mathbf{r}| = r = \sqrt{x^2 + y^2 + z^2} \tag{D.10}$$

$$\cos(\theta) = \frac{\mathbf{r} \cdot \mathbf{r}_s}{rr_s} = \frac{xr_{s_1} + yr_{s_2} + zr_{s_3}}{r_s\sqrt{x^2 + y^2 + z^2}}, \tag{D.11}$$

$$\frac{\partial C(r)}{\partial x_i} = \frac{q}{4\pi\varepsilon_o r_s} n \left(\frac{r}{r_s}\right)^{n-1} \frac{\partial r}{\partial x_i} + D_n(n+1)\frac{1}{r^{n+2}}\frac{\partial r}{\partial x_i} \tag{D.12}$$

APPENDIX E: DERIVATION OF INTEGRAL EQUATIONS

Here we derive equations (2.28) and (2.33) from equations (2.25) and (2.32), respectively.

E.1   Outside BIE

For the outside integral equation, we have

$$\int_{\mathbb{R}^3 \smallsetminus (\Omega \cup B(\mathbf{r}',\rho))} \varepsilon_o \left(G_o(\mathbf{r},\mathbf{r}')\nabla^2 w_o(\mathbf{r}) - w_o(\mathbf{r})\nabla^2 G_o(\mathbf{r},\mathbf{r}') \right) \mathrm{d}\mathbf{r} = 0 \qquad (\text{E.13})$$

Now we can apply Green's second identity. The boundary of $\mathbb{R}^3 \smallsetminus (\Omega \cup B(\mathbf{r}',\rho))$ is split into four parts,

$$0 = I + II + III + IV$$

Part I: The integral on the infinite interface. As both $G(\mathbf{r},\mathbf{r}')$ and $w(\mathbf{r})$ vanish at infinity, $I = 0$.

Part II: The integral on the interface of the layered structure (if any exists). By the boundary conditions, the terms in the integral cancel and $II = 0$.

Part III: The integral on the surface of the sphere.

$$IV = -\oint_S \varepsilon_o \left(G_o(\mathbf{r},\mathbf{r}')\frac{\partial w(\mathbf{r})}{\partial \mathbf{n}} - w(\mathbf{r})\frac{\partial G_o(\mathbf{r},\mathbf{r}')}{\partial \mathbf{n}} \right) \mathrm{d}S(\mathbf{r}).$$

Part IV: The integral on $\partial B(\mathbf{r}',\rho)$:

$$IV = \oint_{\partial B(\mathbf{r}',\rho)} \varepsilon_o \left(G_o(\mathbf{r},\mathbf{r}')\frac{\partial w_o(\mathbf{r})}{\partial \mathbf{n}} - w(\mathbf{r})\frac{\partial G_o(\mathbf{r},\mathbf{r}')}{\partial \mathbf{n}} \right) \mathrm{d}S(\mathbf{r}) \qquad (\text{E.14})$$

For fixed $\mathbf{r}'$ on $B(\mathbf{r}', \rho)$, we have that

$$|G(\mathbf{r}, \mathbf{r}')| = \left| \frac{1}{4\pi} \frac{e^{-i\lambda|\mathbf{r}-\mathbf{r}'|}}{|\mathbf{r} - \mathbf{r}'|} \right| = \left| \frac{1}{4\pi} \frac{e^{-i\lambda\rho}}{\rho} \right|$$

and

$$\left| \frac{\partial G(\mathbf{r}, \mathbf{r}')}{\partial \mathbf{n}} \right| = \left| \frac{\partial G(\mathbf{r}, \mathbf{r}')}{\partial \mathbf{r}} \right| = \left| \frac{1}{4\pi} \left(\frac{-i\lambda e^{-i\lambda|\mathbf{r}-\mathbf{r}'|}}{|\mathbf{r} - \mathbf{r}'|} - \frac{e^{-i\lambda|\mathbf{r}-\mathbf{r}'|}}{|\mathbf{r} - \mathbf{r}'|^2} \right) \right|$$

$$\leq \left| \frac{1}{4\pi} \left(\frac{-i\lambda e^{-i\lambda\rho}}{\rho} - \frac{e^{-i\lambda\rho}}{\rho^2} \right) \right|$$

We break integral IV into three pieces whose sum is IV:

$$\begin{aligned}
IV = &\lim_{\rho \to 0} \oint_{\partial B(\mathbf{r}', \rho)} G(\mathbf{r}, \mathbf{r}') \frac{\partial w(\mathbf{r})}{\partial \mathbf{n}} \, dS(\mathbf{r}) \\
&- \lim_{\rho \to 0} \oint_{\partial B(\mathbf{r}', \rho)} \frac{\partial G(\mathbf{r}, \mathbf{r}')}{\partial \mathbf{n}} (w(\mathbf{r}) - w(\mathbf{r}')) \, dS(\mathbf{r}) \\
&- \lim_{\rho \to 0} \oint_{\partial B(\mathbf{r}', \rho)} w(\mathbf{r}') \frac{\partial G(\mathbf{r}, \mathbf{r}')}{\partial \mathbf{n}} \, dS(\mathbf{r})
\end{aligned} \tag{E.15}$$

Now each of these three integrals behave a certain way in the limit as $\rho \to 0$

1)

$$\begin{aligned}
\lim_{\rho \to 0} \left| \oint_{\partial B(\mathbf{r},', \rho)} G(\mathbf{r}, \mathbf{r}') \frac{\partial w(\mathbf{r})}{\partial \mathbf{n}} \, dS(\mathbf{r}) \right| &\leq \sup \left| \frac{\partial w(\mathbf{r})}{\partial \mathbf{n}} \right| \oint_{\partial B(\mathbf{r}', \rho)} |G(\mathbf{r}, \mathbf{r}')| \, dS(\mathbf{r}) \\
&= \lim_{\rho \to 0} \sup \left| \frac{\partial w(\mathbf{r})}{\partial \mathbf{n}} \right| \cdot \left| \frac{1}{4\pi} \frac{e^{-i\lambda\rho}}{\rho} \right| \cdot 4\pi\rho^2 \\
&= \lim_{\rho \to 0} \sup \left| \frac{\partial w(\mathbf{r})}{\partial \mathbf{n}} \right| \cdot \left| \rho e^{-i\lambda\rho} \right| \to 0 \text{ as } \rho \to 0
\end{aligned} \tag{E.16}$$

and

2)

$$\lim_{\rho \to 0} \oint_{\partial B(\mathbf{r}',\rho)} \frac{\partial G(\mathbf{r},\mathbf{r}')}{\partial \mathbf{n}}(w(\mathbf{r}) - w(\mathbf{r}'))\,\mathrm{d}S(\mathbf{r})$$

$$\leq \lim_{\rho \to 0} \sup_{\mathbf{r},\mathbf{r}' \in B} |w(\mathbf{r}) - w(\mathbf{r}')| \oint_{\partial B(\mathbf{r}',\rho)} \frac{\partial G(\mathbf{r},\mathbf{r}')}{\partial \mathbf{n}}\,\mathrm{d}S(\mathbf{r})$$

$$= \lim_{\rho \to 0} \sup_{\mathbf{r},\mathbf{r}' \in B} |w(\mathbf{r}) - w(\mathbf{r}')| \cdot \frac{1}{4\pi}\left(\frac{-i\lambda e^{-i\lambda\rho}}{\rho} - \frac{e^{-i\lambda\rho}}{\rho^2} \right) \cdot 4\pi\rho^2$$ \hfill (E.17)

$$\to 0 \text{ as } \rho \to 0 \qquad (\text{as } w(\mathbf{r}) = w(\mathbf{r}'))$$

3)

$$\lim_{\rho \to 0} w(\mathbf{r}') \oint_{\partial B(\mathbf{r}',\rho)} \frac{\partial G(\mathbf{r},\mathbf{r}')}{\partial \mathbf{n}}\,\mathrm{d}S(\mathbf{r})$$

$$= \lim_{\rho \to 0} -w(\mathbf{r}') \oint_{\partial B(\mathbf{r}',\rho)} \frac{1}{4\pi}\left(\frac{-i\lambda e^{-i\lambda\rho}}{\rho} - \frac{e^{-i\lambda\rho}}{\rho^2} \right)\,\mathrm{d}S(\mathbf{r})$$

$$= \lim_{\rho \to 0} -w(\mathbf{r}')\left(\frac{1}{4\pi}\left(\frac{-i\lambda e^{-i\lambda\rho}}{\rho} - \frac{e^{-i\lambda\rho}}{\rho^2} \right) \right) \cdot 4\pi\rho^2$$ \hfill (E.18)

$$= \lim_{\rho \to 0} -w(\mathbf{r}')\left(-i\lambda\rho e^{-i\lambda\rho} - e^{-i\lambda\rho} \right)$$

$$\to w(\mathbf{r}')(1) \text{ as } \rho \to 0$$

Now adding 1) +2) +3) together, we have that

$$IV = -w(\mathbf{r}') \text{ as } \rho \to 0$$

Finally, combining parts I - IV yields (2.28):

$$w_o(\mathbf{r}') = \oint_S \varepsilon_o \left(w_o(\mathbf{r})\frac{\partial G_o(\mathbf{r},\mathbf{r}')}{\partial \mathbf{n}} - G_o(\mathbf{r},\mathbf{r}')\frac{\partial w_o(\mathbf{r})}{\partial \mathbf{n}} \right)\,\mathrm{d}S(\mathbf{r})$$

E.2   Inside BIE

For the inside integral equation, we have

$$\int_{\Omega \smallsetminus B(\mathbf{r}',\rho)} \varepsilon_i (G_i(\mathbf{r},\mathbf{r}')\nabla^2 w_i(\mathbf{r}) - w_i(\mathbf{r})\nabla^2 G_i(\mathbf{r},\mathbf{r}')) \, \mathrm{d}S(\mathbf{r}) = 0.$$

We apply Green's second identity and split the boundary of $\Omega \smallsetminus B(\mathbf{r}',\rho)$ into three parts so that

$$I + II + III = 0.$$

Part I: The integral on the interface of the layered structure (if any exists). By the boundary conditions, the terms in the integral cancel and $I = 0$.

Part II: The integral on the surface of the sphere

$$II = \oint_S \varepsilon_i \left(G_i(\mathbf{r},\mathbf{r}')\frac{\partial w(\mathbf{r})}{\partial \mathbf{n}} - w(\mathbf{r})\frac{\partial G_i(\mathbf{r},\mathbf{r}')}{\partial \mathbf{n}} \right) \mathrm{d}S(\mathbf{r}).$$

Part III: The integral on $\partial B(\mathbf{r}',\rho)$ (using the same argument as we did for part IV of outside BIE)

$$III = \oint_{\partial B(\mathbf{r}',\rho)} \varepsilon_i \left(G_i(\mathbf{r},\mathbf{r}')\frac{\partial w(\mathbf{r})}{\partial \mathbf{n}} - w(\mathbf{r})\frac{\partial G_i(\mathbf{r},\mathbf{r}')}{\partial \mathbf{n}} \right) \mathrm{d}S(\mathbf{r})$$

$$= -w(\mathbf{r}') \text{ as } \rho \to 0$$

Combining I - III yields (2.33):

$$w_i(\mathbf{r}') = \oint_S \varepsilon_i \left(G_i(\mathbf{r},\mathbf{r}')\frac{\partial w_i(\mathbf{r})}{\partial \mathbf{n}} - w_i(\mathbf{r})\frac{\partial G_i(\mathbf{r},\mathbf{r}')}{\partial \mathbf{n}} \right) \mathrm{d}S(\mathbf{r})$$

APPENDIX F: DERIVATION OF IDENTITY ON OUT/IN BUBBLE

When deriving a boundary equation for bubble domain Ω_p, regardless of whether the hemisphere is superimposed on the outside or inside of the sphere, we end up with the following boundary equation, where $\partial\Omega_p = S_a \cup \Gamma$:

$$v(\mathbf{r}') = \oint_{S_a \cup \Gamma} \varepsilon(\mathbf{r}) \left(G(\mathbf{r},\mathbf{r}') \frac{\partial v(\mathbf{r})}{\partial \mathbf{n}} - v(\mathbf{r}) \frac{\partial G(\mathbf{r},\mathbf{r}')}{\partial \mathbf{n}} \right) \mathrm{d}S(\mathbf{r}) \tag{F.19}$$

F.1 Bubble on inside of sphere

Consider the case where we superimpose a hemisphere onto the interior of sphere Ω. Then the hypersingular integral that we wish to regularize is written in terms of the interior Green's functions and dielectric constants. Further, in adapting (F.19) with the proper normal vector notation, this equation becomes:

$$\begin{aligned}
v(\mathbf{r}') = &\oint_{S_a} \varepsilon_i(\mathbf{r}) \left(G_i(\mathbf{r},\mathbf{r}') \frac{\partial v(\mathbf{r})}{\partial \mathbf{n}_o} - v(\mathbf{r}) \frac{\partial G_i(\mathbf{r},\mathbf{r}')}{\partial \mathbf{n}_o} \right) \mathrm{d}S(\mathbf{r}) \\
&+ \oint_{\Gamma} \varepsilon_i(\mathbf{r}) \left(G_i(\mathbf{r},\mathbf{r}') \frac{\partial v(\mathbf{r})}{\partial \mathbf{n}_\Gamma} - v(\mathbf{r}) \frac{\partial G_i(\mathbf{r},\mathbf{r}')}{\partial \mathbf{n}_\Gamma} \right) \mathrm{d}S(\mathbf{r})
\end{aligned} \tag{F.20}$$

Taking the normal derivative of (F.20) with respect to $\mathbf{r}'$ and taking the limit as $\mathbf{r}'$ goes to $\mathbf{p}$ from inside the domain:

$$\begin{aligned}
\frac{1}{2} \frac{\partial v(\mathbf{p})}{\partial \mathbf{n}_i} = &\oint_{S_a} \varepsilon_i(\mathbf{r}) \left(\frac{\partial G_i(\mathbf{r},\mathbf{r}')}{\partial \mathbf{n}_i'} \frac{\partial v(\mathbf{r})}{\partial \mathbf{n}_o} - v(\mathbf{r}) \frac{\partial^2 G_i(\mathbf{r},\mathbf{r}')}{\partial \mathbf{n}_i' \partial \mathbf{n}_o} \right) \\
&+ \oint_{\Gamma} \varepsilon_i(\mathbf{r}) \left(\frac{\partial G_i(\mathbf{r},\mathbf{r}')}{\partial \mathbf{n}_i'} \frac{\partial v(\mathbf{r})}{\partial \mathbf{n}_\Gamma} - v(\mathbf{r}) \frac{\partial^2 G_i(\mathbf{r},\mathbf{r}')}{\partial \mathbf{n}_i' \partial \mathbf{n}_\Gamma} \right) \\
\Longrightarrow -\frac{1}{2} \frac{\partial v(\mathbf{p})}{\partial \mathbf{n}_o} = &\oint_{S_a} \varepsilon_i(\mathbf{r}) \left(-\frac{\partial G_i(\mathbf{r},\mathbf{r}')}{\partial \mathbf{n}_o'} \frac{\partial v(\mathbf{r})}{\partial \mathbf{n}_o} + v(\mathbf{r}) \frac{\partial^2 G_i(\mathbf{r},\mathbf{r}')}{\partial \mathbf{n}_o' \partial \mathbf{n}_o} \right) \mathrm{d}S(\mathbf{r}) \\
&+ \oint_{\Gamma} \varepsilon_i(\mathbf{r}) \left(-\frac{\partial G_i(\mathbf{r},\mathbf{r}')}{\partial \mathbf{n}_o'} \frac{\partial v(\mathbf{r})}{\partial \mathbf{n}_\Gamma} + v(\mathbf{r}) \frac{\partial^2 G_i(\mathbf{r},\mathbf{r}')}{\partial \mathbf{n}_o' \partial \mathbf{n}_\Gamma} \right)
\end{aligned} \tag{F.21}$$

If we set this equation equal to zero by moving all of the terms over to the left-hand side and then multiply the whole equation by negative one, we get the corresponding identity used in the main text.

F.2 Bubble on outside of sphere

Now consider the case where we superimpose a hemisphere onto the exterior of the sphere Ω. Then we have a choice to use the exterior Green's functions or the sometimes-layered interior Green's functions. We will drop the indices then here. Using the appropriate notation for the normal vectors, we have

$$
\begin{aligned}
v(\mathbf{r}') = &\oint_{S_a} \varepsilon_i(\mathbf{r}) \left(G_i(\mathbf{r},\mathbf{r}') \frac{\partial v(\mathbf{r})}{\partial \mathbf{n}_i} - v(\mathbf{r}) \frac{\partial G_i(\mathbf{r},\mathbf{r}')}{\partial \mathbf{n}_i} \right) \mathrm{d}S(\mathbf{r}) \\
&+ \oint_{\Gamma} \varepsilon_i(\mathbf{r}) \left(G_i(\mathbf{r},\mathbf{r}') \frac{\partial v(\mathbf{r})}{\partial \mathbf{n}_\Gamma} - v(\mathbf{r}) \frac{\partial G_i(\mathbf{r},\mathbf{r}')}{\partial \mathbf{n}_\Gamma} \right) \mathrm{d}S(\mathbf{r})
\end{aligned}
\tag{F.22}
$$

Taking the normal derivative of (F.22) with respect to $\mathbf{r}'$ and taking the limit as $\mathbf{r}'$ goes to $\mathbf{p}$ on the boundary, we have

$$
\begin{aligned}
\frac{1}{2}\frac{\partial v(\mathbf{p})}{\partial \mathbf{n}_o} = &\oint_{S_a} \varepsilon_i(\mathbf{r}) \left(\frac{\partial G_i(\mathbf{r},\mathbf{r}')}{\partial \mathbf{n}_o'} \frac{\partial v(\mathbf{r})}{\partial \mathbf{n}_i} - v(\mathbf{r}) \frac{\partial^2 G_i(\mathbf{r},\mathbf{r}')}{\partial \mathbf{n}_o' \partial \mathbf{n}_i} \right) \\
&+ \oint_{\Gamma} \varepsilon_i(\mathbf{r}) \left(\frac{\partial G_i(\mathbf{r},\mathbf{r}')}{\partial \mathbf{n}_o'} \frac{\partial v(\mathbf{r})}{\partial \mathbf{n}_\Gamma} - v(\mathbf{r}) \frac{\partial^2 G_i(\mathbf{r},\mathbf{r}')}{\partial \mathbf{n}_o' \partial \mathbf{n}_\Gamma} \right) \\
\implies \frac{1}{2}\frac{\partial v(\mathbf{p})}{\partial \mathbf{n}_o} = &\oint_{S_a} \varepsilon_i(\mathbf{r}) \left(-\frac{\partial G_i(\mathbf{r},\mathbf{r}')}{\partial \mathbf{n}_o'} \frac{\partial v(\mathbf{r})}{\partial \mathbf{n}_o} + v(\mathbf{r}) \frac{\partial^2 G_i(\mathbf{r},\mathbf{r}')}{\partial \mathbf{n}_o' \partial \mathbf{n}_o} \right) \mathrm{d}S(\mathbf{r}) \\
&+ \oint_{\Gamma} \varepsilon_i(\mathbf{r}) \left(\frac{\partial G_i(\mathbf{r},\mathbf{r}')}{\partial \mathbf{n}_o'} \frac{\partial v(\mathbf{r})}{\partial \mathbf{n}_\Gamma} - v(\mathbf{r}) \frac{\partial^2 G_i(\mathbf{r},\mathbf{r}')}{\partial \mathbf{n}_o' \partial \mathbf{n}_\Gamma} \right)
\end{aligned}
\tag{F.23}
$$

Subtracting all terms to the left-hand side of the equation yields the corresponding identity used for this case.